ANALYSIS OF NITRIC OXIDE TRANSFER AND RELEASE RATE FOR A CYSTEINE MODIFIED POLYMER

By

JUN GU

Bachelor of Science
East China University of Science and Technology
Shanghai, P. R. China
July, 2001

Submitted to the Faculty of the
Graduate College of the
Oklahoma State University
in partial fulfillment of
the requirements for
the Degree of
DOCTOR OF PHILOSOPHY
May 2010

ANALYSIS OF NITRIC OXIDE TRANSFER AND

RELEASE RATE FOR A CYSTEINE

MODIFIED POLYMER

Dissertation Approved:

Dr. Randy S. Lewis
Dissertation Adviser

Dr. AJ Johannes

Dr. Gary Foutch

Dr. Sundar Madihally

Dr. Warren T. Ford

Dr. A. Gordon Emslie
Dean of the Graduate College

ACKNOWLEDGEMENTS

First, I am grateful to my advisor, Dr. Randy Lewis for his constant mentoring and encouragement throughout my journey to Ph.D. It was Dr. Lewis who fostered me to become an initiative and independent researcher. I am also thankful for his effort and inspiration in writing publications and preparing presentations. It's my honor to work with an advisor like Dr. Lewis and I will cherish this wonderful period of time for lifetime. I would also like to acknowledge the other members of my committee, Dr. AJ Johannes, Dr. Gary Foutch, Dr. Sundar Madihally and Dr. Warren T. Ford, not only for their participation in this project, but also for the valuable insight and suggestions they provided throughout my research.

I would like to thank my past and present labmates, Dr. Heather Fahlenkamp and Dr. Vignesh Muthuvijayan for their sincere help and valuable inputs. I also want to express my gratitude to other graduate students in the department, especially Jian Xu for training me to use scanning electron microscope.

I am grateful to the School of Chemical Engineering for providing me financial support and I appreciate all the staffs in the School of Chemical Engineering for making my study at Oklahoma State University a great experience.

Finally, I would like to dedicate this dissertation to my wife, Li and my parents, Changsheng and Juanjuan. Without their solid support and constant love, I could never accomplish this important step in my life.

TABLE OF CONTENTS

Chapter Page

1 INTRODUCTION....1
1.1 Objective #1: S-nitrosocysteine (CySNO) Decomposition in Polymer-free Solution....7
1.2 Objective #2: S-nitroso-bovine-serum-albumin (BSANO) Transnitrosation with Free Cysteine (CySH)....8
1.3 Objective #3: Immobilization of CySH on PET Surface....8
1.4 Objective #4: BSANO Transnitrosation Kinetics with Immobilized CySH and Prediction of NO Flux from Cys-PET in a Flow System....9
2 LITERATURE REVIEW....11
2.1 Platelet Activation and Inhibition Mechanism....13
2.1.1 Platelet Activation....13
2.1.2 Platelet Inhibition....16
2.2 Biochemistry of Nitric Oxide and S-nitrosothiol....17
2.2.1 NO Biosynthesis....17
2.2.2 Platelet Inhibition by Nitric Oxide....18
2.2.3 Nitric Oxide and S-nitrosothiol....21
2.2.4 Transnitrosation: Transfer of Nitric Oxide between S-Nitrosothiols....30
2.3 Previous Research....31
2.3.1 Design of an Apparatus to Study NO Inhibition of Platelet on Surface....32
2.3.2 Cysteine Immobilization and Surface Characterization....35
2.3.3 Testing the Platelet Inhibition on Modified Polymer Surface *in vitro*....39

3 S-NITROSOCYSTEINE DECOMPOSITION IN FREE SOLUTION....41
3.1 Introduction....41
3.2 Materials and Methods....42
3.2.1 Materials....42
3.2.2 CySNO and Buffer Preparation....43
3.2.3 CySNO Decomposition....44
3.3 Results....46
3.3.1 CySNO Decomposition Rate Constant (k_{obs})....46
3.3.2 Effect of Buffer Purity on k_{obs}....48
3.3.3 Effect of pH on k_{obs}....53
3.4 Discussion....53
3.5 Conclusions....60

4 S-NITROSO BOVINE SERUM ALBUMIN (BSANO) TRANSNITROSATION WITH FREE CYSTEINE....62
4.1 Introduction....62
4.2 Materials and Methods....65
4.2.1 Materials....65
4.2.2 BSANO Preparation....65
4.2.3 BSANO Transnitrosation with Free Cysteine....66
4.2.4 BSANO Separation Test....68
4.2.5 Chemiluminescence Method....69
4.2.6 Saville Method....73
4.2.7 Cysteine Self-oxidation Assay by Ellman's Method....74
4.3 Results....75
4.3.1 BSANO Nitrosation and Separation Test....75
4.3.2 Transnitrosation Kinetics....77
4.3.3 Transnitrosation/Decomposition Reactions and Modeling Setup....87
4.3.4 Determination of Rate Parameters....90
4.4 Discussion....110
4.5 Conclusions....115

5 IMMOBILIZATION OF L-CYSTEINE ON PET SURFACE....116
5.1 Introduction....116
5.2 Materials and Methods....121
5.2.1 Materials....121
5.2.2 PET Modification....121
5.2.3 CySH Immobilization....122
5.2.4 Cysteine Surface Concentration Analysis....127
5.2.5 Imine Bond and Amide Bond Stability Test....129
5.2.6 Cysteine Modified Polymer Surface Property Analysis....129
5.2.7 Light and Air Effect on CySH Modified Polymer and Long Term Storage Test....129
5.3 Results....130
5.3.1 Cysteine Surface Concentration Measurement....130
5.3.2 Stability of Imine Bond and Amide Bond....131
5.3.3 Polymer Surface Change after Modification....135
5.3.4 Light and Air Effect on CySH Modified Polymer and Long Term Storage Test....141
5.4 Discussion....141
5.5 Conclusions....149

6 BSANO TRANSNITROSATION WITH CYSH MODIFIED PET AND MODELING IN FLOW SYSTEM....151
6.1 Introduction....151

6.2 Materials and Methods.....153
6.2.1 Materials.....153
6.2.2 Transnitrosation Reaction between PET-N(i)-CySH and BSANO Solution.....154
6.2.3 Data Analysis and Modeling.....155
6.3 Results.....165
6.3.1 Transnitrosation between BSANO and Immobilized CySH.....165
6.3.2 Transnitrosation Modeling in Flow System.....169
6.4 Discussion.....171
6.4.1 Transnitrosation Reaction between BSANO and Immobilized CySH....171
6.4.2 Factors That Influence NO Flux from the CySH Modified Polymer.....176
6.5 Conclusions.....178

7 CONCLUSIONS AND FUTURE WORK.....180
7.1 Major Accomplishments of the Study.....181
7.2 Future Work.....185

8 REFERENCES.....187

LIST OF TABLES

Table Page

1.1 Numbers of Medical Devices Used Each Year in U.S.....2

2.1 Extinction Coefficients for Several S-nitrosothiols at 334 nm.....26

2.2 Enzymes Systems that Break Down GSNO *In* Vitro.....29

3.1 Metal Contamination Level for Low and High Purity Salts (wt%).....52

4.1 Kinetic Data for Transnitrosation between S-nitroso Albumin (RSNO) and Thiols (RSH).....64

4.2 Percentage of BSANO Transnitrosated after 10 min or 4 Hours with Different Ascorbic Acid Concentrations (0 to 198 μM).....80

4.3 Values of k_f and k_r for Transnitrosation Experiments in Low Purity Phosphate Buffer at pH=7.4 with Different Ascorbic Acid Concentrations.....98

4.4 Values of k_{dc} and k_{oc}, with fixed average k_f and k_r values (as shown in Table 4.3), for Transnitrosation Experiments in Low Purity Phosphate Buffer at pH=7.4 with Different Ascorbic Acid Concentrations.....101

6.1 S-nitroso Human Serum Albumin (HSANO) Concentration in Plasma.....174

LIST OF FIGURES

Figure Page

1.1 Annual numbers of articles with the word "biocompatibility" in topic....4

2.1 Haemostasis sequence involving the platelets at different levels....12

2.2 Platelet agonists and responses....15

2.3 NO biosynthesis is through oxidation of the guanidinium nitrogen of L-arginine....19

2.4 Summary of the chemistry of the redox-interrelated forms of NO of potential biological significance....23

2.5 Thin-slit flow chamber device used to investigate the inhibition of platelet deposition on a biomaterial surface under flow conditions via the local delivery of gaseous nitric oxide....34

2.6 Illustration of the concept for the design that exploits endogenous NO and naturally-occurring mechanisms to increase the haemocompatibility of blood-contacting surfaces....36

2.7 Reaction schemes of immobilizing L-cysteine onto the surface of polyethylene terephthalate (PET) and polyurethane (PU) 38

3.1 CySNO decomposition profile as a function of pH in low-purity phosphate buffer..47

3.2 CySNO decomposition profile in non-buffer solution compared to buffer solution....49

3.3 First-order decay constant (k_{obs}) for CySNO decomposition in various phosphate buffers....50

3.4 First-order decay constant (k_{obs}) for CySNO decomposition in non-phosphate buffers....54

3.5 Fraction of species B (f_B) as a function of pH....59

4.1 Chemiluminescence experiment setup....71

4.2 Results for microcentrifuge filter analysis.....76

4.3 BSANO and CySNO concentration time profiles following the initiation of transnitrosation.....78

4.4 BSANO and CySNO concentration time profiles following the initiation of transnitrosation with 0μM or 20 μM AA.....81

4.5 BSANO and CySNO concentration time profiles following the initiation of transnitrosation with 148 μM or 198 μM AA.....82

4.6 BSANO and CySNO concentration time profiles following the initiation of transnitrosation with 50 μM or 500 μM AA.....83

4.7 BSANO and CySNO concentration time profiles following the initiation of transnitrosation with 200 μM AA.....84

4.8 Cysteine self-oxidation in buffers and deionized water at 4 ºC and 25 ºC.....86

4.9 Simulated BSANO concentration profiles using the base-case kinetic parameters along with variations in the k_f parameter.....93

4.10 Simulated BSANO concentration profiles using the base-case kinetic parameters along with variations in the k_r parameter.....93

4.11 Simulated BSANO concentration profiles using the base-case kinetic parameters along with variations in the k_{oc} parameter.....94

4.12 Simulated BSANO concentration profiles using the base-case kinetic parameters along with variations in the k_{oa} parameter.....94

4.13 Simulated BSANO concentration profiles using the base-case kinetic parameters along with variations in the k_{dc} parameter.....95

4.14 Scientist 3.0 regression result graphic output for the transnitrosation with 500 μM AA and 50 μM CySH with initial BSANO concentration at 62.27 μM.....99

4.15 Result of data fitting for variable k_f and k_r showed that there is no sign of correlation between the two constant and ascorbic acid concentration.....100

4.16 Scientist 3.0 regression result graphic output for the transnitrosation with 0 μM AA and 50 μM CySH (Run #1) 102

4.17 Scientist 3.0 regression result graphic output for the transnitrosation with 0 μM AA and 50 μM CySH (Run #2) 103

4.18 Scientist 3.0 regression result graphic output for the transnitrosation with 50 μM AA and 50 μM CySH (Run #1) 104

4.19 Scientist 3.0 regression result graphic output for the transnitrosation with 50 μM AA and 50 μM CySH (Run #2) 105

4.20 Scientist 3.0 regression result graphic output for the transnitrosation with 148 μM AA and 50 μM CySH.....106

4.21 Scientist 3.0 regression result graphic output for the transnitrosation with 198 μM AA and 50 μM CySH.....107

4.22 Scientist 3.0 regression result graphic output for the transnitrosation with 200 μM AA and 25 μM CySH.....108

4.23 Scientist 3.0 regression result graphic output for the transnitrosation with 500 μM AA and 50 μM CySH.....109

4.24 Result of data fitting for CySNO decomposition kinetic parameter k_{dc} versus ascorbic concentration.....111

4.25 Result of data fitting for CySH oxidation (by copper ion) kinetic parameter k_{oc} versus ascorbic concentration.....112

5.1 Reaction scheme for PET aminolysis by ethylenediamine.....118

5.2 Reaction scheme for PET carboxylation.....123

5.3 CySH immobilization on the aminolyzed PET using DCCI coupling.....126

5.4 CySH surface concentration on PET modified by different methods.....132

5.5 CySH surface amount and amount in the solution when the modified polymer (PET-N(i)-CySH) was incubated in low purity phosphate buffer at 25 ˚C and 37 ˚C.....134

5.6 CySH surface amount and amount in the solution when the modified polymer (PET-N(a)-CySH) was incubated in low purity phosphate buffer at 25 ˚C.....136

5.7 CySH surface amount and amount in the solution when the modified polymer (PET-C(a)-CySH) was incubated in low purity phosphate buffer at 25 ˚C.....137

5.8 CySH surface concentration when the modified polymer (PET-C(a)-CySH(E) was incubated in low purity phosphate buffer at 25 ˚C.....138

5.9 CySH surface concentration when the modified polymer (PET-N(a,e)-CySH was incubated in low purity phosphate buffer at 25 ˚C.....139

5.10 SEM image of PET surface change after different treatment.....140

5.11 PET-N(i)-CySH oxidation under different storage condition.....142

5.12 PET-N(i)-CySH long term storage test.....143

5.13 Possible CySH chain formation and thiol ester bond formation between the thiol group on the CySH chain and carboxyl group on the PET.....146

6.1 Simulation of CySNO surface concentration time profile when PET-CySH contacts a constant concentration of HSANO.....157

6.2 Modeling geometry of tubular reaction system.....162

6.3 BSANO concentration change during transnitrosation with immobilized cysteine (using PET-N(i)-CySH).....167

6.4 CySH surface concentration (PET-N(i)-CySH) change during transnitrosation with BSANO.....168

6.5 Dimensionless simulation of Human Serum albumin (HSANO) concentration profile within a tube with inner surface covered with Cysteine (CySH).....170

6.6 2-D contour (with concentration gradient) graph for dimensionless simulation of HSANO concentration profile within a tube with inner surface covered with CySH.....172

6.7 NO flux profile along the length of the tube at the inner wall surface (γ=1) of the tube calculated from the dimensionless simulation of Human Serum albumin (HSANO) concentration profile within a tube with the inner surface covered with Cysteine (CySH).....173

NOMENCLATURE

AA	Ascorbic acid
AA^-	Ascorbic acid anion
AA^{2-}	Ascorbic acid dianion
ADP	Adenosine diphosphate
AlbSH	Albumin
AlbSNO	S-nitrosoalbumin
APTES	3-Aminopropyltriethoxysilane
Ar, Ar’	Aromatic amine
ARA	Arachidonate acid
b	Half-thickness of the flow slit
Boc-Cys(Trt)-OH	N-(tert-butoxycarbonyl)-S-trityl-L-cysteine
BSA	Bovine serum albumin
BSA^-	Bovine serum albumin anion
BSANO	Nitrosated bovine serum albumin
C	Cysteine surface concentration
C_0	Initial cysteine surface concentration
C_A	Concentration of component A
C_{A0}	Initial concentration of component A
Ca-CAM	Calcium- calmodulin complex

cAMP	Cyclic adenosine 3’,5’-monophosphate
C_B	Concentration of component B
C_C	Concentration of component C
cGMP	Cyclic guanosine 3’,5’-monophosphate
C_{H+}	Concentration of hydrogen ion
cm	Centimeter
^{51}Cr	Chromium-51
C_T	Total concentration of ion impurities
COOH	Carboxyl group
CyS^-	Cysteine anion
CyS-CyS	Disulfide cysteine
CySH/Cys	Cysteine
CySH(E)	Cysteine ethylester
Cys-PET	Cysteine modified PET
CySNO	S-nitrosocysteine
D_A	Molecular diffusivity of component A
DAG	Diacylglycerol
DCCI	N,n'-dicyclohexylcarbodiimide
DHA	Dehydroascorbic acid
DI	Deionized
DNA	Deoxyribonucleic acid
DTNB	5,5-Dithiobis (2-nitrosbenzoic acid) (Ellman’s reagent)
DTPA	Diethylene triamine pentaacetic acid

ED	Ethylenediamine
EDC	1-ethyl-3-(3-dimethylaminopropyl)-carbodiimide hydrochloride
EDRF	Endothelium-derived relaxing factor
EDTA	Ethylenediaminetetraacetic acid
EMP	4-ethylmorpholine
f_B	Fraction of component B
fmol	Femtomole
g	Gram
GA	Glutaraldehyde
GlyCySNO	S-nitrosocysteinylglycine
GSH	Glutathione
GSNO	S-nitrosoglutathione
GTP	Guanosine triphosphate
H	Height of tube
HI	Hydriodic acid
HSA	Human serum albumin
HSANO	S-nitroso human serum albumin
HCl	Hydrochloric acid
HMW	High molecular weight
HNO_2	Nitrous acid
HOBt	1-hydroxybenzotriazole
HPLC	High-performance liquid chromatography
hr	Hour

$h\nu$	Photon's energy
IP_3	Inositol 1,4,5-triphosphate
k	Actual rate constant
k_1, k_2	Actual rate constant for AA oxidation by copper
K_1, K_2, K_3, K_4, K_5	Equilibrium constants of reactions
$k_{A,S}$	Surface consumption rate constant of HSANO on CyS-PET
kDa	Kilodalton
K	Transnitrosation equilibrium constant
$K_{a,C}$	Acid dissociation equilibrium constant for cysteine
k_{da}	CySNO decomposition (by ascorbic acid) rate constant
k_{db}	BSANO decomposition rate constant
k_{dc}	CySNO decomposition (by Cu^{+}) rate constant
k_f	Forward reaction rate constant of transnitrosation
KI	Potassium iodide
k_{oc}	Cysteine oxidation (by Cu^{2+}) rate constant
k_{oa}	Ascorbic acid oxidation (by Cu^{2+}) rate constant
k_{oo}	Cysteine autoxidation rate constant
k_r	Reverse reaction rate constant of transnitrosation
k_{obs}	Observed rate constant
κ	Nondimensionalization coefficient
L	Length of tube
LMW	Low molecular weight
m	Meter

M	Molar
MES	2-(N-morpholino)ethanesulfonic acid
min	Minute
mL	Milliliter
mM	Millimolar
mol	Mole
mV	Millivolt
MW	Molecular weight
N_2O_3	Dinitrogen trioxide
NaCl	Sodium chloride
NADPH	Nicotinamide adenine dinucleotide phosphate
NaOH	Sodium hydroxide
NEM	N-Ethylmaleimide
NH_2	Primary amine group
nm	Nanometer
nM	Nanomolar
nmol	Nanomole
NO	Nitric Oxide
NO_x	Nitrogen oxide donors
NO^+	Nitrosonium
NO^-	Nitroxyl
NO_2^-	Nitrite
NOA	Nitric oxide analyzer

NOS	NO synthase
O_2^-	Superoxide
OD	Optical density
OD_0	Initial optical density
ODE	Ordinary differential equation
ONOOH	Peroxynitrite
PA_2	Phospholipase A_2
PBS	Phosphate buffered saline
PDE	Partial differential equation
PET	Poly(ethylene terephthalate)
PET-C(a)-CySH	Cysteine modified carboxylated PET (amide bond)
PET-C(a)-CySH(E)	Cysteine ethylester modified carboxylated PET (amide bond)
PET-C(a)-Gly	Glycine modified carboxylated PET (amide bond)
PET-COOH	Carboxylated PET
PET-GA	Glutaraldehyde modified PET
PET-N(a)-CySH	Cysteine modified aminolyzed PET (amide bond, DCCI method)
PET-N(a)-Gly	Glycine modified aminolyzed PET (amide bond, DCCI method)
PET-N(a,e)-CySH	Cysteine modified aminolyzed PET (amide bond, EDC method)
PET-NH_2	Aminolyzed PET
PET-N(i)-CySH	Cysteine modified aminolyzed PET (imine bond)
pM	Picomolar
PMT	Photomultiplier tube
PU	Polyurethane

ρ	Density of fluid
Q	Volumetric flow rate
φ	Nondimensionalized concentration variable
r	Independent variable in radial direction
r_A	Reaction rate of component A in bulk liquid
γ	Nondimensionalized variable in radial direction
R	Radius of tube
Γ	Wall shear rate
R_A	Surface consumption rate of HSANO in bulk liquid
$R_{A,S}$	Surface consumption rate of HSANO on Cys-PET
RBC	Red blood cell
rpm	Revolutions per minute
RS•	Thiol radical
RSH, R'SH	Thiol
RSNO, R'SNO	S-nitrosothiol
RSSR	Disulfide
s	Second
S	Surface area of modified polymer
SEM	Scanning electron microscopy
sGC	Soluble guanylate cyclase
SH	Sulfhydryl group
SNAP	S-nitroso-N-acetylpenicillamine
t	Time independent variable

Tris	Tris[hydroxymethyl]aminomethane
TXA_2	Thromboxane A_2
θ	Angular independent variable
μL	Microliter
μM	Micromolar
UV-Vis	Ultraviolet-visible
V	Volume of reaction system
W	Slit width
wt%	Weight percentage
z	Independent variable in axial direction
ζ	Nondimensionalized independent variable in axial direction

CHAPTER 1

INTRODUCTION

Biomaterials have been used in the medical field for approximately one hundred years [Bhat 2002]. Although there is controversy over the term “biomaterial”, a widely accepted definition for biomaterials is: "A material intended to interface with biological systems to evaluate, treat, augment or replace any tissue, organ or function of the body." [Williams 1999]. It is important to note that living natural materials, such as tissues, should be called “biological materials” and should not be included in the definition of biomaterials [Shi 2005].

In recent years, there has been an increased interest in biomaterial applications in the medical field. Some common examples are artificial joints, heart valves, and contact lenses. Table 1.1 shows the major applications of biomaterials, with a total U.S. market of $9 billion in 2000 [Ratner *et al.* 2004]. Despite some biomaterial successes during the past few years, one of the most constant problems is the “biocompatibility” of the biomaterial. Biocompatibility is “the ability of a biomaterial to perform its desired function with respect to a medical therapy, without eliciting any undesirable local or systemic effects in the recipient or beneficiary of that therapy, but generating the most appropriate beneficial cellular or tissue response in that specific situation, and optimizing the clinically relevant performance of that therapy” [Williams 2008]. Thus, two key

Table 1.1 Numbers of Medical Devices Used Each Year in U.S. (Global numbers are typically 2-3 times the U.S. numbers) [Ratner *et al.* 2004] .

Medical Devices	Numbers of Usage/yr
Catheter	200,000,000
Blood Bags	40,000,000
Contact lens (2000)	30,000,000
Intraocular lens (2003)	2,500,000
Coronary stents	1,500,000
Dental implant (2000)	910,000
Hip and knee prostheses (2002)	500,000
Pacemaker	400,000
Renal dialyzer (2001)	320,000
Vascular graft	300,000
Heart-Lung (Oxygenators)	300,000
Breast implant	250,000
Heart valve	100,000

aspects of biomaterials need to be evaluated: performance of desired functions and assessment of interference with the biological system.

Research of biocompatible materials has drawn more and more attention since first introduced in the literature in 1967. Publication data shows that it has become an almost exponentially growing topic in research within the past twenty years as shown in Figure 1.1. Due to the complexity and diversity of the circumstances in which biomaterials are being used, biocompatibility issues are very complicated. Although, many creative works have been performed to improve the biocompatibility of materials, some key draw backs still remain unsolved, especially in long-term implantable medical devices [Williams 2008]. One major long-term problem of current blood-contacting biomaterials is haemocompatibility, which includes platelet adhesion, activation, and aggregation, followed by thrombus formation and detaching (shedding emboli) [Hayward and Chapman 1984; Courtney *et al.* 1994; Williams 2008]. These adverse host responses can further lead to the severe health problems, including severe bleeding resulting from platelet depletion, life-threatening stroke due to emboli transported to the brain and ischemia (lack of oxygen), and death of downstream tissue due to thrombosis formation.

The prevalent strategy for enhancing the haemocompatibility of biomedical polymers is surface modification. Modifications include grafting anticoagulants such as heparin [Marconi *et al.* 1996; Thorslund *et al.* 2005] and hirudin [Lahann *et al.* 2001; Lin and Tseng 2001], increasing the surface hydrophilicity via poly(ethyleneoxide) [Amiji and Park 1993], and passivation by coupling albumin to the surface [Amiji and Park 1993; De Queiroz *et al.* 1997]. However, some problems still exist with such methods.

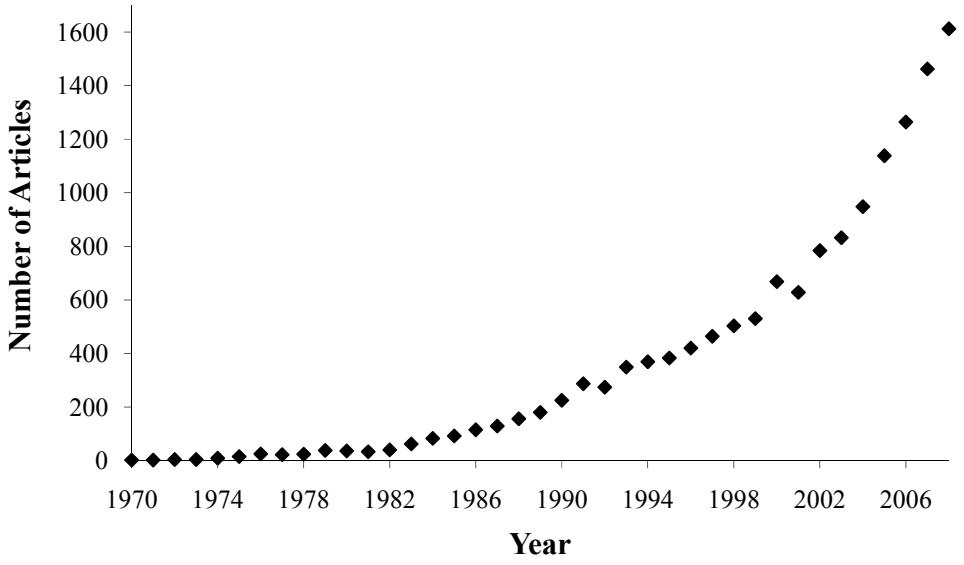

Figure 1.1 Annual numbers of articles with the word "biocompatibility" in topic (data obtained from ISI Web of Knowledge)

The immobilized active proteins, such as albumin and hirudin, are susceptible to conformational changes and enzymatic deterioration *in vivo* and are often only suitable for short-term applications [Bamford and Al-Lamee 1992; Muntean 1999; Williams 2008].

Recently, nitric oxide (NO), a well-known anti-platelet factor which is endogenously generated by endothelia cells, has been used to improve the haemocompatibility of biomaterials [Bohl and West 2000; Frost *et al.* 2005]. However, these biomaterials still have their limitations, including limited lifetime release of NO or a non-constant NO release rate. Recently, a polymer which uses endogenous NO to minimize platelet adhesion has been designed [Duan and Lewis 2002] and the minimum NO flux for complete platelet inhibition on the polymer surface has been determined to be 0.3-0.6 fmol/(cm^2·s) [Ramamurthi and Lewis 2000]. The polymer exploited endogenous NO (S-nitrosothiols, RSNO) to generate an NO flux from the polymer surface. Therefore, the polymer did not involve incorporating limited amount of NO donors into the polymer.

The design concept was based on the following theory. First, there is abundant S-nitrosothiols (mostly S-nitroso-albumin with concentrations around the μM level [MacArthur *et al.* 2007]) in the blood providing an unlimited NO resource for the modified polymer [Stamler and Loscalzo 1992]. Second, NO can be transferred between different thiol compounds. The transfer rate is fast and preferentially transferred from S-nitroso-albumin to cysteine [Meyer *et al.* 1994; Wang *et al.* 2001]. It also has been shown that NO can be transferred *in vivo* from S-nitroso bovine serum albumin (BSANO) to L-cysteine [Scharfstein 1994]. Third, S-nitrosocysteine (the compound

formed once NO is transferred to cysteine) is unstable with trace concentrations of some metal ions catalysis, such that NO is released to inhibit platelet adhesion [Askew *et al.* 1995; Swift and Williams 1997; Stamler and Toone 2002]. Thus, the above properties of thiols gave rise to the design of attaching cysteine to the surface of a polymer so that NO can be transferred from S-nitroso-albumin to the cysteine on the polymer and then released to inhibit platelet adhesion and aggregation.

Previous experimental results showed significant inhibition of platelet adhesion to the modified polymer surface. However, complete inhibition still has not been achieved despite several optimization attempts of this polymer [Duan 2001; Fahlenkamp 2003]. Thus, this work focused on the kinetics of the reactions between a cysteine-modified biomaterial and the S-nitrosothiols to predict the NO release rate of this modified biomaterial surface for comparison with the release rate required for complete inhibition of platelet adhesion in physiological conditions. Specifically, this work explored and developed the kinetic model of the multiple reactions between a cysteine-modified polyethylene terephthalate polymer (Cys-PET) and nitroso bovine serum albumin (BSANO) in various *in vitro* conditions and predicted the NO release rate from the polymer surface. Meanwhile, various potential deactivating factors of the polymer were studied so that an optimized storage condition could be determined for the polymer and the effective life time of the polymer could be estimated in the physiological condition.

Although transnitrosation kinetics in free solution have been studied earlier [Meyer *et al.* 1994; Hogg 1999; Wang *et al.* 2001; Hu and Chou 2006], this study is unique since there is no reported kinetic study for the transnitrosation and release of NO involving immobilized components applied to the minimization of platelet adhesion. In

addition, reported kinetic data for the transnitrosation between S-nitroso proteins and low molecular weight thiols are not consistent and complete [Meyer *et al.* 1994; Zhang and Means 1996; Hogg 1999; Wang *et al.* 2001], thus this study can help to fill this gap. The kinetic model will also be helpful to reveal the possible reasons that cause the incomplete inhibition of platelet adhesion. Thus, more pertinent optimizations of the polymer can be made. The work was accomplished through five objectives.

1.1 Objective #1: S-nitrosocysteine (CySNO) Decomposition in Polymer-free Solution.

The hypothesis was that various factors can affect CySNO decomposition such as light, pH and metal ion. The decomposition rate is one of the dominant parameters that can affect NO release rate from the polymer surface. Thus, by studying the CySNO decomposition in the polymer-free solution condition, behaviors of the CySNO in the immobilized form can be predicted. Because NO is extremely reactive due to its free radical essence [Wang *et al.* 2002], it is hard to measure the NO release rate directly from the polymer. Thus an indirect method was used through monitoring the CySNO disappearance rate which can be quantified by spectrophotometric analysis. In this study, CySNO decomposition in various buffers with different purity grades at different pH was studied and a chelate effect was also studied. In addition, light effects from the spectrophotometer were also evaluated and results from two spectrophotometers were compared. Finally, a possible mechanism for CySNO decomposition, involving metal ion concentration and pH, was presented.

1.2 Objective #2: S-nitroso-bovine-serum-albumin (BSANO) Transnitrosation with Free Cysteine (CySH).

In order to better understand the transnitrosation between BSANO and immobilized cysteine (CySH), transnitrosation with free CySH (not bound to polymer) was studied first. As NO transfer is hard to monitor directly as mentioned earlier, the kinetics were studied through monitoring BSANO and CySNO concentration changes with time in batch conditions. Molecular weight filtration was used to separate BSANO and CySNO and a chemiluminescence method was used to measuring their concentrations. A mathematic model was developed to fit the experiment data and key kinetic parameters were calculated using data analysis software. Ascorbic acid effects on the transnitrosation were also studied due to its well known ability of promoting the NO release from nitrosothiols [Holmes and Williams 2000; Smith and Dasgupta 2000].

1.3 Objective #3: Immobilization of CySH on PET Surface.

The hypothesis was that the imine bond which is formed during previous developed immobilization techniques might be unstable in neutral pH solution and the peptide bond can be a good candidate for immobilization, also CySH itself can be oxidized by various factors. Previous studies showed that cysteine can be detached from PET in acidic condition completely within 1 hour [Duan and Lewis 2002; Gappa-Fahlenkamp *et al.* 2004] probably due to imine bond hydrolysis [Vazquez *et al.* 1990; Migneault *et al.* 2004]. In order assess this hypothesis, Cys-PET made by the previous method was incubated in buffer solutions and the CySH concentration in the solution and on the polymer was monitored through Ellman's method and chemiluminescence

method, respectively. Afterwards, the kinetics of CySH detaching from the PET surface were studied. To overcome the potential unstable bond, several alternative methods were developed to attach cysteine or its derivatives on the PET surface via a peptide bond. The stability of the new CySH modified polymer in aqueous solution was evaluated. The immobilized CySH oxidation due to different environment conditions was studied by monitoring CySH surface concentration during various treatments, such as light, air and temperature. The light and air effect was studied only for dry conditions, while for the aqueous condition, only temperature effect was studied as the modified polymer is intended to be used in an oxygenated environment without light (*in vivo*). A detailed kinetic model was developed based on the experimental data and an optimized storage condition was determined.

1.4 Objective #4: BSANO Transnitrosation Kinetics with Immobilized CySH and Prediction of NO Flux from Cys-PET in a Flow System.

The hypothesis was that the partial platelet inhibition previously observed was due to insufficient NO release from the modified polymer surface. In order to assess the hypothesis, Cys-PET and BSANO transnitrosation followed by CySNO decomposition in batch conditions were monitored by measuring BSANO and cysteine surface concentration changes using a chemiluminescence based assay which was previously established. A mathematical model was developed similarly as in object #2 and key kinetic parameters were determined. The kinetic model and parameters were then applied to a tubular flow reactor (with laminar flow) and the NO flux from the polymer surface at steady state was predicted using a mathematical model. Various factors, including flow rate, BSANO concentration, cysteine surface concentration and CySNO

decomposition rate constant and transnitrosation reaction equilibrium constant, were evaluated as to their effect on the NO release rate. The predicted NO was compared with the minimum NO flux required to inhibit platelet adhesion as mentioned earlier.

CHAPTER 2

REVIEW OF LITERATURE

Platelets hold an important role in the haemostatic response. Platelets prevent the loss of blood following a wound by adhering to the site of vascular damage and then forming a thrombus that can stop bleeding. A more detailed illustration of the haemostasis sequence is shown in Figure 2.1. Briefly, platelets adhere to the vascular damage site in a few seconds after injury. Then platelet aggregation starts and it forms a loose and permeable haemostatic plug which can close up the rupture. As more platelets are attracted to the site, the plug becomes impermeable and then the coagulation cascade starts, forming fibrin fibrils which can fortify the primary thrombus and finally forming a stronger thrombus to stop bleeding [Roderique and Wynands 1967; Blockmans *et al.* 1995]. However, such positive mechanisms can cause significant adverse sequences when foreign materials are in contact with blood [Authi *et al.* 1993]. Platelet adhesion to materials, when applied to medical devices, can adversely affect the material performance.

In order to develop a haemocompatible biomaterial, the mechanism of the interaction between the foreign material and blood must be fully understood. This chapter will first focus on the mechanism of haemostatic response in the biological

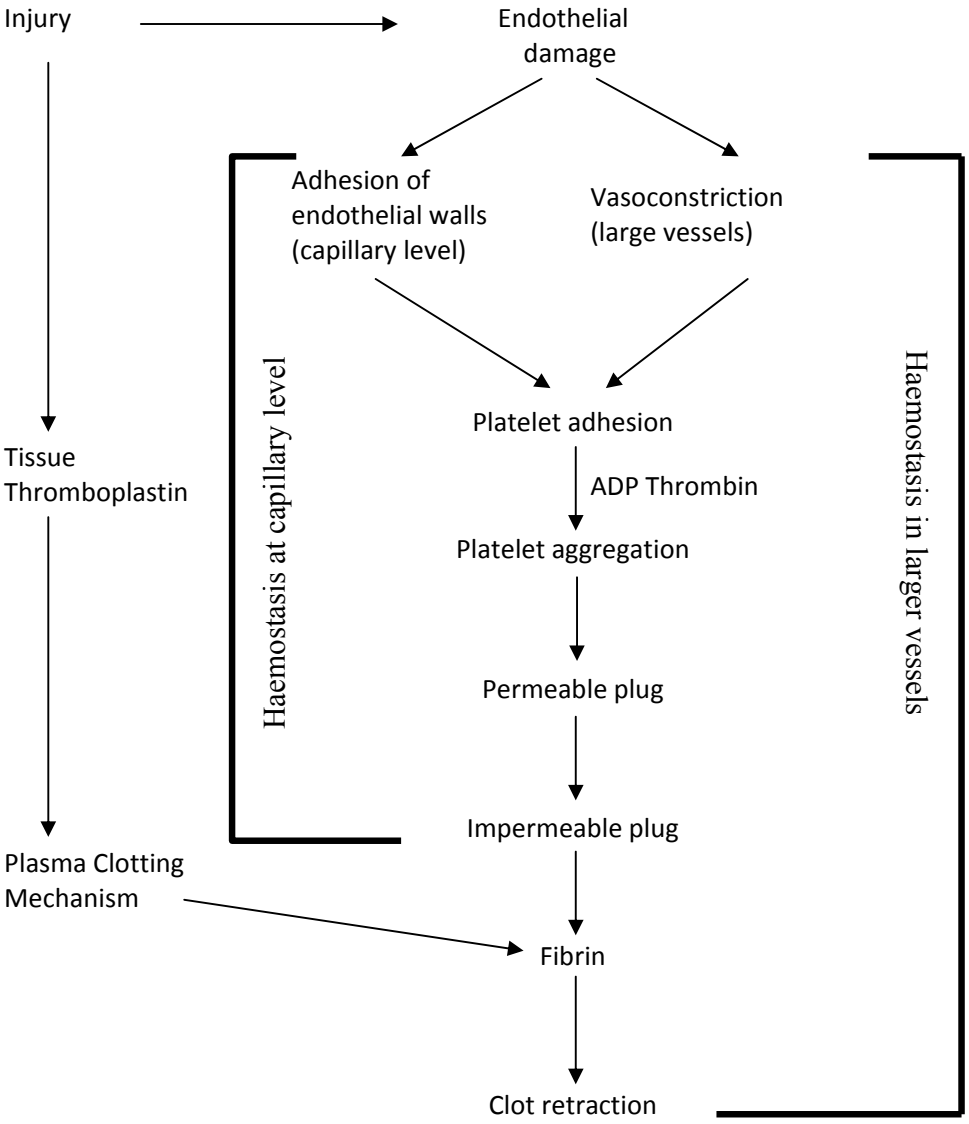

Figure 2.1 Haemostasis sequence involving the platelets at different levels. Figure modified from [Roderique and Wynands 1967].

system, which includes platelet activation and inhibition. Afterwards, the biochemistry of nitric oxide (NO) and its interaction with thiols in blood, to form S-nitrosothiols, will be explored, leading to the rationale of using cysteine-modified polymers to inhibit platelet adhesion. Finally, a brief review of current haemocompatible biomaterials including the previous work done by our group will be given.

2.1 Platelet Activation and Inhibition Mechanism

2.1.1 Platelet Activation

Platelet activation can be observed when platelets change their shape from disk-like to sphere and form long extensions called pseudopodia. Although the detailed pathways of platelet activation are very complicated, the pathways all involve interactions between agonists and the corresponding receptors in the platelet membrane [Ashby *et al.* 1990; Blockmans *et al.* 1995]. These responses can be categorized into three different patterns based on the agonists that initiate the responses [Authi *et al.* 1993].

Direct Response. Platelets are induced by thrombin and Platelet-Activating Factor (PAF), the latter is a potent phospholipid activator. These agonist-receptor interactions can cause platelet aggregation, thromboxane A_2 (TXA_2) synthesis and secretion from all three storage granules in the platelet. ADP then interacts with TXA_2 to enhance platelet aggregation.

Adhesion-dependent Response. This response is initiated when platelets interact with collagen fibrils and then spread on the fibrils. This causes the secretion of TXA_2 synthesis from all three storage granules and an increase in the phosphatidylserine

content of the outer leaflet of the plasma membrane. This enhanced extracellular exposure of phosphatidylserine triggers the formation of factor X and prothrombin activation complexes on the activated platelets and forms localized thrombin in the surrounding area of the site where platelets are exposed to collagen. This response only occurs in an area of vascular damage where collagen is exposed. If the collagen concentration is low, collagen alone won't initialize this response and usually the response is additionally dependent upon the interaction with released products such as ADP and TXA_2. Thus, this response can be remarkably reduced if ADP or TXA_2 is removed.

Aggregation-dependent Response. If the initial aggregation caused by agonist-receptor interactions is not strong enough, TXA_2 synthesis may be triggered and TXA_2 will be secreted from the storage granules. This response is induced by agonists such as ADP, adrenaline and 5-hydroxytrytamine (5HT). However, this response won't lead to lysosomal secretion or enhanced phosphatidylserine which is unlike the direct response mentioned earlier. Figure 2.2 shows different platelet agonists and responses.

Once the receptors in the platelet membrane binds the corresponding agonists, the cascade of intracellular second messengers, including inositol 1,4,5-triphosphate (IP_3), and diacylglycerol (DAG), is triggered. IP_3 causes Ca^{2+} secretion from the platelet dense tubular system, which leads to the arachidonate acid (ARA) release by phospholipase A_2 (PA_2) [Brass 1991; Haynes 1993; Puri and Colman 1997]. ARA is the precursor of TXA_2 which can permeate out of cell and interact with receptors on the platelet surface and leads to further activation. Meanwhile, DAG activates protein kinase C, initiating

granule secretion and fibrinogen receptor exposure [Savi and Herbert 1996]. Another important player during the platelet activation is the G protein family, which mediates

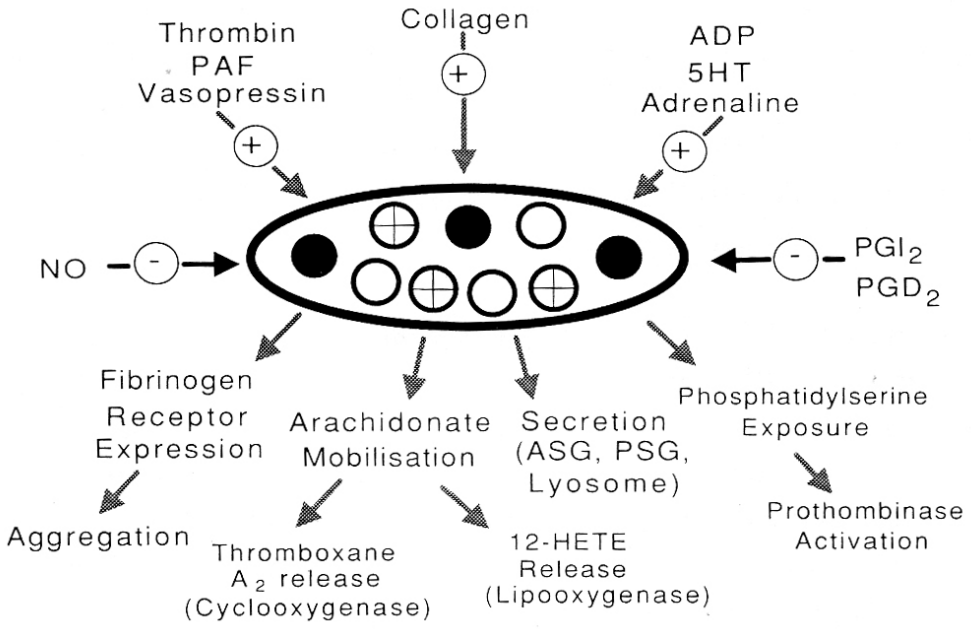

Figure 2.2 Platelet agonists and responses. The "+" symbol indicates an excitatory agonist and the "-" symbol represents an inhibitory agonist. [Authi *et al.* 1993].

various agonist-receptor interactions [Brass *et al.* 1993]. G proteins were believed to manipulate phosphoinosititde hydrolysis and 3',5'-monophosphate (cAMP) formation. They are also involved in PA_2 activation, which leads to the secretion of TXA_2 precursor formation as mentioned earlier [Haynes 1993].

2.1.2 Platelet Inhibition

Regulation of platelet activation is critical for the homeostasis of the vascular wall because excessive platelet activation can cause a thrombo-embolic phenomena, especially in the arterial vessels [Blockmans *et al.* 1995]. The activation of human platelets is inhibited by various chemicals, including thrombin inhibitor (e.g. hirudin) [Glusa 1991], ADP scavengers (e.g. apyrase) [Walsh *et al.* 1977], TXA_2 generation inhibitors (e.g. aspirin) [Vane 1994] and physiological and pharmacological agents which can elevate intraplatelet cyclic nucleotides [Haynes 1993]. In physiological conditions, vascular endothelial cells synthesize and secrete various platelet inhibitors. The most important two inhibitors are prostacyclin and the endothelium-derived relaxing factor (EDRF), which boost levels of the cAMP and cGMP, respectively, in human platelets [Haynes 1993; Vane 1994].

EDRF was first discovered by Furchgott and Zawadzki in 1980 when it was recognized as an endothelium-derived labile humeral substance which is responsible for mediating the vascular relaxations induced by acetylcholine [Furchgott and Zawadzki 1980]. Later, EDRF was found to be a potent inhibitor of platelet aggregation [Azuma *et al.* 1986; Radomski *et al.* 1992] and that it elevates cGMP levels in platelets or other target cells [Furchgott and Zawadzki 1980; Radomski *et al.* 1992]. This behavior of EDRF was then shown to be identical to that of nitric oxide (NO) by different research

groups [Furchgott 1988; Ignarro *et al.* 1988]. Additional results confirmed this analysis and it is now widely accepted that NO is EDRF [Radomski and Moncada 1993].

2.2 Biochemistry of Nitric Oxide and S-nitrosothiol

NO is a diffusible and extremely reactive molecular messenger with diverse biological functions throughout the body including the vascular, immune, and nervous systems due to its free radical essence [Moncada *et al.* 1991; Butler and Williams 1993; Änggård 1994; Knowles 1997; Murayama and Nomura 1998; Louis 1999; Gladwin *et al.* 2003]. In the central nervous system, NO adjusts synaptic plasticity and affects brain development, memory formation and behaviors. In the peripheral nervous system, NO acts as a neurotransmitter to regulate viscera motility, local blood flow and neuroendocrine function [Christopherson and Bredt 1997; Michel and Feron 1997]. NO is also responsible for controlling infection in which macrophages express an inducible NO synthase in response to immunological or inflammatory stimulation [Nathan 1997]. Also, the continuous generation of NO by the vascular endothelia cells is critical for the regulation of blood pressure and blood flow [Michel and Feron 1997; Loscalzo 2001]. Finally, the endothelium-derived NO has a critical role in preventing premature platelet adhesion and aggregation [Moncada *et al.* 1991; Loscalzo 2001].

2.2.1 NO Biosynthesis

NO is synthesized by the oxidation of the guanidinium nitrogen of amino acid L-arginine, resulting in L-citrulline as the coproduct [Knowles and Moncada 1994; Williams 2003]. The mechanism is a two-stage stereo-specific reaction involving molecular oxygen and reduced nicotinamide adenine dinucleotide phosphate (NADPH)

as coenzyme, with the aid of cofactors such as calcium ions and tetrahydrobiopterin (Figure 2.3) [Williams 2003]. This formation of NO from L-arginine is catalyzed by NO synthase (NOS) [Knowles and Moncada 1994; Mayer *et al.* 1998]. There are three different NOS isoforms that have been discovered so far:

- nNOS (neuronal NO synthase): a calcium and calmodulin (Ca-CAM)-dependent constitutive enzyme present in neurons and skeletal muscle, which generates NO as a neurotransmitter [Schmidt and Walter 1994; Christopherson and Bredt 1997; Mayer *et al.* 1998].
- iNOS (inducible NO synthase): a calcium-independent isoform isolated from macrophages, vascular smooth muscle cells, and hepatocytes which is induced by specific cytokines such as bacterial and viral infections [Nathan 1997; Williams 2003].
- eNOS (endothelial NOS): a Ca-CAM regulated constitutive form found in vascular endothelial cells, which produces NO and releases it into blood stream [Michel and Feron 1997].

nNOS and eNOS are also called constitutive NOS (cNOS) because they are dependent on calcium ion. The distribution of these three isoforms overlaps in many tissues and cell types and their subcelluar locations are variable. Meanwhile, the same isoform in different cells may have different biological functions, and the eNOS and nNOS are also inducible [Michel and Feron 1997].

2.2.2 Platelet Inhibition by Nitric Oxide

One of the most distinguished properties of NO is its unspecified signaling due to its lipophilic and free radical properties. This is quite different from the usual signaling

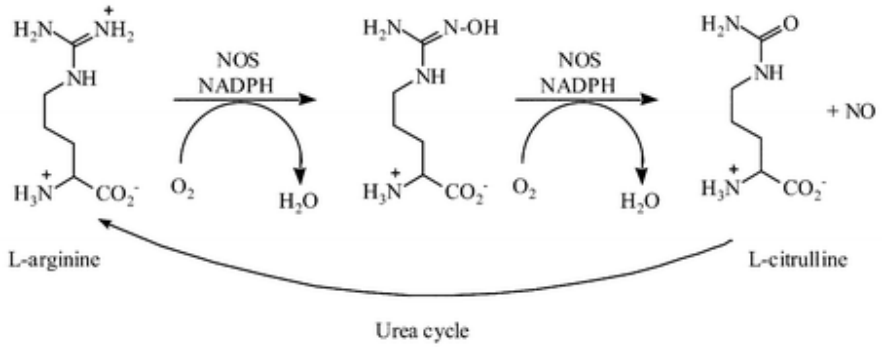

Figure 2.3 NO biosynthesis is through oxidation of the guanidinium nitrogen of L-arginine. This reaction catalyzed by nitric oxide synthase (NOS) with coenzyme NADPH. Oxygen is the electron acceptor [Williams 2003].

process in which signaling messengers interact with particular receptors on target cells to induce a specific response. NO can diffuse to virtually anywhere to interact with many targets including metal- and thiol-containing molecules and soluble guanylate cyclase [Moncada *et al.* 1991; Radomski and Moncada 1993; Williams 2003]. Although this process may seem to be random, these unique properties of NO are critical to mediate many of its biological functions.

Guanylate cyclase exists in both cytosolic and particulate fractions of cells [Brass 1991; Ivanova *et al.* 1994]. Particulate guanylate cyclase is found in the plasma membrane of many cells and so far five isoforms have been recognized. The soluble isoform of guanylate cyclase (sGC) plays a essential role in the NO-cGMP signal transduction pathway [Ivanova *et al.* 1994]. sGC is a Mn^{2+}-dependent enzyme found in the cytosolic fraction of most mammalian cells and is very abundant in platelets [Guthmann *et al.* 1992]. A key characteristic of sGC is the presence of heme as a prosthetic group. NO interacts with sGC through this heme group to evoke a conformational change that stimulates the conversion of GTP to cGMP [Radomski and Moncada 1993; Änggård 1994].

It has been well documented that the key mechanism by which NO inhibits platelet activation is through activation of platelet sGC to increase levels of cGMP [Radomski and Moncada 1993; Williams 2003]. Besides the sGC pathway, NO actions that are independent of cGMP production have also been described [Gordge *et al.* 1996]. These include NO-mediated ADP ribosylation, inhibition of glyceraldehyde-3-phosphate dehydrogenase and inhibition of intracellular calcium mobilization [Dimmeler and Brüne

1992; Feldman 1993; Brune B. 1998]. However, the relative importance of such non-sGC/cGMP independent actions of NO has not yet been fully understood.

The effects of NO on platelet differ substantially from those of many other antiplatelet agents. Compared to cyclooxygenase inhibitor acetylsalicylic acid (aspirin), which irreversibly inhibits platelet activation by preventing the formation of the pro-aggregatory TXA_2 [Vane 1994], NO inhibits platelet activation at an earlier stage and its effects are rapid and reversible [Radomski and Moncada 1993; Williams 2003]. Thus, in addition to inhibiting platelet adhesion to the vessel wall, NO also interferes with the initial thrombus formation by inhibiting aggregation and autocrine stimulations. This interference prevents platelet recruitment to the vicinity [Freedman *et al.* 1995; Freedman *et al.* 1997; Williams 2003].

2.2.3 Nitric Oxide and S-nitrosothiol

As a messenger molecule involving many physiological functions, NO needs to be transferred to various target tissues. However, due to its high reactivity with molecular oxygen, superoxide anion and heme/non-heme iron, its half life is less than 5 seconds in biological systems [Nathan 1992; Archer 1993]. In order to overcome this problem, biological systems develop an effective method to suppress the activity of NO, namely, binding NO to thiol groups. Stamler *et al.* observed that NO can react with cellular thiols to form S-nitrosothiols (RSNO), thus extending the half-life and spatial impact of NO [Stamler *et al.* 1992b]. Stamler also suggested that RSNOs act as nitrosonium (NO^+) and nitroxyl (NO^-) donors with chemical reactivities different from those of NO, which donors are capable of forming and modifying proteins and are present in mammalian tissue [Stamler *et al.* 1992b]. S-nitrosothiols have also been shown to have similar

biological actions as NO and play an important role in many processes, including platelet inhibition, signal transduction, DNA repair, host defense, blood pressure control, ion channel regulation and neurotransmission [Radomski *et al.* 1992; Lander *et al.* 1996; Gow *et al.* 1997; Brune B. 1998; Persichini *et al.* 1998]. In order to understand the S-nitrosothiol/NO functions in the physiological conditions, the basic biochemistry of S-nitrosothiol/NO need to be elaborated. Figure 2.4 shows a summary of the major NO derivatives with different redox status. A detailed explanation of the reactions involved is discussed below.

Synthesis. S-nitrosothiol can be synthesized *in vitro* by mixing thiol (RSH) and acidic nitrite via the following reactions in aqueous solution.

$$HNO_2 + H^+ \rightarrow NO^+ + H_2O \quad (2.1)$$

$$RSH + NO^+ \rightarrow RSNO + H^+ \quad (2.2)$$

The S-nitrosation (or S-nitrosylation) reactions can be quite rapid (ranging from less than half minute to a few minutes) under certain circumstances [Stamler *et al.* 1992a; Williams 1996; Zhang *et al.* 1996]. Although this method was later shown to be unspecific for S-nitrosation due to its ability to nitrosate amine and hydroxyl group, it is still widely used for preparing S-nitrosothiols because the thiol groups have a much higher affinity to nitrosation agents, thus getting nitrosated very fast [Aldred *et al.* 1982; Zhang *et al.* 1996].

Nitrosation of thiols can also take place with gaseous NO in aqueous solution at neutral pH when oxygen exists. The mechanism involves oxygen converting NO into N_2O_3, which is a known strong nitrosation agent [Wink *et al.* 1993; Lewis and Deen 1994]:

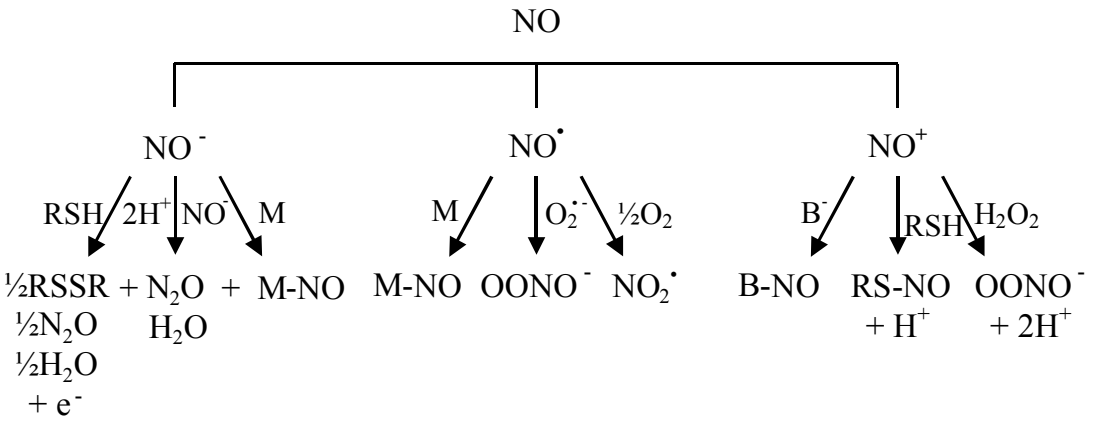

Figure 2.4 Summary of the chemistry of the redox-interrelated forms of NO of potential biological significance. The primary reactions of $NO^{\cdot}$ involve oxygen, superoxide, and redox metals (M). NO^- is reactive with metals and with thiols (RSH). Spontaneous dimerization of NO^- results in the formation of N_2O. Nitrosation reactions involve RSH and addition to bases (B^-), including peroxide [Stamler and Loscalzo 1992].

$$2NO + O_2 \rightarrow 2NO_2 \tag{2.3}$$

$$NO + NO_2 \Leftrightarrow N_2O_3 \tag{2.4}$$

$$N_2O_3 + RSH \rightarrow RSNO + NO_2^- + H^+ \tag{2.5}$$

These reaction mechanisms may serve as a pathway for *in vivo* S-nitrosation formation, although no direct evidence is provided. Recently, it has been reported that even in the absence of oxygen, thiol can still be nitrosated by NO with the mediation of an hemoglobin-iron complex [Palmerini 2002]. On the other hand, it was also reported that peroxynitrite (ONOOH) may nitrosate thiols such as glutathione [Wu *et al.* 1994; van der Vliet *et al.* 1998] according to:

$$GSH + ONOOH \rightarrow GSNO + H_2O_2 \tag{2.6}$$

Gow *et al.* proposed a mechanism for the formation of RSNOs *in vivo* (under physiological conditions) [Gow, 1997]. In this mechanism, NO reacts directly with reduced thiol to produce a radical intermediate, RSNOH. This intermediate then reduces an available electron acceptor to produce RSNO. Under aerobic conditions, O_2 acts as the electron acceptor and is reduced to produce superoxide (O_2^-).

$$RSH + NO \Leftrightarrow RSNOH \tag{2.7}$$

$$RSNOH + O_2 \rightarrow RSNO + H^+ + O_2^- \tag{2.8}$$

$$O_2^- + NO \rightarrow ONOO^- \tag{2.9}$$

The above reaction mechanisms clarify that RSNO can also be synthesized under a wide variety of physiological conditions.

S-nitrosothiols have relatively high extinction coefficients in the range of 330-350 nm. This property can be used to directly measure the concentration of S-nitrosothiol at

sub-mM levels [Stubauer *et al.* 1999; Vanin *et al.* 2004]. Table 2.1 lists the extinction coefficients of some common S-nitrosothiols at 334nm [Gordge *et al.* 1996].

RSNO has also been reported to be formed *in vivo* from many thiol compounds [Butler *et al.* 1995; Lander 1997]. S-nitrosoalbumin (AlbSNO), S-nitrosoglutathione (GSNO), or S-nitrosocysteine (CySNO) have been detected and quantified *in vivo* and their physiological functions has been shown to be similar to NO itself [Kluge *et al.* 1997]. The single free cysteine of serum albumin, Cys-34, has been shown to be particularly reactive toward NO under physiological conditions, primarily because that the pK_a of its sulfhydryl group (8.5) is close to that of cysteine itself (8.0) [Tong 2003]. Human plasma contains micromolar or sub-micromolar level RSNOs, of which 96% are S-nitrosoproteins, 82% of which is accounted for by AlbSNO. However, plasma level of free nitric oxide is only in the 3 nM range [Stamler *et al.* 1992b; Giustarini *et al.* 2007]. Thus, it has been hypothesized that AlbSNO serves as a reservoir with which plasma levels of highly reactive, short-lived free NO can be regulated. The chemical half-life of released NO is very short and is inactivated within ~0.2 s [Kelm and Schrader 1990]. On the other hand, RSNOs are usually very stable compounds, especially the AlbSNO which has a half-life of 40 min [Stamler *et al.* 1992a].

Decomposition. The stability of most the S-nitrosothiol is much better compared to NO. The thioester bond is a slightly polar covalent bond and it is not susceptible to homolysis to form radicals unless irradiated with strong light [Hogg 2002]. However this bond is very unstable due to trace metal ions contamination in solution [John McAninly 1993; Williams 1996; Stamler and Toone 2002]. The general form of this reaction is as follows:

Table 2.1 Extinction Coefficients for Several S-nitrosothiols at 334 nm [Gordge *et al.* 1996].

RSNO	**Extinction coefficients ($mM^{-1}cm^{-1}$)**
S-nitrosocysteine	0.74
S-nitrosohomocysteine	0.73
S-Nitroso-N-acetylpenicillamine	1.00
S-nitroso-N-acetyl-cysteine	0.87
S-nitrosoglutathione	0.85
S-nitrosoalbumin	0.87

$$RSNO \rightarrow NO + \frac{1}{2} RSSR \quad (2.10)$$

This instability is directly related to the metal ion concentration and it leads to sporadic decomposition rates due to the various contamination level of metal ions in solution [Hogg 2002; Stamler and Toone 2002]. For example, S-nitrosocysteine (CySNO) half-life was reported to be 30 seconds by Meyer et al, while Arnelle and Stamler measured it as 60 min [Meyer *et al.* 1994; Arnelle and Stamler 1995]. Studies have shown that even at μM level, copper ions can effectively catalyze this decomposition [Williams 1996]. Initially, Cu^{2+} was believed to be the active form that is responsible for the decomposition, but additional studies confirmed that Cu^{+} is the real species. A detailed mechanism has been established as follows [Askew *et al.* 1995; Dicks *et al.* 1996; Stubauer *et al.* 1999]:

$$RS^{-} + Cu^{2+} \rightarrow RS\cdot + Cu^{+} \quad (2.11)$$

$$RSNO + Cu^{+} \rightarrow RS^{-} + Cu^{2+} + NO \quad (2.12)$$

$$2RS\cdot \rightarrow RSSR \quad (2.13)$$

Chelating agents which can complex with Cu^{+} has been shown to suppress the biological function of RSNO to some extent [Gordge *et al.* 1995].

On the other hand, the structure of the nitrosothiol can also affect the stability of RSNO in solution significantly, although no direct correlation has been found [Noble and Williams 2000]. For example, Nobel and Williams reported that the CySNO decomposition rate is on the order of 10^3 faster than S-nitrosocysteinylglycine (GlyCySNO) [Noble and Williams 2000]. As for S-nitroso proteins, this stability can be even higher. Pietraforte *et al.* (1995) showed that S-nitroso bovine serum albumin (BSANO) is very stable in PBS buffer at 37ºC even in absence of metal ion chelators.

Scorza *et al.* (1996) observed no NO release from BSANO within 3 hours with a chelator (DTPA) and thiol deactivator (NEM).

In biological systems, RSNO concentrations, locations and bioactivities are usually regulated by catabolic processes rather than by synthesis. Several enzymes have been shown to break down low molecular weight (LMW) RSNOs *in vitro*, as shown in Table 2.2 [Askew *et al.* 1995; Freedman *et al.* 1995; Hou *et al.* 1996; Trujillo *et al.* 1998]. The relative distribution of these enzymes in different tissues could dramatically alter RSNO bioactivities. In the lung, for example, γ-glutamyl transpeptidase, which converts GSNO to S-nitrosocysteinylglycine, may give a greater membrane permeability for submucosal/smooth muscle bioactivity [Hogg *et al.* 1997]. In addition, glutathione peroxidase may produce NO with the net effect of inactivating GSNO and eliminating NO_x through NO expiration and/or reaction of NO with heme iron(II) [Freedman *et al.* 1995; Hou *et al.* 1996].

RSNO decomposition can also be induced by inorganic reaction. Intermediate Fe(S)NO formulation involving LMW thiol groups may result in RSNO catabolism [Vanin *et al.* 1997]. Inorganic reactions with copper are closely related to S-nitrosocysteine decomposition *in vitro* as previously discussed [Singh *et al.* 1996a]. Although these may seem to be less relevant *in vivo*, where free Cu^+ concentrations are low, protein bound Cu^+ is still capable of promoting NO release from RSNO at a comparatively lower speed [Dicks and Williams 1996]. It has been reported that Cu^+ chelation results in inhibition of bioactivities, which are thought to be related to GSNO catabolism in platelets and cardiac myocytes [Gordge *et al.* 1996; Mayer *et al.* 1998]. The RSNO catabolic effects of other biological transition metals are negligible compared

Table 2.2 Enzymes Systems that Break Down GSNO *In Vitro* [Askew *et al.* 1995; Freedman *et al.* 1995; Hou *et al.* 1996; Trujillo *et al.* 1998]

Enzyme	**Nitrogen oxide product**
(Thioredoxin) Thioredoxin Reductase	Nitric Oxide
Glutathione Peroxidase	Nitric Oxide
γ-Glutamyl Transpeptidase	S-nitrosocysteinylglycine
(Xanthine) Xanthine Oxidase	Peroxynitrite
Glutathione Dependent Formaldehyde Dehydrogenase	Hydroxylamine

with those of Cu and Fe [McAninly *et al.* 1993]. On the other hand, O_2^- has been shown to cause CySNO and GSNO breakdown with second order reaction kinetics in RSNO and first order in O_2^- [Aleryani *et al.* 1998; Jourd'heuil *et al.* 2000]. Based on the rate constant k ($3\text{-}6\times10^8$ $M^{-2}s^{-1}$), micromolar RSNO concentrations would be degraded only very slowly (~pM min^{-1}) by these reactions in the presence of nanomolar O_2^- concentrations under physiological conditions.

2.2.4 Transnitrosation: Transfer of Nitric Oxide between S-Nitrosothiols

Although plasma albumin can reacts with NO to form AlbSNO in physiological conditions, the limited intracellular access of AlbSNO indicates that NO might be transferred from plasma AlbSNO pool to affect biological function. NO exchange among thiols has been already reported in non-physiological conditions [Bennett *et al.* 1986; Keaney 1993]. Scharfstein *et al.* have demonstrated that the transnitrosation between AlbSNO and LMW thiols (i.e., cysteine), occurs rapidly and completely *in vitro* under physiological conditions, as shown below [Scharfstein 1994].

$$\text{AlbSNO} + \text{CySH} \Leftrightarrow \text{AlbSH} + \text{CySNO} \qquad (2.14)$$

After NO is transferred to LMW thiols, these smaller, more diffusible NO adducts can be used to transport NO more efficiently to the vascular smooth muscle cell or platelet surface.

Hemoglobin can also be nitrosated by NO through its single β-chain reduced Cys-93 under conditions of high oxygen affinity and the resulting SNO-hemoglobin leads to LMW RSNO formation through transnitrosation reactions [Jia *et al.* 1996; Gow *et al.* 1997; Giustarini *et al.* 2004]. The circulatory system may provide end organs with a stable supply of LMW RSNOs which can diffuse into tissues from the erythrocytes [Jia *et*

al. 1996]. Furthermore, NOS activation itself may form RSNOs, probably via intermediate $ONOO^-$ in the presence of thiols [Schmidt and Walter 1994; Gow *et al.* 1997]. Finally, other RSNO synthetic reactions may occur *in vivo*, such as protein nitrosation by nitrous acid (HNO_2) in acidic organelles, although these reactions remain to be verified.

2.3 Previous Research

The prevalent strategy for enhancing the haemocompatibility of biomedical polymers is surface modification. Modifications include grafting anticoagulants such as heparin and hirudin [Marconi *et al.* 1996], increasing the surface hydrophilicity via poly(ethyleneoxide) [Amiji and Park 1993], and passivation by coupling albumin to the surface [De Queiroz *et al.* 1997]. Also, polymers that have multiple functional molecules have also been studied in which heparin and albumin were both immobilized to increase the thromboresistance of biomedical polymers [Marconi *et al.* 1996]. However, some problems still exist with such methods. The immobilized active proteins are susceptible to conformational changes and enzymatic deterioration *in vivo* and are often suitable for only short-term applications. To date, none of these methods can generate a complete non-thrombogenic surface.

A new approach of haemocompatible polymer that is widely studied is a nitric oxide donor polymer. As discussed earlier, NO, a small messenger molecule, serves to inhibit platelet adhesion, aggregation, and activation as well as relax smooth muscles and modulate neurotransmission. Vascular endothelial cells synthesize and release NO and prostacyclin to make vessel walls completely compatible with platelet. The estimated NO flux rate from the blood vessel is 6800 $fmol \cdot cm^2 \cdot s^{-1}$ [Vaughn *et al.* 1998]. To mimic the

inner surface of the blood vessel, significant studies have been devoted to incorporate diazeniumdiolate NO donors into polymer surfaces to reduce platelet adhesion, aggregation, and the formation of thrombus on the thrombogenic surfaces [Annich G M 2000; Bohl and West 2000; Folts 2000].

Research on NO donor polymers demonstrates that localized NO release through incorporating NO donors into polymer surfaces may be an effective strategy for solving the haemocompatibility problems associated with blood-contacting medical devices. There are various NO donors incorporated in different polymers [Maalej *et al.* 1999; Annich G M 2000; Bohl and West 2000; Folts 2000]. However, some limitations of NO-releasing polymers, including non-constant release rates and limited life span and toxic concerns from donor residues, are difficult or impossible to be resolved which may essentially limit the applications of this technology.

2.3.1 Design of an Apparatus to Study NO Inhibition of Platelet on Surface

In order to overcome the above limitations of the current haemocompatible polymers, a new design of polymer was proposed. The first work in our research group was to establish valid guidelines for the local delivery of NO to reduce platelet deposition on biomaterials. This included the development of a suitable NO delivery device to study NO inhibition of platelet-biomaterial interactions *in vitro*, and the development of a mathematical model to predict aqueous NO concentration and flux profiles required to inhibit platelet attachment to biomaterials [Ramamurthi and Lewis 1997; Ramamurthi and Lewis 1998].

A thin-slit flow chamber device (shown in Figure 2.5) was designed to study the inhibition of platelet deposition on polymer surfaces under various flow conditions via

the local delivery of gaseous NO. A collagen-coated polymer was exposed to a flowing platelet suspension while NO gas permeated through the polymer and entering into the solution. The platelets were labeled with either a fluorescence dye or ^{51}Cr in order to study the platelet attachment to the polymer surface either qualitatively or quantitatively. Perfusion rates were determined based on wall shear rate requirements. The study showed that platelet-surface interactions are highly dependent on wall shear rates [Ramamurthi and Lewis 2000]. Although physiologically relevant shear rates range between 40 and 5000 s^{-1} [Turitto 1982], the shear rates tested were restricted between 125 and 500 s^{-1}, in order to minimize surface platelet aggregation and thrombus formation at higher shear rate. The wall shear rate (γ in s^{-1}) was determined from laminar flow analysis in a slit flow chamber according to:

$$\gamma = \frac{3}{2}\frac{Q}{60Wb^2} \tag{2.15}$$

where Q is the volumetric flow rate (cm^3 min^{-1}), W is the slit width (cm), and b is the half-thickness of the flow slit (cm). Based on the geometry of the flow slit, a volumetric flow rate of 1 ml min^{-1} corresponds to a shear rate of 250 s^{-1} and a Reynolds number of 2.

In order to predict aqueous NO spatial concentrations and fluxes profiles within the slit flow chamber reactor, a steady-state dimensionless continuity equation for NO was developed and solved numerically [Ramamurthi and Lewis 1997]. This study showed that the minimum surface NO concentrations and fluxes required to inhibit platelet deposition are 0.1 nM and 0.3-0.6 fmol·cm^{-2}·s^{-1}, respectively. Comparing this value to the estimated NO flux from the vascular cell mentioned earlier (which is 6800 fmol·cm^{-2}·s^{-1}), it is obvious that the platelets can be fully inhibited at the physiological NO flux rate. For the modified polymer, since the concentration of RSNOs in plasma

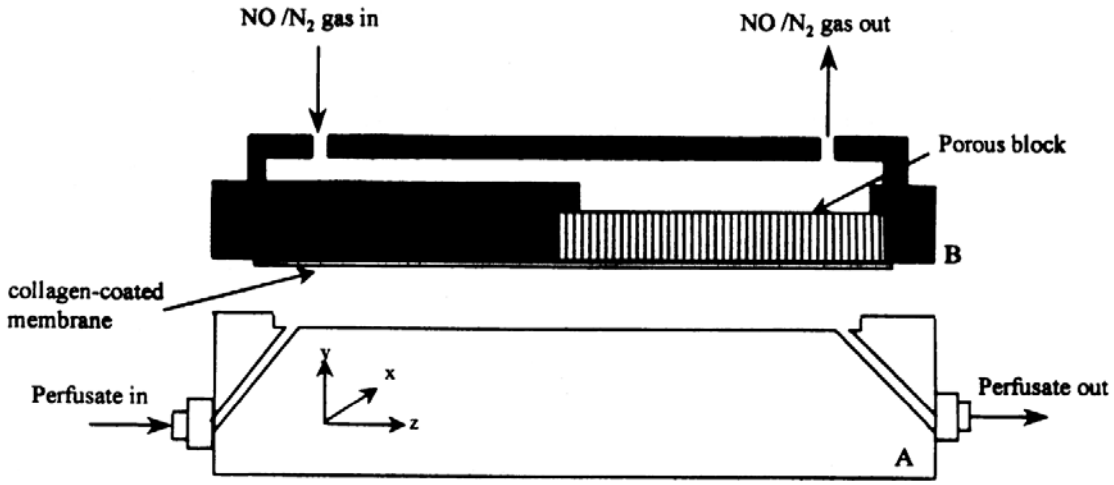

Figure 2.5 Thin-slit flow chamber device used to investigate the inhibition of platelet deposition on a biomaterial surface under flow conditions via the local delivery of gaseous nitric oxide [Ramamurthi and Lewis 1998].

have been shown to be in the micromolar or sub-micromolar range [Giustarini *et al.* 2007], there is a sufficient supply of NO that can be transferred to the surface of the cysteine-modified polymer by transnitrosation in order to inhibit platelet deposition on the surface.

2.3.2 Cysteine Immobilization and Surface Characterization

The next part of the research was to develop a cysteine modified surface which was first characterized and then used in studies involving platelets and plasma in order to test the design's ability to inhibit platelet adhesion to the surface [Duan 2001; Duan and Lewis 2002]. The basic concept for this modified polymer involves transnitrosation between the S-nitroso-albumin and the immobilized cysteine followed by S-nitroso-cysteine decomposition which releases NO to inhibit platelet adhesion to the polymer surface (Figure 2.6).

Two polymers which are widely used in blood-contacting applications, polyurethane (PU) and polyethylene terephthalate (PET), were chosen as the model polymer to attach cysteine. There are three reactive groups on cysteine that can be used for immobilization: the primary amine ($-NH_2$), carboxyl (-COOH) and the thiol (-SH). Since a free thiol group is required for the transnitrosation reaction with RSNOs in the blood followed by the release of NO into surroundings to prevent platelet attachment, therefore, only the amino group and the carboxyl group are available for immobilization. The amino group of cysteine was finally chosen as the reaction group for attaching cysteine on polymer surface because glutaraldehyde cross-linking through amino group is convenient and efficient and had been widely used [Jayakrishnan and Jameela 1996; Marconi *et al.* 1996; Seifert *et al.* 1997]. PU and PET have inert surfaces and have to be

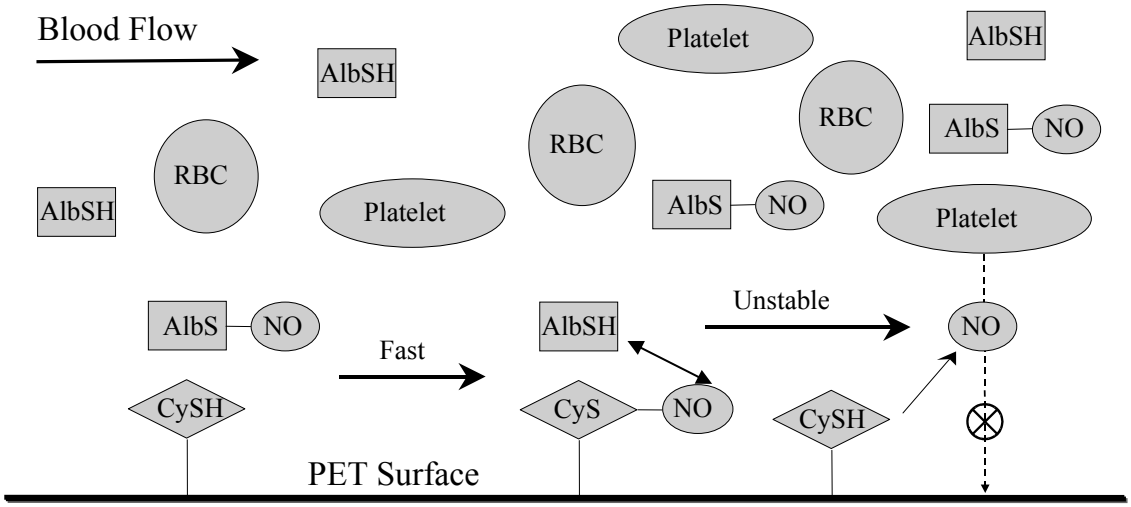

Figure 2.6 Illustration of the concept for the design that exploits endogenous NO and naturally-occurring mechanisms to increase the haemocompatibility of blood-contacting surfaces. Nitric oxide (NO) is transferred from S-nitroso serum albumin (AlbSNO) to cysteine (CySH), which is attached on the surface of polyethylene terephthalate (PET) film. This forms unstable S-nitrosocysteine (CySNO) which then decomposes and releases NO to inhibit platelet adhesion on the PET surface.

chemically modified to introduce reactive groups for immobilization. Therefore, PET and PU were treated with ethylenediamine (ED) and 3-aminopropyltriethoxysilane (APTES) to form a primary amine group on the polymer surfaces. The complete reaction scheme used to attach cysteine to PET and PU is shown in Figure 2.7. Later on, this process was optimized and different thiol containing molecules (e.g., 2-iminothiolane, cysteine polypeptide) were successfully attached to PET [Fahlenkamp 2003].

The cysteine surface concentration was then quantified by a chemiluminescence-based assay. Modified polymers were first treated by acidic nitrite solution (nitrite in excess) so that the immobilized cysteine is nitrosated. This step also breaks off the cysteine molecules from the polymers due to the unstable imine bond under acidic conditions [Carey and Sundberg 2007]. After nitrosation, the nitrosated cysteine the solution and the excess nitrite can be converted to NO by the use of reducing agents and measured by a NO chemiluminescence analyzer. The reducing solutions are made up of acidic acid with potassium iodide and can be adjusted for measuring different nitrite product by adding different agents. For assaying the total nitrite (NO_2^- + CySNO), an excess of free iodine is added in order to convert the CySNO and the excess nitrite into NO. On the other hand, adding excess of cysteine to the reducing solution can suppress 90% conversion of CySNO to NO, while exerts no effect on nitrite detection. Therefore, the concentration of the nitrosated cysteine can be determined by calculating the difference between the measurements from the two reducing solutions [Duan 2001]. The detection limit for nitrite using this method was as low as 0.02 nmol per injection. The intra-assay variability was less than 2% and the inter-assay variability was less than 5%. The calculated cysteine surface concentration on PET and PU surfaces were 8.1±1.1

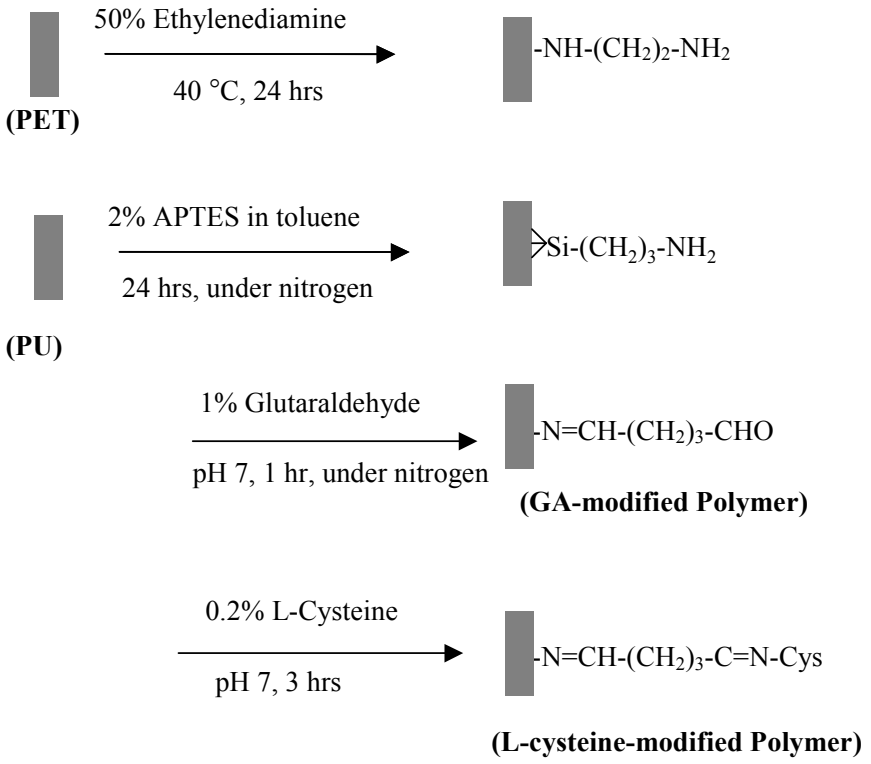

Figure 2.7 Reaction schemes of immobilizing L-cysteine onto the surface of polyethylene terephthalate (PET) and polyurethane (PU) by first adding an amine group by the use of ethylenediamine and 3-aminopropyltriethoxysilane (APTES), respectively and then using glutaraldehyde as a crosslinker to attach cysteine on the polymer surface [Duan and Lewis 2002].

nmol/cm^2 (n=5) and 5.2 ± 0.9 nmol/cm^2 (n=3), respectively. Later, a modified reducing solution containing copper chloride and cysteine in phosphate buffer (pH 7.4) was developed with better accuracy by Fahlenkamp [Gappa-Fahlenkamp *et al.* 2004].

2.3.3 Testing the Platelet Inhibition on Modified Polymer Surface *in vitro*

A preliminary experiment showed that the both cysteine modified PET and PU cause significant BSANO concentration decrease during incubation in PBS buffer, indicating that the modified polymers are capable of transferring NO from BSANO in After this, the two modified PET and PU polymers were tested in both batch and flow conditions in order to verify their haemocompatibility with platelets. The platelets were radio-labeled with isotope ^{51}Cr so that the amount of platelets could be quantified by measuring the radioactivity of the labeled platelets. Control samples for this study were glycine-modified PET and PU samples under the same experimental conditions. The batch test showed that the cysteine modified PET and PU samples does not have noticeable antiplatelet effect when no plasma presenting in the platelet suspension. However, when 50% plasma was present in the platelet suspension, the number of platelets attached to the modified polymer surfaces was reduced by ~60% and ~50%, respectively, as compared to the control. In the flow test, ,similar to the batch test, the presence of plasma significantly reduced the number of platelets attached to the modified polymer to ~55% and ~25%, respectively, as compared to the control [Duan 2001]. The results of this study indicate that in order for the cysteine modified polymers to inhibit platelet adhesion on the surfaces, they must be exposed to a source of RSNOs, which are found in plasma, so that NO can be transferred to the surface of the material and then released from the surface.

In order to further improve the haemocompatibility of this cysteine modified polymer so that it can completely inhibit platelet adhesion, the NO release rate from the modified polymer under physiological condition needs to be quantified and compared to the minimum NO flux required for platelet inhibition which was mentioned earlier. Assessment of the release rate will help determine whether the incomplete inhibition results from an insufficient NO flux from the polymer surface.

To determine the release rate, the kinetics of the transnitrosation between BSANO and the cysteine on the polymer, followed by CySNO decomposition, need to be investigated since there is no available kinetic data for the transnitrosation involving immobilized cysteine. Chapters 3 and 4 focus on the transnitrosation between CySNO and BSA in free solution. Stability issues of the cysteine on the polymer are addressed in Chapters 5. Finally, the kinetics of transnitrosation reactions between the modified polymer and BSANO are discussed and a mathematical model for predicting NO flux from the modified polymer surface in a tubular reactor is established in Chapter 6. In addition, various environmental factors are examined for their influences on the NO release rate from the polymer surface.

CHAPTER 3

S-NITROSOCYSTEINE DECOMPOSITION IN FREE SOLUTION

3.1 Introduction

S-nitrosothiols (RSNOs) play a significant role in many biological processes. As the main reservoir of nitric oxide (NO), RSNOs are involved in several processes including platelet deactivation, smooth muscle relaxation, immunosupression, neuro-transmission, and host defense [Richardson and Benjamin 2002]. Although the mechanisms of RSNO interactions *in vivo* are complex, the biological actions of RSNOs are often associated with the transfer (transnitrosation) and/or release of NO [Kelm 1999].

In order to analyze the kinetics of the NO flux from the cysteine modified polymer, the key kinetic parameter that directly controls the release rate, which is the S-nitrosocysteine decomposition rate as mentioned in the previous chapter, must be fully studied first. Although the decomposition rate for immobilized S-nitrosocysteine might be different from that of free S-nitrosocysteine in solution (due to the conformation change after the immobilization) it has been previously shown that immobilized S-nitrosocysteine decomposition is very susceptible to metal ions, similar to free S-nitrosocysteine decomposition [Duan 2001]. Thus, it is possible that both the immobilized and free S-nitrosocysteine exert similar behaviors in response to various

environmental conditions such as temperature, pH, metals and light [Williams 1999; Stamler and Toone 2002]. Therefore, it is beneficial to study S-nitrosocysteine decomposition in free solution before assessing decomposition on an immobilized polymer.

In this chapter, studies were focused on assessing and characterizing the free CySNO decomposition rate in solution over a broad pH range with various buffer purities for further application in the polymer modeling. Previous studies have shown that CySNO is stable in acidic (pH<5) and alkaline (pH>9) pH, while in the pH range of 6-8 CySNO decomposition occurs very rapidly [Vanin *et al.* 1997]. However, information on how the magnitude of the decomposition rate changes over the pH range of 5 to 9, particularly near physiological pH, is not given and such information would be beneficial to understand the control in which pH has on CySNO decomposition. In addition to pH effects, several studies have shown that metal ions including copper [Askew *et al.* 1995], iron [McAninly *et al.* 1993], and mercury [Swift and Williams 1997] are responsible for RSNO decomposition, although several of the studies were performed at or near pH 7.4 rather than over a wide pH range. Analysis over a wide pH range would be beneficial for determining if pH effects on CySNO decomposition were similar among various buffers containing metal ion contaminants.

3.2 Materials and Methods

3.2.1 Materials

L-cysteine, sodium nitrite, desferal (deferoxamine mesylate salt), citric acid and Tris-base were obtained from Sigma-Aldrich. Low-purity sodium phosphate dibasic

(Certified ACS, ≥99.0%, Cat. # S374-500), low-purity sodium phosphate monobasic (Certified ACS, ≥98.0%, Cat # S369-500), 12 M hydrochloric acid, ferrous sulfate, sodium hydroxide and pH 4.0/7.0/10.0 standard buffers were purchased from Fisher Scientific. High- purity sodium phosphate dibasic (Trace Select, ≥99.99%, Cat. # 71629) and sodium phosphate monobasic (Trace Select, ≥99.99%, Cat. # 71492) were purchased from Fluka. 1M NaOH and 1 M HCl were purchased from Cole-Parmer. 10× Gibco Phosphate-Buffered Saline (PBS), pH 7.4 was purchased from Invitrogen. All solutions in this work used purified water that was prepared by passage of reverse osmosis water through a pretreatment filter to remove colloids and bacteria, then passaged through two dionization columns, and finally passaged through a column to remove organics. This purified water was used for all the works in the other chapters, unless specified.

3.2.2 CySNO and Buffer Preparation

CySNO was made by acidic nitrosation as described in Chapter 2 (see section 2.2.3) [Byler *et al.* 1983; Kuo 2003]. Briefly, in a 15 mL centrifuge tube covered with aluminum foil, 3 mL of a 10 mM cysteine solution was mixed with 4 mL of a 10 mM sodium nitrite solution in the presence of 1 mL of 1 M HCl for 5 minutes to promote nitrosation of cysteine at acidic conditions. Following nitrosation, 1 mL of 1 M NaOH was added to neutralize the solution. A pH test paper was used to verify that the solution is neutralized. The final concentration of CySNO was approximately 3.33 mM. For studies in which the chelator desferal was used, 2 mL of 5 mM desferal was added to 8 mL of freshly-prepared CySNO. Thus, the final concentration of CySNO was approximately 2.67 mM with a desferal concentration of 1 mM.

Various buffers with different pH controlling ranges [Beynon 1996] were prepared to assess CySNO decomposition kinetics as a function of pH. The NaH_2PO_4-Na_2HPO_4 buffer, for controlling the pH between 5 and 8, was made by adding 100 mM Na_2HPO_4 slowly into 50 mL of 100 mM NaH_2PO_4 until the desired pH was obtained, with continuous mixing by micro-stirrer. The pH was continuously monitored by an Accumet semi-micro combination pH electrode (Cole-Parmer Instrument, Vernon Hills, IL) connected to an Oakton pH/CON510 Benchtop meter (Oakton Instruments, Vernon Hills, IL). The final phosphate concentration was 100 mM. This buffer was prepared using both low-purity and high-purity sources. The glycine-NaOH buffer, for controlling the pH between 7.5 and 10.5, was made similarly by slowly adding 10 M NaOH into 100 mL of 100 mM glycine until the desired pH was obtained. Since the NaOH volume added was very small (only a few droplets) compared to the glycine solution volume, the final glycine concentration after pH adjustment remained essentially at 100 mM. The glycine-HCl buffer (for pH control between 5 and 8) was similarly made by adding 12 M HCl into 100 mL of 100 mM glycine solution. For the Citric acid-Tris -NaOH buffer (for pH control between 5 and 9), 10 M NaOH was added into 100 mL of a 100 mM Citric-acid-Tris base solution. For these latter two buffers, the final concentrations were essentially 100 mM due to the small amounts of HCl or NaOH added.

3.2.3 CySNO Decomposition

Decomposition studies were performed by adding equal amounts of the CySNO solution with the buffer solution in either a 96-well microplate (usually 50 μL CySNO plus 50 μL buffer) for analyzing with a microplate reader or a semi-micro cuvette (usually 1 mL CySNO plus 1mL buffer was added to a 4 mL amber vial for mixing after

which a 1 ml sample was transferred into a semi-micro cuvette, as mixing the CySNO with buffer in the semi-micro cuvette directly is difficult) for analyzing with the UV-Vis spectrophotometer. Thus, for most studies, the final concentrations of buffer salts and CySNO were 50 mM and 1.67 mM, respectively. In the case where 10× Gibco PBS was used, the final total phosphate concentration of Gibco PBS was 5×, which is approximately 20 mM according to the product specification label. For the desferal studies, the final CySNO concentration was 1.34 mM. For the high purity buffer study containing added metal iron, 10 mM $FeSO_4$ was made freshly and diluted to a final iron concentration of 4.57 μM with high purity buffer. This final concentration of iron was made to be comparable to the maximum iron level of the low purity buffer, since 1 L of low purity buffer (pH 7.4) was made with approximately 11.50 g of Na_2HPO_4 (0.002 wt% max iron impurity) and 2.62 g of NaH_2PO_4 (0.001 wt% max iron impurity), which resulted in a potential maximum iron concentration of 4.57 μM.

Spectrophotometric absorbance changes of the mixture at 340 nm, proportional to the CySNO concentration, were monitored immediately after mixing using either a Packard® SpectraCount™ Microplate Photometer (BS10000, Packard Instrument Co., Meriden, IL) or a Varian UV-Vis Spectrophotometer (Cary 50 Bio, Varian, Inc., Palo Alto, CA). The corresponding buffer was used as blank. The spectrophotometer was used for the low-purity phosphate experiments (exemplifying faster decay) since it gives better consistency in assessing fast kinetics as compared to the plate reader (data not shown). The chemiluminescence method was not used for these experiments because the concentration of S-nitrosocysteine was high enough to be measured by a spectrophotometer directly and S-nitrosocysteine decomposition is very fast such that a

rapid and easy measurement is needed. The pH of the mixture was monitored before and after the decomposition studies using a micro pH electrode (PHR-146B, Lazarlab Research Laboratories, CA) connected to an Accumet mV/pH meter (AP62, Thermo Fisher Scientific Inc, Pittsburgh, PA) to assess any possible changes in pH after mixing the CySNO with the buffer and during the decomposition studies. Both pH meters were calibrated by 3-point standardization using pH 4.0, 7.0 and 10.0 standard buffers prior to measurement.

3.3 Results

3.3.1 CySNO Decomposition Rate Constant (k_{obs})

For assessing the rate at which CySNO decomposed with time, the concentration of CySNO was measured with time at each pH and buffer condition. Since the concentration is proportional to the optical density (OD) at 340 nm, Figure 3.1 shows a plot of OD (divided by the initial OD) versus time for several of the low-purity NaH_2PO_4-Na_2HPO_4 buffer experiments. The trend shows that CySNO disappears the slowest at pH 5.85, then disappears faster as the pH increases to pH 7.33 to 7.45, then starts to slow down again after pH 7.45.

Since CySNO is known to decompose in the presence of metal ions [McAninly *et al.* 1993; Dicks and Williams 1996; Williams 1996; Burg *et al.* 2000], the CySNO decomposition was modeled as a pseudo first-order decay according to

$$\frac{d[CySNO]}{dt} = -k_{obs}[CySNO] \tag{3.1}$$

where k_{obs} is the observed first-order decomposition rate constant and [CySNO] is the CySNO concentration. The metal ion concentrations contributing to the decomposition

rate are incorporated into k_{obs}, which is similar to the analysis used to model the decomposition of S-nitrosated glutathione (GSNO) in the presence of ascorbic acid and

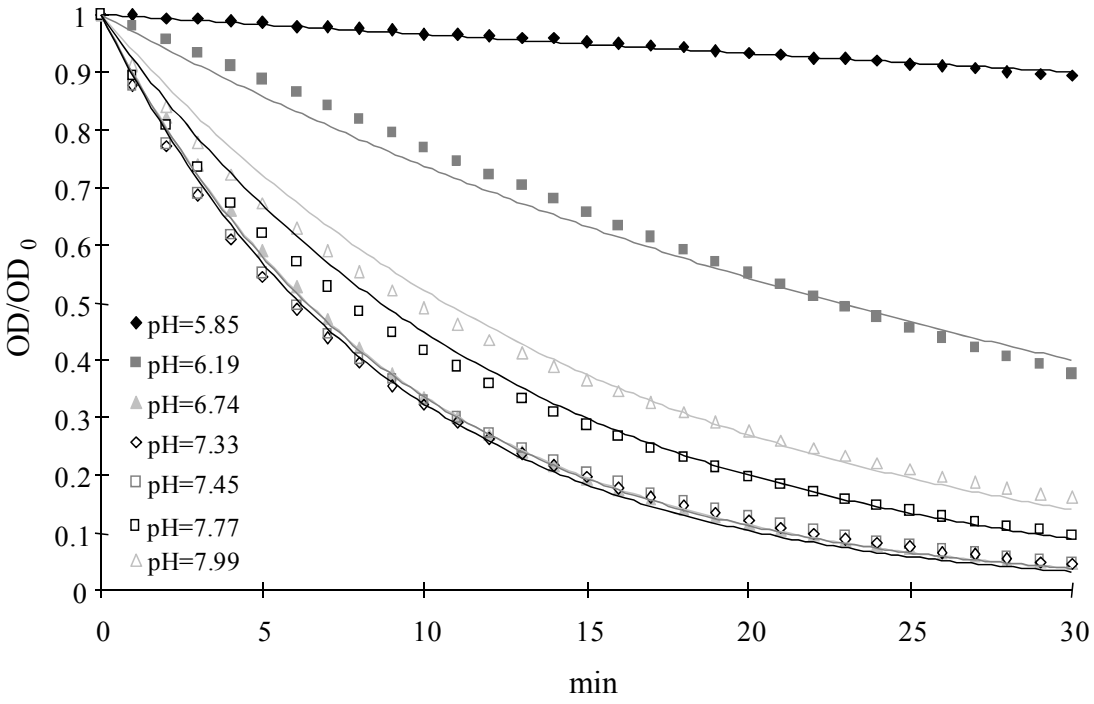

Figure 3.1 CySNO decomposition profile as a function of pH in low-purity phosphate buffer. (n=2) The optical density (OD) time profile, which is proportional to the CySNO concentration, is shown as a function of pH in the presence of low-purity phosphate buffer. The solid lines are exponential fitting.

copper ions [Scorza *et al.* 1996; Smith and Dasgupta 2000]. The rate at which NO is generated would be represented by k_{obs}[CySNO]. Since the OD is proportional to [CySNO], [CySNO] can be replaced by the OD in Equation 3.1. Integration of Equation 3.1 results in:

$$\frac{OD}{OD_0} = e^{-k_{obs} \cdot t} \tag{3.2}$$

Thus a plot of $-\ln(OD/OD_0)$ versus time from the information in Figure 3.1 would yield a slope equal to k_{obs}. The lines shown in Figure 3.1 represent the model (Equation 3.2) for the calculated k_{obs} values, thus confirming the correctness of the pseudo first-order decay model. In all cases, the standard error of k_{obs} obtained from the curve fit was less than 1.5%. Interestingly, if there was no buffer to control the pH (in water or 0.5 M NaCl solution), CySNO decomposition shown in Figure 3.2 did not correspond to a first-order decay model that was consistent with buffered solutions (phosphate or Gibco PBS). The lack of a first-order decay model for the non-buffered solutions was likely a result of changing pH since the pH changed 3-4 units throughout the experiment due to the formation of nitric acid from NO and oxygen [Lewis and Deen 1994].

3.3.2 Effect of Buffer Purity on k_{obs}

In Figure 3.3, the values of k_{obs} are plotted as a function of pH for three separate buffer solutions: a) low-purity NaH_2PO_4-Na_2HPO_4, b) high-purity NaH_2PO_4-Na_2HPO_4, and c) low-purity NaH_2PO_4-Na_2HPO_4 with the addition of the chelating agent desferal. In addition, k_{obs} is shown for one experiment in which Fe^{2+} was added to high purity NaH_2PO_4-Na_2HPO_4 buffer (final concentration of 4.57 μM) to show the effect of a metal ion contaminant on k_{obs}. The error bars representing the standard errors for the curve fits

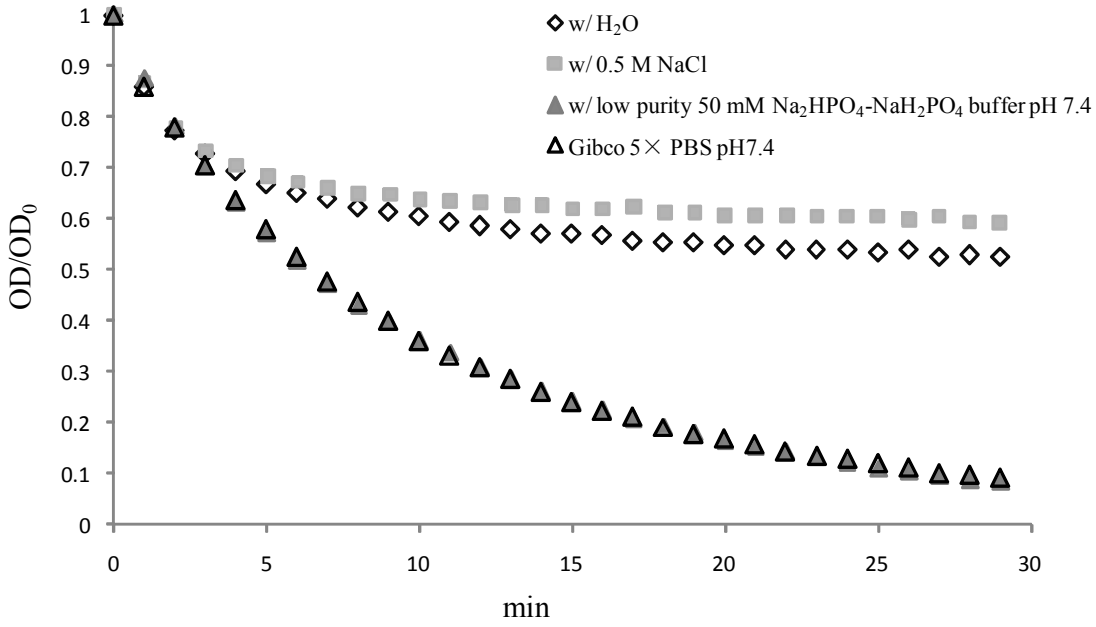

Figure 3.2 CySNO decomposition profile in non-buffer solution (water or 0.5 M NaCl) compared to buffer solution (in 50 mM low-purity phosphate buffer or Gibco 5× PBS). (n=2) The decomposition profile in non-buffer solution did not correlate with the first order decay model shown.

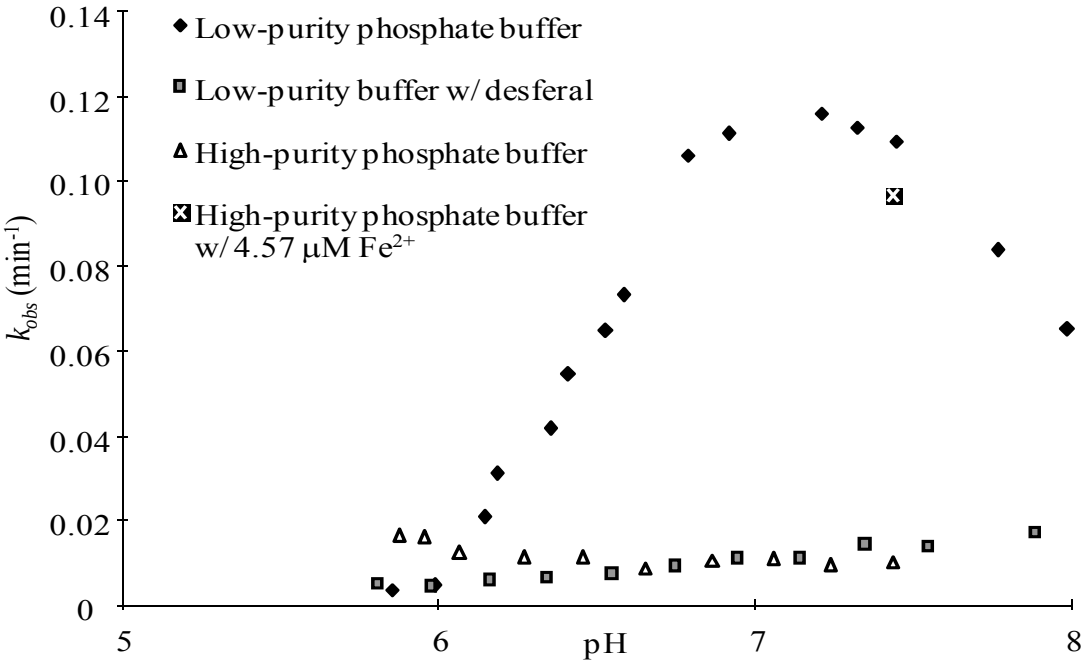

Figure 3.3 First-order decay constant (k_{obs}) for CySNO decomposition in various phosphate buffers. k_{obs}, as calculated from Equation 3.2 using experimental time data, is shown as a function of pH for low-purity phosphate buffer, low-purity phosphate buffer in the presence of the chelator desferal, high-purity phosphate buffer, and 4.57 μM Fe^{2+} in high-purity phosphate buffer.

are not shown since they were less than 1.5% for all points. As shown in Figure 3.3, k_{obs} maximizes near physiological pH and approaches zero near pH 6 for the low-purity buffer. Thus at pH 6 and below, CySNO decomposition (or the release of NO) does not occur. There is no data for pH >8 since this buffer is only capable of controlling the pH in the 5.5 to 8 range. For each pH experiment, the pH of the solution was well controlled during the decomposition- the pH only varied within ± 0.02.

As compared to the low-purity buffer, both 1 mM desferal and high-purity buffer significantly reduced the decomposition of CySNO, essentially showing little decomposition over the entire pH range. According to product specifications (Table 3.1), the low-purity phosphate buffer contained phosphate salts that had iron contamination up to 0.002 wt% and heavy metals contamination (Ag, As, Bi, Cd, Cu, Hg, Mo, Pb, Sb, and Sn [Schmidt *et al.* 2005]) up to 0.001 wt%. For the desferal study, the desferal reduced the metal ion contaminants (particularly Fe^{3+} [Vanin *et al.* 1997]) in the low-purity phosphate buffer via chelating action. Similarly, the high-purity phosphate buffer was made of much purer phosphate salts with iron contamination less than 0.000005 wt% and heavy metals less than 0.00002 wt% (Table 3.1). With the addition of Fe^{2+} to the high-purity phosphate buffer at pH 7.44 to obtain an iron concentration similar to the maximum iron content in the low-purity phosphate salts, k_{obs} increased significantly and was close to the k_{obs} for the low-purity phosphate buffer (the small difference may be due to other metal ion contaminants). These results demonstrate the importance of metal ions in CySNO decomposition and that the metal ions for this study came from the phosphate salts. The importance of metal ions in CySNO was previously observed although the effects of pH on the process were not assessed [Burg *et al.* 2000; Vanin *et al.* 2004].

Table 3.1 Metal Contamination level for low and high purity salts (wt%)

	Low Purity Salts		High Purity Salts	
Contaminant	Na_2HPO_4	NaH_2PO_4	Na_2HPO_4	NaH_2PO_4
Fe	≤0.002	≤0.001	≤0.000005	≤0.000005
Heavy Metals	≤0.001 (as Pb)*	≤0.001 (as Pb)*	0.000018**	0.000013**

Note. * Fisher Scientific did not have detailed compositions regarding the heavy metal content. Usually, heavy metals concentration is determined by adding Na_2S into the solution and comparing the darkness of the solution with a standard Pb solution mixed with Na_2S (sulfide ion reacts with heavy metals to develop darkness). A common list of heavy metals includes Ag, As, Bi, Cd, Cu, Hg, Mo, Pb, Sb, and Sn [Schmidt *et al.* 2005]. Contaminant levels were obtained from the label.

** Sigma-Aldrich provides detailed concentration levels for each metal on the label, thus this value is calculated by adding up the corresponding heavy metal concentrations.

3.3.3 Effect of pH on k_{obs}

Although Figure 3.3 showed that k_{obs} was negligible below pH 6 and increased to a maximum near physiological pH, further studies were performed to assess the pH effect on k_{obs} over a wider pH range and in the presence of other buffers. Since the phosphate buffer is not as efficient above pH 8, a citric acid-Tris-NaOH buffer, a glycine-HCl buffer, and a glycine-NaOH buffer were also evaluated to assess the effects of CySNO decomposition over a wider pH range. Figure 3.4 shows k_{obs} as a function of pH for the three buffers. Similar to the phosphate buffer studies in Figure 3.3, k_{obs} maximized near physiological pH and approached zero for pH <6 and >9.5. The citric acid-Tris-NaOH buffer had higher values of k_{obs} compared to the glycine buffers, which is likely a result of greater metal ion contamination in the chemicals used to prepare the buffer. The citric acid-Tris-NaOH buffer results were similar to those of the low-purity phosphate buffer, suggesting that contaminants rather than key buffer ingredients contribute to CySNO decomposition.

3.4 Discussion

The major findings from this chapter showed that the rate constant characterizing CySNO decomposition maximized near physiological pH (independent of the type of buffer), the rate constant dropped off rapidly within approximately ±1.5 pH units, and the metal ion contamination of the buffers affected the rate constant. It is interesting to note that the greatest decomposition occurred near physiological pH and that the release rate is controlled within a narrow pH band regardless of the metal ion content. Although the NO chemistry in biological systems is complex, the maximum release of NO from

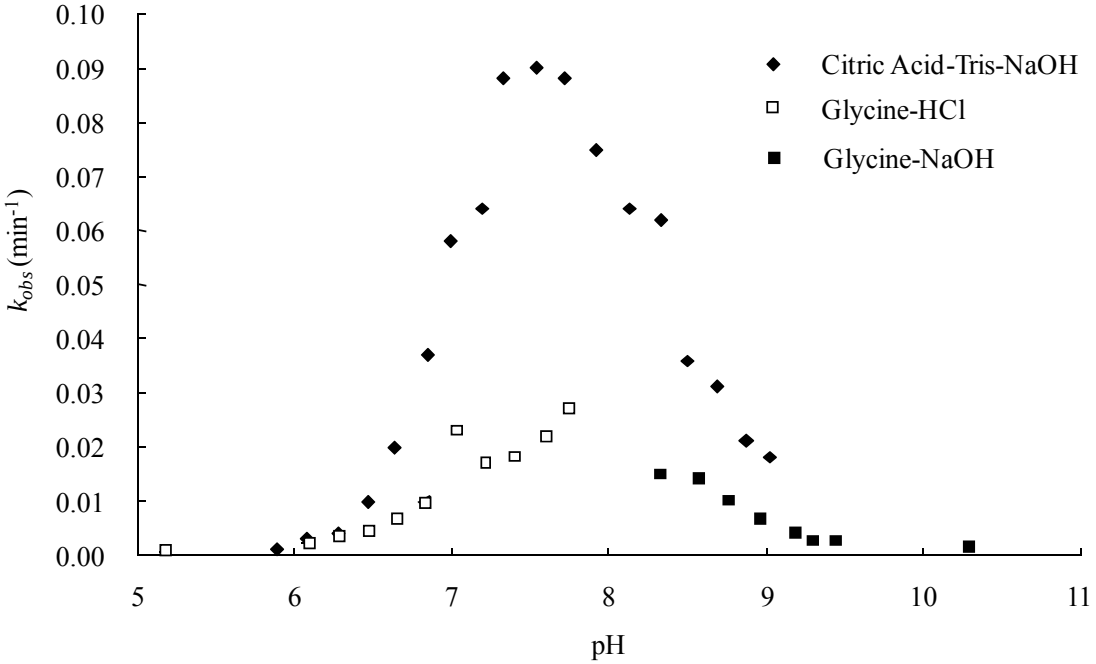

Figure 3.4 First-order decay constant (k_{obs}) for CySNO decomposition in non-phosphate buffers. k_{obs}, as calculated from Equation 3.2 using experimental time data, is shown as a function of pH for citric acid-Tris-NaOH buffer, glycine-HCl buffer, and glycine-NaOH buffer.

CySNO would thus occur near physiological pH. It would be beneficial to assess whether other RSNOs show similar trends.

The question arises as to why the decomposition rate maximizes near physiological pH. Previous studies assessing the decomposition rate of nitrosated glutathione in the presence of ascorbic acid showed that the decomposition rate was negligible below pH 5.5 but increased with increasing pH up to pH 7.7 [Smith and Dasgupta 2000]. The results showed evidence that the species promoting the greatest NO release was the ascorbic acid dianion. Equilibrium analysis that included the other two forms of ascorbic acid (ascorbic acid monoanion and ascorbic acid) showed that the dianion fraction of the total ascorbic acid increased as the pH increased, leading to a higher decomposition rate. Studies were not performed above pH 7.7 so an upper limit of the decomposition rate was not observed -- although the dianion fraction should theoretically reach unity and the decomposition rate should maintain a maximum level above a certain pH. However, these findings differ from the CySNO decomposition results where CySNO maximizes near physiological pH with metal ions and then decreases as the pH is increased or decreased. The action of Cu^{2+} on glutathione decomposition was also assessed but only at pH 7.45. Nevertheless, similar to this work that showed increasing the buffer impurity increased the decomposition rate, increasing the Cu^{2+} concentration increased the glutathione decomposition rate.

Recently, the effect of pH on CySNO decomposition in the absence of metal ions, but in the presence of excess cysteine, showed a maximum decomposition rate at approximately pH 8 with decreasing rates as the pH increased or decreased from pH 8 [Adam *et al.* 2005]. Thus, the results showed a similar effect of pH on the decomposition

rate as reported in this work. The mechanistic explanation for the pH effect involved an equilibrium model of several forms of cysteine. The decomposition mechanism was independent of metal ions and generated nitrogen gas instead of NO. In this work, excess cysteine was not present such that the decomposition mechanism would not be applicable. In addition, this decomposition pathway requires excessive cysteine at the mM amounts and estimates of the cysteine concentration in human plasma is less than 100 μM [Richie *et al.* 1996]. Therefore, this mechanism may not be as applicable in the physiological environment as compared to metal catalyzed decomposition—although further experiments would need to be performed to assess the dominating pathways leading to CySNO decomposition in a physiological environment.

Unlike the two mechanisms mentioned above involving either excess cysteine with CySNO or ascorbic acid with nitrosated glutathione, the results of this work provide a plausible explanation that several species of a metal ion contaminant (such as copper or iron) exist in equilibrium and that the dominant species at physiological pH (rather than the species at high pH in the case of ascorbic acid) is the species involved in the CySNO decomposition. For example, various forms of a metal contaminant (ex. Cu^{2+}, Cu^{+}, and Cu represented as A, B and C) could exist in equilibrium such that:

$$A \Leftrightarrow B + H^{+} \tag{3.3}$$

$$B \Leftrightarrow C + H^{+} \tag{3.4}$$

At equilibrium, $C_A = C_B C_{H+}/K_1$ and $C_C = K_2 C_B / C_{H+}$ where K_1 and K_2 are the equilibrium constants for the reactions in Equations 3.3 and 3.4, respectively. If only species B contributed to the decomposition, the fraction of B ($f_B = C_B/(C_A+C_B+C_C)$) contributing to decomposition would be pH dependent according to

$$f_B = \frac{1}{\left(1 + C_{H+} / K_1 + K_2 / C_{H+}\right)} \tag{3.5}$$

In Equation 3.5, activity coefficients are considered unity. If k_{obs} was represented as kC_B = kf_BC_T where C_T is the total species of copper present in solution (which is independent of pH) and k is the true first-order decomposition rate constant (also independent of pH), then a plot of f_B versus pH would yield the same curvature as k_{obs} versus pH for a given combination of K_1 and K_2 values. For instance, with $K_2 >> K_1$, at low pH the term K_2/C_{H+} would dominate the denominator in Equation 3.5 leading to f_B (and thus k_{obs}) approaching zero. Similarly at high pH, the term C_{H+}/K_1 would dominate the denominator such that f_B (or k_{obs}) also approaches zero. At an intermediate pH, f_B would reach a maximum.

An alternative model would be the dissolution of a single metal contaminant in solution such as was shown for the complete dissolution of cuprous oxide (represented as D below) in water to generate three forms of Cu^+ [Palmer *et al.* 2004] - again noting that Cu^+ is the species that has been shown to contribute to RSNO decomposition [Williams 1996; Burg *et al.* 2000]. In this scenario,

$$0.5D + H^+ \Leftrightarrow A + 0.5H_2O \tag{3.6}$$

$$0.5D + 0.5H_2O \Leftrightarrow B \tag{3.7}$$

$$0.5D + 1.5H_2O \Leftrightarrow C + H^+ \tag{3.8}$$

where A, B, and C represent the three forms of Cu^+ in solution. At equilibrium, the fraction of B in solution (f_B) is

$$f_B = \frac{1}{\left(1 + C_{H+} / (K_4 / K_3) + (K_5 / K_4) / C_{H+}\right)} \tag{3.9}$$

where K_3, K_4, and K_5 are the equilibrium constants for Equations 3.6, 3.7 and 3.8, respectively. It is noteworthy that Equation 3.9 is of the same form as Equation 3.5. Therefore, similar to the scenario presented for Equation 3.5 above, it is feasible to have f_B (or k_{obs}) approach zero at low and high pH and to maximize at an intermediate pH. For such a scenario to occur, K_5/K_4 must be much greater than K_4/K_3.

Figure 3.5 shows f_B versus pH for a variety of K_1 and K_2 values (or similarly, K_4/K_3 and K_5/K_4 values). The curvature, with values approaching zero at low and high pH, is similar to that shown in Figures 3.3 and 3.4, demonstrating the feasibility that species B in equilibrium with several other species is one plausible explanation for the effect of pH on CySNO decomposition involving metal ions. For both models presented above, species A or C participating in the CySNO decomposition would not lead to k_{obs} approaching zero at both pH extremes while maximizing at an intermediate pH. For $K_2/K_1 = 10^4$, it can be seen that decreasing K_2 shifts the f_B maximum from a lower pH to a higher pH while maintaining the same maximum value. When keeping K_1 constant (for example, $K_1=10^{-9}$), decreasing the ratio of K_2/K_1 increases the maximum value of f_B and slightly increases the pH at which the maximum occurs. Since $k_{obs} = f_B k C_T$, k_{obs} has a similar pH profile as f_B except the height of the curve depends upon the constant factor kC_T which is independent of pH. kC_T is constant and independent of pH since k is the true first-order decomposition rate constant and C_T is the total concentration of ion impurities. Although beyond the scope of this article, further studies need to be performed to confirm the appropriate model (i.e. multiple scenarios were given above) and determine the model parameters once the metal ion contaminant(s) are determined.

The maximum decomposition occurring near physiological pH (between 7.35 and 7.45 [Cooney 1976]) indicates that blood naturally provides an optimized condition to decompose CySNO, leading to optimal release of NO. Under acidosis conditions

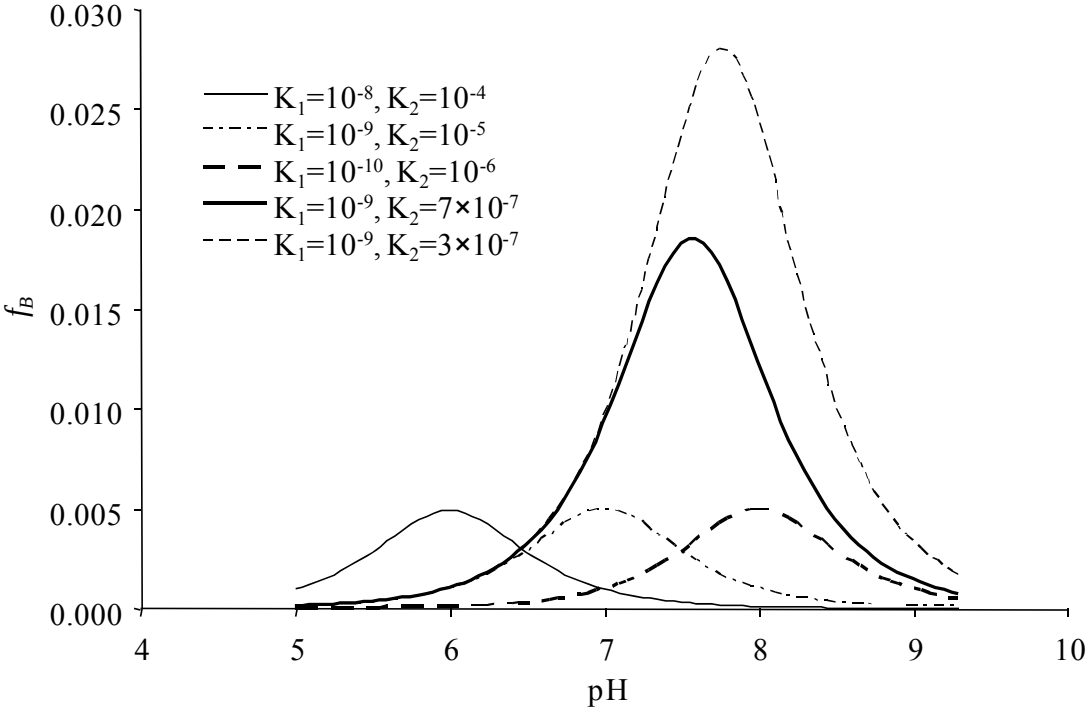

Figure 3.5 Fraction of species B (f_B) as a function of pH. Equation 3.5, representing the fraction of one form of ion species in equilibrium with other forms of the same ion species, is plotted as a function of equilibrium constants for the equilibrium reactions given in Equations 3.3 and 3.4.

(pH<7.35), the decomposition rate is relatively stable until the pH drops below 6.8. However, since the reported life-compatible pH range for blood is between 6.3 and 8.0 [Hinderling and Hartmann 2005], the CySNO decomposition rate can be reduced up to 50% at these pH extremes. Therefore, any physiological process involving CySNO decomposition in blood can potentially be affected under extreme acidosis/alkalosis conditions.

Another physiological process that can be affected by CySNO decomposition involves neurotransmission in which the localized environment in the synaptosomes is maintained at pH 7.04 ± 0.07 by bicarbonate ion [Richardson and Benjamin 2002]. According to this study, this pH indicates that CySNO decomposition (and NO release) is maximized when NO is involved in modulating the neurotransmission [Murayama and Nomura 1998]. In the event that pH control by bicarbonate is diminished such that the localized pH decreases below 7, NO release can also be diminished and potentially affect neurotransmission.

Finally, studies involving CySNO decomposition must be carefully performed and evaluated since pH and buffer purity contribute significantly to the decomposition rate. Knowledge of the decomposition rate is important for assessing the kinetics of the cysteine modified polymer and providing helpful information for temporarily preserving the CySNO solution and avoid any experimental error arising from CySNO decomposition during the measurement in the later chapters.

3.5 Conclusions

In this chapter, the CySNO decomposition rate was studied in different buffers (with varying metal ion impurities) at varying pH conditions. A chelator (deferoxamine

mesylate salt) was also used to assess how scavenging metal ions affects the decomposition rate over a wide pH range. The kinetic rate constant, characterizing the rate at which CySNO decomposes with time, was measured at each condition (pH and buffer content) with results showing that the rate constant maximized near physiological pH under all buffer solutions studied. An equilibrium model of metal ions as a function of pH provides a plausible explanation for the pH dependence on the experimental decomposition rate. The results of this work validate reasons for apparent discrepancies in RSNO decomposition studies [Mathews and Kerr 1993; Meyer *et al.* 1994; Pietraforte 1995; Scorza *et al.* 1996] and demonstrate the strong correlation between physiological pH and the maximum CySNO decomposition rate.

The important findings are:

1) CySNO decomposition maximizes near physiological pH regardless of the buffer, since trace metal ion exists in all buffer salts.

2) The model presented above gives a representative curvature similar to experimental observations and provides a plausible explanation for the pH dependence on CySNO decomposition,

3) CySNO decomposition can be very sensitive to environmental conditions, especially near the physiological pH, thus an accurate spectroscopy instrument, like Cary 50 UV-Vis spectrophotometer, is recommended.

4) The buffer purity (or C_T) greatly affects the decomposition rate, especially at near physiological pH.

CHAPTER 4

S-NITROSO BOVINE SERUM ALBUMIN (BSANO) TRANSNITROSATION WITH FREE CYSTEINE

4.1 Introduction

In biological systems, transnitrosation can occur with constituents containing at least one of two functioning groups, amines and thiols [Loeppky *et al.* 1987; Park 1988; Yanagimoto *et al.* 2007]. Transnitrosation reactions facilitate many signal transmissions in biological systems [Butler *et al.* 1994; Gaston *et al.* 2003; Marozkina *et al.* 2008]. As mentioned in Chapter 2, S-transnitrosation, which is the transfer of an NO moiety between two thiol molecules, is a key reaction involved in the mechanism of cysteine-modified polymers used to minimize platelet adhesion. The transnitrosation reaction is:

$$RSNO + R'SH \rightleftharpoons RSH + R'SNO \tag{4.1}$$

One possible mechanism for Equation 4.1 is [Hu and Chou 2006]:

$$R'SH \rightleftharpoons R'S^- + H^+ \tag{4.2}$$

$$R'S^- + RSNO \rightarrow RS^- + R'SNO \tag{4.3}$$

In order to conduct a kinetic analysis of transnitrosation, the reactants and the products need to be separated at a given point in the reaction and then measured. An

HPLC method has been used by several research groups to achieve this goal [Hogg 1999; Tsikas *et al.* 1999; Hu and Chou 2006]. The reaction is a second order reversible reaction, as determined by monitoring the concentration changes for RSNO and R'SH [Meyer *et al.* 1994; Hogg 1999]. Additionally, kinetic data for reactions between different thiols and S-nitrosothiols were acquired using different methods [Wang *et al.* 2001; Hu and Chou 2006]. However, not much kinetic analysis has been done for the transnitrosation between S-nitroso protein (such as S-nitroso bovine albumin) and low molecular weight thiols (such as cysteine).

Table 4.1 gives a recent summary of the transnitrosation kinetic data for S-nitroso albumin and low molecular weight thiols. From this list, it is evident that the current kinetic data is very limited with some inconsistencies. The kinetic data obtained was mostly acquired from spectrophotometric measurements which are not very sensitive compared to chemiluminescence methods [Samouilov and Zweier 1998; MacArthur *et al.* 2007]. Since this work involves transnitrosation between S-nitroso bovine albumin (BSANO) and cysteine (CySH), it would be beneficial to evaluate the kinetic constants for the transnitrosation between BSANO and free CySH before studying the transnitrosation kinetics of the cysteine modified polymer.

In this chapter, transnitrosation kinetics between BSANO and cysteine in solution, followed by S-nitrosocysteine (CySNO) decomposition, were evaluated using a molecular weight separation method coupled with a KI/I_2-based chemiluminescence analysis of RSNO (either BSANO or CySNO). Additionally, ascorbic acid (AA) effects on transnitrosation and NO release were identified since ascorbic acid has been found to

Table 4.1 Kinetic data for transnitrosation between S-nitroso albumin (RSNO) and thiols (RSH).

RSNO	RSH	k_f ($\mu M^{-1}hr^{-1}$)	k_r($\mu M^{-1}hr^{-1}$)	K_{eq}	Method	Reference
BSANO	CySH	2.203×10^{-4}			OD_{335}	[Wang *et al.* 2001]
			0.0468		OD_{412} w/ DTNB	[Zhang and Means 1996]
	GSH	0.068±0.08	0.692±0.049	0.120	HPLC, A_{336}	[Hogg 1999]
		6.048×10^{-3}			$OD_{330\text{-}370}$ and $OD_{500\text{-}600}$	[Wang *et al.* 2001]
			0.208		OD_{340}, Griess Method and spectral deconvolution	[Rossi *et al.* 1997]
			0.1872		OD_{412} w/ DTNB	[Zhang and Means 1996]
HSANO	CySH	0.0328			OD_{334}	[Meyer *et al.* 1994]
				0.75	HPLC, OD_{333}	[Tsikas *et al.* 1999]
	GSH	0.01152			OD_{334}	[Meyer *et al.* 1994]
				0.59	HPLC, OD_{333}	[Tsikas *et al.* 1999]

Abbreviations: GSH, glutathione; CySH, L-cysteine; BSANO, S-nitroso-bovine serum albumin; HSANO, S-nitroso-human albumin; k_f, forward reaction rate constant; k_r, reverse reaction rate constant; K_{eq}, equilibrium constant. A_{xxx}, Spectrophotometric measurement at wave length of xxx nm; HPLC, High-performance liquid chromatography; DTNB, 5,5'-dithio-(2-nitrobenzoate).

promote the NO release from S-nitrosothiols [Holmes and Williams 2000; Smith and Dasgupta 2000; Xu *et al.* 2000; Aquart and Dasgupta 2004] and is contained abundantly on transnitrosation and NO release were identified since ascorbic acid has been found to promote the NO release from S-nitrosothiols [Holmes and Williams 2000; Smith and Dasgupta 2000; Xu *et al.* 2000; Aquart and Dasgupta 2004] and is contained abundantly in human plasma (ranging from 20 μM to 60 μM) [Khaw *et al.* 2001; Jamaati *et al.* 2006].

4.2 Materials and Methods

4.2.1. Materials

Glacial acetic acid, potassium iodide, and sodium nitrite were purchased from Fisher Scientific (Fairlawn, NJ). Low-purity sodium phosphate dibasic (Certified ACS, ≥99.0%, Cat. # S374-500), low-purity sodium phosphate monobasic (Certified ACS, ≥98.0%, Cat # S369-500), 12 M hydrochloric acid and sodium hydroxide were purchased from Fisher Scientific. 1M NaOH and 1 M HCl were purchased from Cole-Parmer. Bovine serum albumin (BSA), ammonia sulfamate, sulfanilamide, iodine, L-cysteine (CySH), N-ethylmaleimide (NEM), 5,5-dithiobis (2-nitrobenzoic acid) (DTNB) and all the other reagents were purchased from Sigma Chemical Co. (St. Louis, MO). NANOSEP 500 μL microcentrifuge filter tubes with a cutoff molecular weight of 10k were purchased from PALL Corporation. Kimble 4mL and 1.8 mL amber vials were purchased from VWR.

4.2.2. BSANO Preparation

The BSANO solution was made similarly as the CySNO described in Chapter 3. Briefly, 2 mM BSA was made freshly by dissolving BSANO using the HPLC water in a 15mL centrifuge tube. Then, 1760 μL of 2 mM BSA solution was mixed with 640 μL of 4mM $NaNO_2$. This solution can be made and stored at 4 ºC for a few months. The total moles of BSA is less than the $NaNO_2$ because the BSA usually contains around 0.6 thiol groups per molecule [Wang *et al.* 2001]. To initiate nitrosation, 800 μL 1M HCl was added to the BSA solution and the tube was set on a hand-motion shaker (Cole-Parmer, Vernon Hills, IL) shaking at 60 times/min at room temperature. After 10 minutes, the nitrosation reaction was terminated by adding 15 μL 5% ammonium sulfamate for 5 minutes to scavenge the excess nitrite. Prolonged nitrosation is not recommended as excess nitrite can react with primary amine groups in the BSA molecule to slowly form N-nitrosation products [Zhang *et al.* 1996] which are not desirable because N-nitroso albumin can also have transnitrosation reactions with other thiols [Yanagimoto *et al.* 2007]. Finally, 800 μL 1M NaOH was added to the solution to neutralize the acid and make the pH near 7. This freshly made BSANO solution was further mixed with 5985 μL HPLC water and 10 mL 100 mM NaH_2PO_4-Na_2HPO_4 (pH=7.4, low purity) buffer to bring the final volume to 20 mL containing 50mM NaH_2PO_4-Na_2HPO_4 buffer. This final mixture is referred to as the BSANO solution in the following sections. The BSANO final concentration was usually around 100 μM although, in some cases, BSANO was diluted further to around 60 μM.

4.2.3. BSANO Transnitrosation with Free Cysteine.

To initiate transnitrosation, BSANO solution (4mL) was added to a 4mL amber vial and then 20.1 μL of 10mM cysteine solution (freshly made) was added so that the

final cysteine concentration was approximately 50 μM. In the case where AA effects were studied, 10mM freshly made AA was added into corresponding vials to achieve a desired final AA concentration ranging between 20 and 500 μM. The control sample that did not contain cysteine was made by adding HPLC water with a volume equal to the cysteine solution added. In the case of AA being involved, the same amount of AA was added into the control sample. All the vials were set on a hand-motion shaker at room temperature, shaking at 60 times/min for a couple of hours. All experiments were duplicated and performed at 25 ºC.

During the reaction, at specific times (usually 5 to 6 times), 300μL sample solution was drawn using a pipette and added into a microcentrifuge filter tube with a MW cutoff of 10kDa (see Section 4.2.4) to separate CySNO from BSANO for detection. In each filter tube, 50 μL of 100 μM NEM was added and mixed by hand for 30 sec to quench the thiol so that transnitrosation stopped [Mochizuki *et al.* 2005]. Afterwards, 50 μL of 1N HCl was added in order to inhibit CySNO decomposition. The centrifuge filter tubes were then centrifuged at 13000 rpm for 8 min in order to obtain a retentate solution of BSANO, CySNO, and NO_2^- (which formed during the CySNO decomposition) and a filtrate solution of CySNO and NO_2^- (these two species freely flowed through the filter). The filtrate (200 μL), containing the CySNO, was moved into another tube and mixed with 50μL of 0.33% ammonium sulfamate in order to quench the residual NO_2^-. The mixed solution (20 μL) was then measured by a KI/I_2-based chemiluminescence method (see Section 4.2.5) to determine the CySNO concentration. At the same time, 25 μL unfiltered sample was also treated with 50 μL of 100 μM NEM and 175μL 0.33% acidic ammonium sulfamate solution. The sample was then measured immediately by a KI/I_2-

based chemiluminescence method to determine the total S-nitrosothiol (BSANO + CySNO) concentration. In all cases, dilution effects were taken into account to obtain the true CySNO and BSANO concentrations during transnitrosation.

4.2.4. BSANO Separation Test

Since microcentrifuge filter tubes were used in the process to separate BSANO from CySNO following transnitrosation studies, it was important to test how well BSANO could be retained in the retentate solution. Therefore, 400 μL of a BSANO solution (without ammonium sulfamate treatment) was added into two microcentrifuge tubes. The centrifuge filter tubes were then centrifuged at 13000 rpm for 8 minutes using a Spectrafuge 16M Microcentrifuge (Labnet International, Inc, Woodbridge, NJ) in order to separate NO_2^- (remaining from BSANO preparation) from BSANO. Following filtration, 25 μL filtrate was collected from each filter tube and transferred into another regular centrifuge tube containing an equal volume of HPLC water. Finally, the filtrate sample was immediately measured by the Saville method (see Section 4.2.6) to measure both the NO_2^- concentration and total nitrite (NO_2^- + BSANO) concentration. It is expected that the NO_2^- concentration and total nitrite concentration should be the same since BSANO should not go through the filter. Meanwhile, another 20 μL un-filtered sample, which was collected directly from BSANO solution, was diluted to the same ratio as the filtrate sample and measured by the Saville method to assess the retained the NO_2^- concentration and total nitrite (NO_2^-+BSANO) concentration. The BSANO concentration was calculated by subtracting the measured NO_2^- concentration from the measured total nitrite concentration.

4.2.5. Chemiluminescence Method

For transnitrosation studies, it was important to measure the CySNO and BSANO concentrations with time. The chemiluminescence method has been widely used for RSNO detection for the past twenty years [Walters 1987; Conboy 1989; Samouilov and Zweier 1998; Marley R *et al.* 2000; Rassaf *et al.* 2002; MacArthur *et al.* 2007]. Its most distinguished advantage is high sensitivity and accuracy [Walters 1987; Conboy 1989; MacArthur *et al.* 2007].

The mechanism of the chemiluminescence method is based on the reaction between nitric oxide (NO) and ozone leading to the formation of an excited form of NO_2 (denoted NO_2^*), which subsequently releases electromagnetic radiation of characteristic frequency, as shown in the reaction steps below:

$$NO + O_3 \rightarrow NO_2^* + O_2 \tag{4.4}$$

$$NO_2^* \rightarrow NO_2 + h\nu \tag{4.5}$$

Emission from NO^*_2 is in the red and near-infrared region of the spectrum and is detected by a thermoelectrically-cooled, red-sensitive photomultiplier tube (PMT). NO from the sample and ozone produced in the electrical discharge of the detector are mixed in the chemiluminescence reaction cell. A red cut-off filter between the reaction cell and the PMT selectively transmits the light emitted by the NO/O_3 reaction for detection by a recorder.

For a liquid sample containing NO_2^- and RSNO, a reducing solution is required to convert NO_2^- and RSNO into NO so that the NO can be detected by chemiluminescence.

One most commonly used reducing solution is a tri-iodide based reducing solution (KI/I_2) which is made by mixing 2.5 mL 0.2 M KI in saturated I_2 solution with 7.5 mL glacial acetic acid. The reaction is rapid and stoichiometric [MacArthur *et al.* 2007]. This reducing solution is capable of reducing both NO_2^- and RSNO to NO for detection. The mechanism to produce NO is [Samouilov and Zweier 1998]:

$$I^- + I_2 \leftrightarrow I_3^- \tag{4.6}$$

$$2NO_2^- + 2I^- + 4H^+ \rightarrow 2NO + I_2 + 2H_2O \tag{4.7}$$

$$2RSNO + I_3^- \rightarrow 2NO^+ + 3I^- + RSSR \tag{4.8}$$

$$2I^- + 2NO^+ \rightarrow I_2 + 2NO \tag{4.9}$$

Figure 4.1 shows the chemiluminescence experimental set-up that was used throughout this project. Briefly, it contains a purging vial with the reducing solution connected to a Sievers 270B chemiluminescence NO analyzer (Sievers Corporation, Boulder, CO). After the reducing solution was added to the purging vial (D × H: 20 mm × 70 mm), the solution was purged by nitrogen via a fritted disk (Pore Diameter: 25-50 μm) at the bottom of the vial. Aqueous samples from the experiments were obtaining using a gas-tight syringe (Hamilton Company, Reno, NV) and then injected into 10 ml of the reducing solution. The NO released from the sample was carried with the nitrogen purge to the detector. The volume of each sample varied between 20 and 200 μl depending on the detection limits. The output signal from the detector was sent to an HP 3396 integrator (Agilent Technologies, Inc., Santa Clara, CA) that calculated the area under each sample peak. The areas were compared to NO_2^- standards for quantification.

In order to measure CySNO in the filtrate following centrifugation of transnitrosation samples or BSANO + CySNO in the unfiltered sample, the sample of

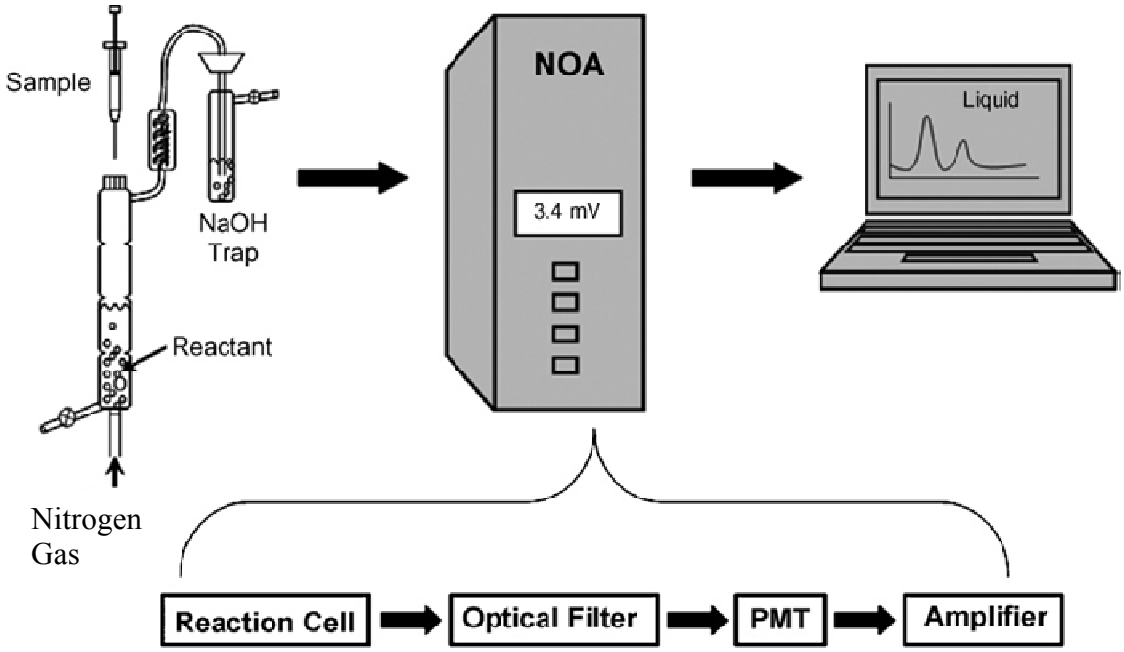

Figure 4.1 Chemiluminescence experiment setup. Samples were injected into the purge vessel containing reducing solution. The NO released from the samples is carried by the nitrogen gas through an ice trap to remove the acetic acid which is harmful for the NOA analyzer. NOA generates ozone to react with NO which produces emission that can be detected by the photomultiplier tube. The signal was transferred to an integrator which can calculate the peak area of the signal. Figure modified from MacArthur *et al*., 2007.

interest was treated with acidic ammonium sulfamate to scavenge NO_2^- (without affecting the RSNO concentration) via the following reaction mechanism.

$$NO_2^- + H^+ + NH_4SO_3NH_2 \rightarrow NH_4HSO_4 + N_2 + H_2O \quad (4.10)$$

After all the NO_2^- was consumed, the sample was then measured using the KI/I_2-based chemiluminescence method as previously described to give the RSNO concentration in the sample. If needed, another portion of the sample without ammonium sulfamate treatment could be measured using the same reducing solution to obtain the total nitrite (NO_2^- and RSNO) concentration. The NO_2^- concentration could then be calculated by subtracting the RSNO concentration from the total nitrite concentration. However, this work only reports the CySNO and BSANO concentrations during transnitrosation. In this work, the above chemiluminescence method was used in order to simplify the measurement and minimize the error propagation since the RSNO could be measured directly.

An alternative method to indirectly measure the RSNO concentration is to use two reducing solutions. In addition to the KI/I_2 reducing solution mentioned above, a KI/cysteine reducing solution can be made to scavenge I_2 and thus prevent I_3^- formation and NO release from the RSNO (see Equation 4.6 and 4.8) such that [Pietraforte 1995; Robak *et al.* 1997]:

$$2CySH + I_2 \rightarrow CyS\text{-}SCy + 2HI \quad (4.11)$$

Thus, this reducing solution can only liberate NO from NO_2^-. By using the KI/I_2 solution (without acidic ammonium sulfamate addition to scavenge NO_2^-) to measure total nitrite and the KI/cysteine solution to measure just NO_2^-, the RSNO concentration could be obtained by the difference [Duan 2001]. However, this method was found to be more

complicated and less accurate since the RSNO concentration is measured by a difference in two measurements.

In addition, one method to measure the RSNO directly which was used previously in the lab is using Cu^{+}/cysteine modified reducing solution (not acidic condition) [Fahlenkamp 2003]. Unfortunately, this method only works well with low molecular weight RSNO, such as CySNO, because when S-nitroso-protein is injected into the purge vessel, significant bubbling occurs (even using antifoam agent) due to the denaturing of the protein. However, this foaming was mostly suppressed when using acetic acid-based reducing solution probably due to the reason that the acid can break the macrostructure of the protein to reduce foaming. Therefore this Cu^{+}/cysteine reducing solution was not used for this work.

4.2.6 Saville Method

This test was used in some of the experiments in order to make a quick test of either free nitrite (NO_2^-) or RSNO concentration where a low nitrite/S-nitrosothiol detection is not required [Jocelyn 1987]. Compared to the chemiluminescence method, the Saville test is easier to set up. However, the lower detection limit for the Saville test is around 100 nM [Huang *et al.* 2007], while the chemiluminescence method can detect to as low as 1 nM [Jobgen *et al.* 2007]. The mechanism of the Saville test is described by Equations 4.12 through Eq. 4.14 [Stamler and Feelisch 1996].

$$RSNO + Hg^{2+} + H_2O \rightarrow HONO + RS\text{-}Hg^{+} + H^{+} \tag{4.12}$$

$$HONO + ArNH_2 + H^{+} \rightarrow ArN^{+} \equiv N + 2H_2O \tag{4.13}$$

$$Ar^{'} + ArN^{+} \equiv N \rightarrow Ar\text{-}N{=}N\text{-}Ar^{'} \tag{4.14}$$

Briefly, NO_2^- alone or NO_2^- released from S-nitrosothiols (due to decomposition catalyzed by Hg^{2+}) react with sulphanilamide (aromatic amine, Ar) to yield the corresponding diazonium salt which couples with N-1-naphthylethylenediamine (second aromatic amine, Ar') to form an intensely colored azo dye for colorimetric assay at OD_{540}.

The detailed experimental procedure is as follows. 50 μL to 100 μL samples were added into a well in a 96-well microplate, then equal volumes of Saville solution A (1% sulfanilamide in 0.5M HCl) to detect NO_2^- or Saville solution B (Saville A with 0.2% $HgCl_2$) to detect total nitrite (S-nitrosothiol + NO_2^-) were added to the well. The plate was maintained at room temperature for 5 min in order to complete the diazonium formation (Equation 4.13). Finally, equal volumes of Saville C (0.02% N-1-naphthylethylenediamine in 0.5M HCl) were added into the well. After 5 min, the mixture was measured by a Packard® SpectraCount™ Microplate Photometer (BS10000, Packard Instrument Co., Meriden, IL) at 540 nm wavelength. The RSNO concentration was obtained by subtracting the NO_2^- concentration from the total nitrite concentration. 20 μM $NaNO_2$ was made freshly for the standard. By comparing the OD_{540} reading from the samples to the one from standard $NaNO_2$ solution, the total nitrite concentration or the free nitrite concentrations in the samples were calculated.

4.2.7 Cysteine Self-oxidation Assay by Ellman's Method

Ellman's assay [Jocelyn 1987] was used to test the cysteine self-oxidation test in the solution without transnitrosation. Briefly, 25 μM cysteine solution was freshly prepared using 50 mM low purity NaH_2PO_4-Na_2HPO_4 (pH=7.4) buffer or deionized water and then 4 mL of cysteine solution was added into a 4 mL amber vial. One group of the vials was maintained on the hand motion shaker at room temperature while the

other one was maintained at 4ºC. Also, one group of vials with 25 μM cysteine was prepared using 50 mM NaH_2PO_4-Na_2HPO_4 and 50 μM AA and this one was also maintained on the hand motion shaker at room temperature. At specific time intervals, 50 μL samples were drawn from each vial and mixed with 50 μL Ellman's reagent in a 96-well microplate for 5 minutes and then measured at 410 nm using a Packard® SpectraCount™ Microplate Photometer (BS10000, Packard Instrument Co., Meriden, IL). A 25 μM cysteine in deionized water was made freshly as the standard. By comparing the OD_{410} reading from the samples to the one from standard CySH solution, the CySH concentrations in the samples were calculated.

Ellman's reagent was made by dissolving DTNB (final concentration 5mM) in a 100 mM NaH_2PO_4-Na_2HPO_4 solution (pH 7.2) with 0.1 mM EDTA. This solution is stable for greater than 2 months if stored in the dark between 0-5°C [Sigma-Aldrich 2002].

4.3 Results

4.3.1 BSANO Nitrosation and Separation Test

Figure 4.2 shows the concentration of free nitrite (NO_2^-), total nitrite (BSANO + NO_2^-), and BSANO in the filtrate and the unfiltered sample following utilization of the microcentrifuge tube. As previously mentioned, the BSANO concentration was calculated according to:

$$[BSANO] = [Total\ nitrite] - [Free\ nitrite] \tag{4.15}$$

Since the solution prior to separation was not treated by acidic ammonium sulfamate to quench NO_2^-, and the NO_2^- was slightly in excess, some free NO_2^- was detected as

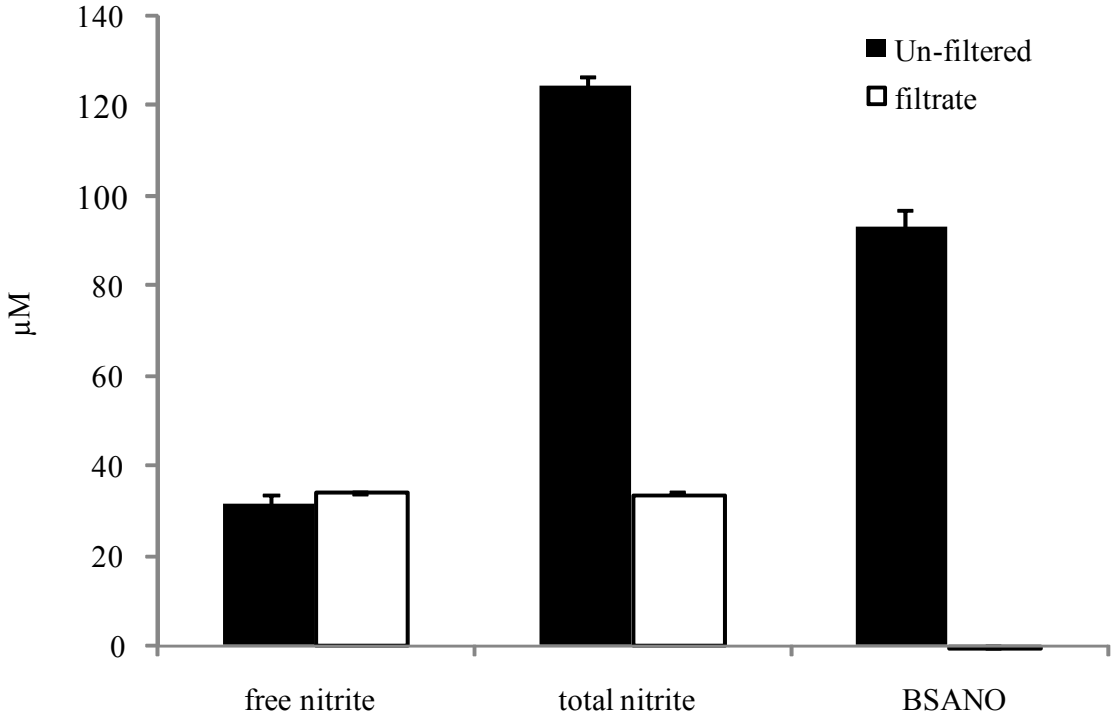

Figure 4.2 Results for microcentrifuge filter analysis. The BSANO concentration is calculated by subtracting the free nitrite data from the total nitrite data. (n=2)

expected. This NO_2^- concentration remained virtually the same in both the filtrate and un-filtered samples, indicating that NO_2^- is not separated but is equally distributed in both the filtrate and retentate. BSANO only existed in the un-filtered sample, indicating that BSANO cannot penetrate through the filter. The molecular weight (MW) cut-off of the filter is 10k Da which is much less than the MW of BSA/BSANO (66.43k Da).

Another important piece of information given by this result is that the measured BSANO concentration was around 93 μM. Based on this value and comparison with the maximum BSANO that could be made (176 μM BSA was nitrosated), the BSANO yield per mol of BSA was calculated as 0.53, which is consistent with the literature value of 0.6 [Zhang and Means 1996]. This incomplete nitrosation is due to the fact that 35–40% of the BSA is in the disulfide form [Carter and Ho 1994]. On the other hand, the measured total nitrite (BSANO + NO_2^-) was around 124 μM, which is about 97% of the moles of $NaNO_2$ added, indicating that most of the original nitrite was accounted for in either BSANO or excess nitrite (negligible N-nitrosation products formed). The 3% that was unaccounted for is probably due to the HNO_2 breaking down and forming NO, which quickly escapes from the solution into the headspace during nitrosation.

4.3.2 Transnitrosation Kinetics

The time profiles of the BSANO and CySNO concentrations during transnitrosation, with or without AA at various concentrations, are shown in Figures 4.3 through Figure 4.7. By fitting the BSANO self-decomposition (no CySH present) to a first-order kinetic model (exponential decay) according to:

$$\frac{d[BSANO]}{dt} = -k_{db}[BSANO] \tag{4.16}$$

Figure 4.3 BSANO and CySNO concentration time profiles following the initiation of transnitrosation. (n=2) Initial conditions were 102 μM BSANO and 50 μM CySH without ascorbic acid. The solid line and the exponential equation represents first order self-decomposition model described by Equation 4.16.

the BSANO self-decomposition rate constant, k_{db}, can be evaluated. The associated k_{db} is shown in each of the figures. In Figure 4.3, in the absence of ascorbic acid, BSANO is very stable even in the low purity phosphate buffer. There is virtually no BSANO decomposition within 24 hours. The k_{db} value in the absence of AA is 0.002 hr^{-1}. In the presence of AA, k_{db} values ranged from 0.008 to 0.011 hr^{-1} (see Figures 4.4-4.7). In general, the results indicate that BSANO is relatively stable during the transnitrosation studies. Its self-decomposition rate did not appear to depend on the AA concentration, although the rate was relatively faster in the presence of AA as compared to no AA, possibly due to the fact that more reduced copper/iron is generated by AA and can catalyze BSANO decomposition [Smith and Dasgupta 2000].

When CySH was added to the BSANO solution, the BSANO concentration dropped drastically within 1 hour for all the experiments (with or without AA), indicating a very fast forward transnitrosation reaction. This was confirmed from the CySNO data which showed a rapid increase of CySNO during the first hour. In the absence of AA, the BSANO decrease was initially rapid and then essentially leveled off. In the presence of AA, the BSANO decrease was also initially rapid and then the decrease continued, with the decrease going faster with increasing AA concentration. Table 4.2 summarizes this aspect, showing the percentage of BSANO lost after 10 min and 4 hours as a function of the AA concentration. The data for 50 μM and 500 μM are not included because the starting BSANO concentration is much lower than the others due to a different dilution method mentioned earlier in Section 4.2.2.

As for the amount of NO transferred from BSANO to CysH, the studies without AA showed that approximately 30 μM NO was transferred within 15 minutes from

Table 4.2 Percentage of BSANO transnitrosated after 10 min or 4 hours with different ascorbic acid concentrations (0 to 198 μM).

Ascorbic Acid Conc. / Reaction Time	0 μM	20 μM	148 μM	198 μM
10 min	33%	36%	49%*	46%*
4 hours	36%	52%	94%	98%

Note: *Data were acquired after 15 min.

Figure 4.4 BSANO and CySNO concentration time profiles following the initiation of transnitrosation. (n=2) Initial conditions were 88μM BSANO and 50 μM CySH with (circle) or without 20μM (triangle) ascorbic acid. The solid line and the exponential equation represents first order self-decomposition model described by Equation 4.16.

Figure 4.5 BSANO and CySNO concentration time profiles following the initiation of transnitrosation. (n=2) Initial conditions were 88μM BSANO and 50 μM CySH with 150 μM (square) or 200 μM (circle) ascorbic acid. The solid line and the exponential equation represents first order self-decomposition model described by Equation 4.16.

Figure 4.6 BSANO and CySNO concentration time profiles following the initiation of transnitrosation. (n=2) Initial conditions were 62.27 μM BSANO and 50 μM CySH with 50 μM (circle) or 500 μM (triangle) ascorbic acid. The solid line and the exponential equation represents first order self-decomposition model described by Equation 4.16.

Figure 4.7 BSANO and CySNO concentration time profiles following the initiation of transnitrosation. (n=2) Initial conditions were 116.5 μM BSANO and 25 μM CySH with 200 μM (triangle) ascorbic acid. The solid line and the exponential equation represents first order self-decomposition model described by Equation 4.16.

BSANO to cysteine (in the form of CySNO) while the BSANO concentration decreased by approximately 30 μM (Figure 4.3 & 4.4). However, essentially no additional NO was transferred during the remainder of the experiment. Since the initial CySH was 50 μM, the amount of NO transferred was less than the initial CySH added, suggesting that CySH was not continually involved in transnitrosation. One possible explanation is that cysteine was oxidized by the oxygen in the solution with the help of metal ions [Bagiyan *et al.* 2003; Bagiyan *et al.* 2004]. Thus, there was a point where no more transnitrosation could occur since all of the CySH became oxidized.

In order to study the kinetics of cysteine autoxidation, an experiment for cysteine oxidation in buffer was conducted. The results are shown in Figure 4.8. It is evident that increasing temperature can accelerate this oxidation process and the decomposition appears to be a zero order reaction, which is consistent with literature [Ehrenberg *et al.* 1989; Bagiyan *et al.* 2004]. The zero order reaction rate constant, k_{oo}, was calculated by a linear fit of the data. Thus, at 25 ºC, in 50 mM low purity NaH_2PO_4-Na_2HPO_4, pH=7.4 buffer, the zero order decomposition rate constant was 0.7103 $\mu M \cdot hr^{-1}$. This result also showed that 50 μM AA cannot stop this self-oxidation at all. This can be explained by the redox potential of dehydroascorbic acid/ascorbic acid (58 mV) is much higher than cystine/cysteine (-340 mV) [Fasman 1976] which means that AA cannot reduce cystine to form cysteine spontaneously.

For the transnitrosation studies with AA, more than 50 μM of NO was transferred depending on the concentration of the AA in the solution (Figures 4.4-4.6). Since the initial CySH was 50 μM, this showed that more NO was transferred than the initial amount of CySH. Thus, CySH oxidation did not completely occur following

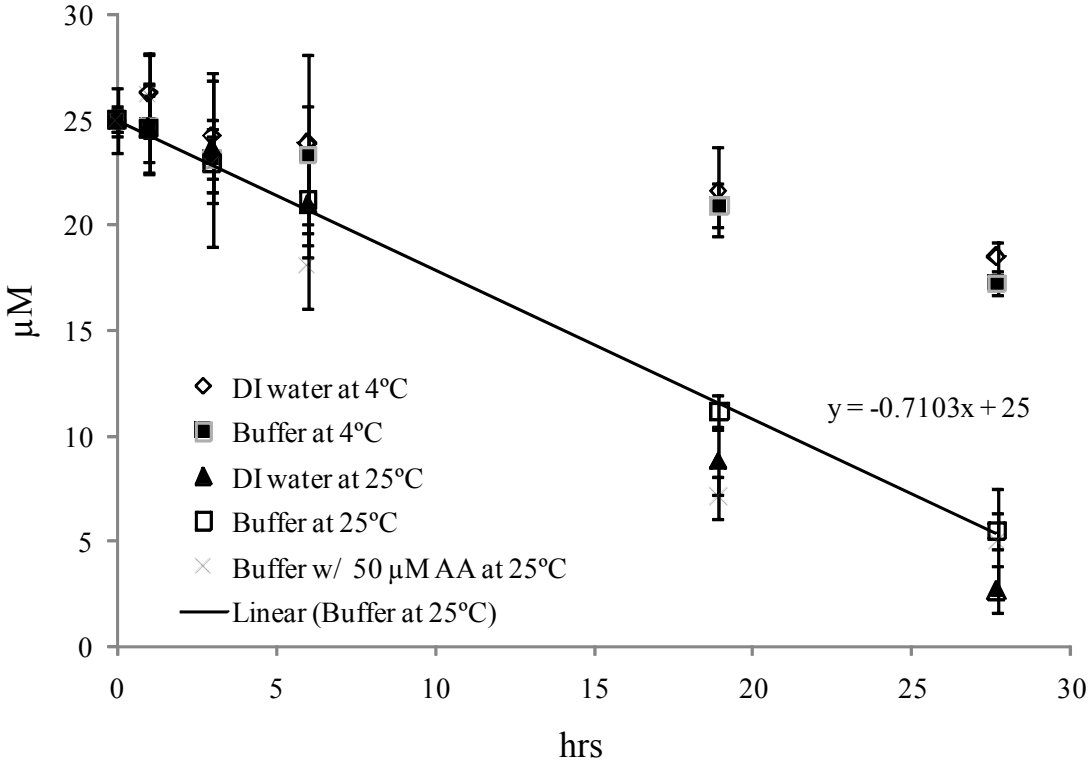

Figure 4.8 Cysteine self-oxidation in buffers (50 mM low purity NaH_2PO_4-Na_2HPO_4, pH=7.4) and deionized water at 4 ºC and 25 ºC. (n=2) Initial cysteine concentration was 25 µM. Open diamond: in deionized water at 4 ºC. Solid square: in buffer at 4 º C. Solid triangle: in deionized water at 25 ºC. Open square: in buffer at 25 ºC. Cross: in buffer with 50 µM ascorbic acid at 25 ºC. The solid line and the linear equation represents zero order autoxidation model reported earlier [Ehrenberg *et al*. 1989; Bagiyan *et al*. 2004].

transnitrosation and NO release, such that CySH could be regenerated during the transnitrosation process. Also CySH autoxidatioin might not be significant in this time frame because transnitrosation was completed within a few hours, whereas it takes more than 28 hours for 25 μM CySH to be fully oxidized as shown in Figure 4.8.

In order to further test the AA effect on the transnitrosation reaction, a study using less initial CySH (25 μM, compared to 50 μM previously) and 200 μM ascorbic acid was performed. In Figure 4.7, approximately 60 μM NO was transferred from BSANO, more than twice the initial amount of CySH. However, the transfer rate started to decrease after a few hours, indicating that CySH autoxidation eventually consumes most of the CySH after about 4 hours, thus no CySH is available for transnitrosation. Additionally, the CySNO concentration dropped to almost zero at approximately 4 hours, which also confirms that transnitrosation essentially stopped.

4.3.3 Transnitrosation/Decomposition Reactions and Modeling Setup

As discussed earlier (see Equations 4.2 & 4.3), the main reactions involved in transnitrosation and decomposition are:

$$BSANO + CyS^- \underset{k_r}{\overset{k_f}{\rightleftharpoons}} CySNO + BSA^- \tag{4.17}$$

$$BSANO + Cu^+ \xrightarrow{k_{db}} BSA^- + NO + Cu^{2+} \tag{4.18}$$

$$Cu^+ + CySNO \xrightarrow{k_{dc}} CyS^- + Cu^{2+} + NO \tag{4.19}$$

Since CyS^- is important in the transnitrosation reaction, it is important to understand the fate of CyS^-, which can be complicated due to various environmental conditions.

If there is no reducing agent, such as AA, Cu^{2+} in solution (which can initially be present or be formed according to Equation 4.19) can oxidize thiol anions to form a disulfide bond and generate Cu^{+} according to [Smith and Dasgupta 2000]:

$$Cu^{2+} + CyS^{-} \xrightarrow{k_{oc}} \frac{1}{2} CyS\text{-}CyS + Cu^{+} \tag{4.20}$$

This disulfide cysteine (CyS-CyS) is stable and would thus reduce the CyS^{-} available for transnitrosation. This is likely what happened in the studies without AA where transnitrosation stopped occurring. If a reducing agent is present, the reducing agent can suppress the available Cu^{2+}, keeping the thiol anion in the reduced form and minimizing the formation of disulfide bonds. For example, AA can react with Cu^{2+} (including Cu^{2+} generated from Equation 4.19) and form dehydroascorbic acid (DHA) and Cu^{+} [Holmes and Williams 2000; Smith and Dasgupta 2000; Aquart and Dasgupta 2004]:

$$AA + Cu^{2+} \xrightarrow{k_{oa}} Cu^{+} + DHA \tag{4.21}$$

Thus, reducing agents can allow for the continual progression of transnitrosation by inhibiting the formation of disulfide bonds. However, AA itself can react directly with CySNO, causing CySNO decomposition and the associated release of NO without the dependence on copper [Holmes and Williams 2000]. The reaction is

$$AA + CySNO \xrightarrow{k_{da}} CyS^{-} + NO + DHA \tag{4.22}$$

Finally, CySH can also be oxidized by molecular oxygen (autoxidation) in a solution containing Cu^{+} according to [Ehrenberg *et al.* 1989]:

$$4CySH + O_2 \xrightarrow[Cu^{+}]{koo} 2CyS\text{-}CyS + 2H_2O \tag{4.23}$$

The value of k_{oo} measured for this work was previously shown in Section 4.3.2.

As shown in all transnitrosation results (Figure 4.3-4.7), the BSANO self-decomposition (Equation 4.18) is extremely slow and can likely be neglected compared to the transnitrosation reactions that diminish the BSANO concentration. The CySNO decomposition reactions in which NO is released (Equations 4.19 and 4.22) are the key reactions that drive the transnitrosation (Equation 4.17) towards the right hand side and keep equilibrium from being established.

Though thiol anions are the actual reactants or products in the above reactions, the rate of reaction can still be written in the form of the total thiol concentration in the solution based on a rapid equilibrium assumption where:

$$CySH \xrightleftharpoons{K_{a,C}} CySH^- + H^+ \tag{4.24}$$

such that,

$$K_{a,C} = \frac{[CyS^-][H^+]}{[CySH]} \tag{4.25}$$

At a certain pH:

$$[CySH] = \frac{10^{-pH} \cdot [CyS^-]}{K_{a,C}} \tag{4.26}$$

Thus,

$$[CySH]_T = \frac{(10^{-pH} + K_{a,C}) \cdot [CyS^-]}{K_{a,C}} = K_C \cdot [CyS^-] \tag{4.27}$$

where $[CySH]_T$ denotes the total cysteine which includes both [CySH] and $[CyS^-]$. Assuming that Equation 4.24 is always at equilibrium (fast equilibrium), any concentration change in the CyS^- will result in a proportional change in the total CySH. Thus, all reaction rate equations involving CyS^- can be written in the form of total

Cysteine, although the rate constant used in a reaction would include the term K_C shown in Equation 4.27. A similar situation can also apply to BSA.

From the reactions given above, the mass balance for all species, assuming a well-mixed system, can be written as follows:

$$\frac{d[BSANO]}{dt} = -k_f[BSANO][CySH]_T + k_r[CySNO][BSA]_T - k_{db}[BSANO] \tag{4.28}$$

$$\frac{d[CySNO]}{dt} = -k_{dc}[CySNO] - k_{da}[AA][CySNO] - k_r[CySNO][BSA]_T + k_f[CySH]_T[BSANO] \tag{4.29}$$

$$\frac{d[BSA]}{dt} = k_f[BSANO][CySH]_T - k_r[CySNO][BSA]_T + k_{db}[BSANO] \tag{4.30}$$

$$\frac{d[CySH]}{dt} = k_r[CySNO][BSA]_T - k_f[CySH]_T[BSANO] - k_{oo} - k_{oc}[CySH]_T + k_{da}[AA][CySNO] + k_{dc}[CySNO] \tag{4.31}$$

$$\frac{d[AA]}{dt} = -k_{da}[AA][CySNO] - k_{oa}[AA] \tag{4.32}$$

The above equations assume that Cu^{2+} and Cu^{+} remain at constant values. Since the total copper concentration is very low compared to the other species in the system, and both copper species are constantly being consumed and regenerated, the change in the copper concentration of both species was assumed to be negligible. Therefore, k_{dc}, k_{oc}, and k_{oa} are actually pseudo rate constants which include the Cu^{2+} or Cu^{+} concentrations.

4.3.4 Determination of Rate Parameters

From the above equations, there are a total of eight kinetic parameters:

- RSNO decomposition: k_{da}, k_{dc}, k_{db}
- Transnitrosation: k_f, k_r

- CySH and ascorbic acid oxidation: k_{oo}, k_{oc}, k_{oa}

Rate constants, k_{db} and k_{oo} were measured from experimental studies shown in Section 4.3.2. The value of k_{da} has previously been studied with a predicted value of 0.00094 hr^{-1} [Holmes and Williams 2000]. Although k_{dc} has been measured and reported in Chapter 3, different AA concentrations will affect the Cu^{+} and Cu^{2+} due to the reaction shown in Equation 4.21. Therefore, the value from Chapter 3 cannot be used. Based on the above analysis, there are five rate parameters left that needed to be determined from the experimental data.

In order to determine the above kinetic rate constants, Scientist 3.0 (Micromath, Saint Louis, MO) was initially used to fit the experiment data of Figures 4.3 to 4.7 to the ordinary differential equations (ODEs; Equations 4.28-4.32). A least square fit algorithm was used during the fitting. However, since there are five unknown parameters, some experimental results did not have enough data points for fitting (less than five) since BSANO disappeared completely within a few hours (see Figure 4.5). Thus, in order to reduce the number of kinetics parameters for fitting, a parameter sensitivity analysis was performed to find out if there were any parameters that could be considered negligible. MathCAD (PTC, Needham MA) was used to solve the ODEs numerically to simulate the BSANO concentration profile.

The base case for the parameter sensitivity analysis assumed an initial condition of 116.48 μM BSANO, 200 μM AA and 25 μM CySH. The following base-case kinetic rate constants were obtained using the previously determined values of k_{db} and k_{oo}, the reported value of k_{da} noted above, and a least square fit of the 25 μM CySH + 116.48 μM BSANO +200 μM AA study. The base-case values are:

$$k_f = 0.2\mu M^{-1} \cdot hr^{-1}$$
$$k_r = 0.8\mu M^{-1} \cdot hr^{-1}$$
$$k_{db} = 0.008 hr^{-1}$$
$$k_{dc} = 0.4 hr^{-1}$$
$$k_{oo} = 0.71\mu M \cdot hr^{-1}$$
$$k_{oc} = 0.1 hr^{-1}$$
$$k_{oa} = 0.2 hr^{-1}$$
$$k_{da} = 0.005\mu M^{-1} \cdot hr^{-1}$$

Through changing the kinetic parameters by plus or minus 10 fold and plotting the BSANO concentration profile, the model sensitivity level regarding each parameter was determined. The results are shown in Figures 4.9 through 4.13. These figures also include the base-case experimental data and the associated fit. According to the figures, a changing k_{oa} had the least effect on the BSANO concentration profile. Thus, the potential for neglecting the reaction incorporating this parameter (Equation 4.21) was considered based on the additional analysis shown below.

The detailed kinetics of ascorbic acid oxidation by copper (Equation 4.21) has been established earlier as follows [Hayakawa *et al.* 1973]:

$$-\frac{d[AA^-]}{dt} = k_1[Cu^{2+}]^2[AA^-] + k_2[Cu^{2+}]^2[AA^{2-}] \tag{4.33}$$

where k_1=3.1×10^4 M^{-2}s^{-1} and k_2=6.1×10^{10} M^{-2}s^{-1}. AA^- and AA^{2-} are different dissociated forms of AA according to:

$$AA \xleftrightarrow{K_1} AA^- + H^+ \tag{4.34}$$

$$AA^- \xleftrightarrow{K_2} AA^{2-} + H^+ \tag{4.35}$$

From the AA pK_a values (pK_1=4.04 and pK_2=11.34) and assuming fast equilibrium, the following results can be calculated (at pH=7.4):

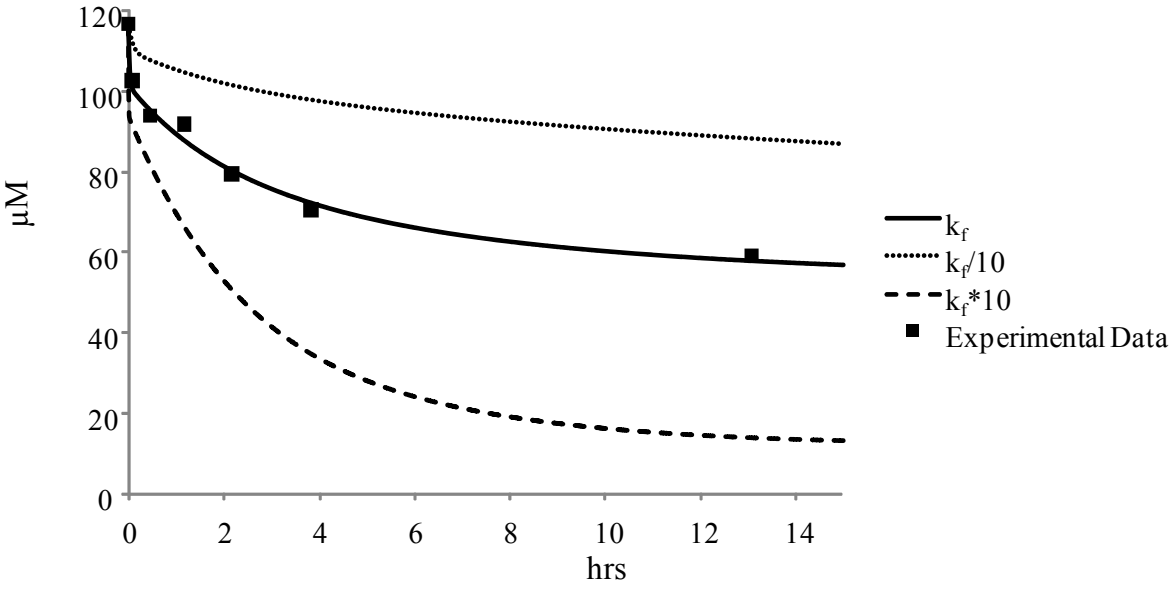

Figure 4.9 Simulated BSANO concentration profiles using the base-case kinetic parameters along with variations in the k_f parameter. The transnitrosation experimental data for the base-case scenario is also shown (solid squares).

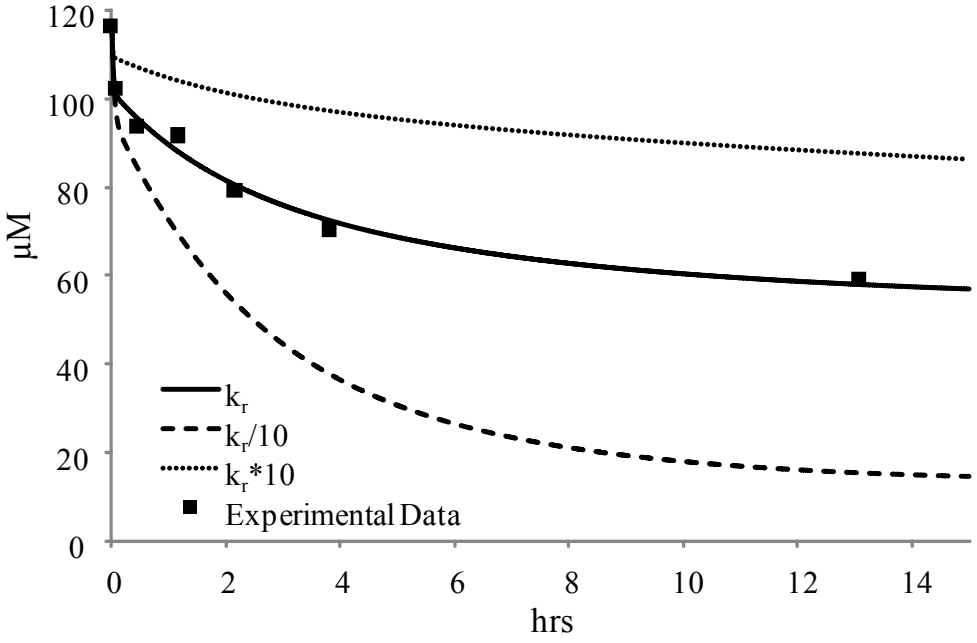

Figure 4.10 Simulated BSANO concentration profiles using the base-case kinetic parameters along with variations in the k_r parameter. The transnitrosation experimental data for the base-case scenario is also shown (solid squares).

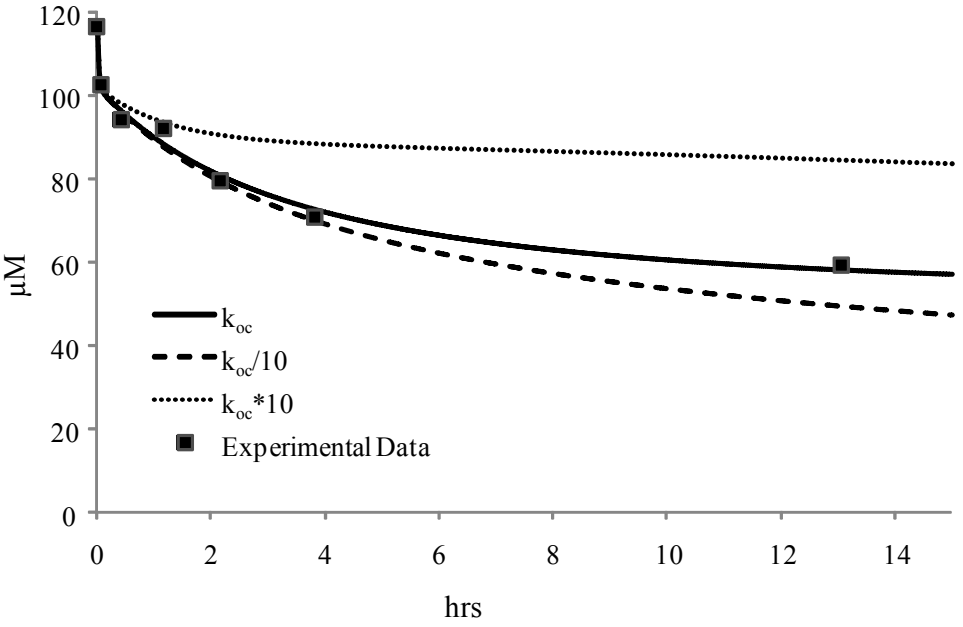

Figure 4.11 Simulated BSANO concentration profiles using the base-case kinetic parameters along with variations in the k_{oc} parameter. The transnitrosation experimental data for the base-case scenario is also shown (solid squares).

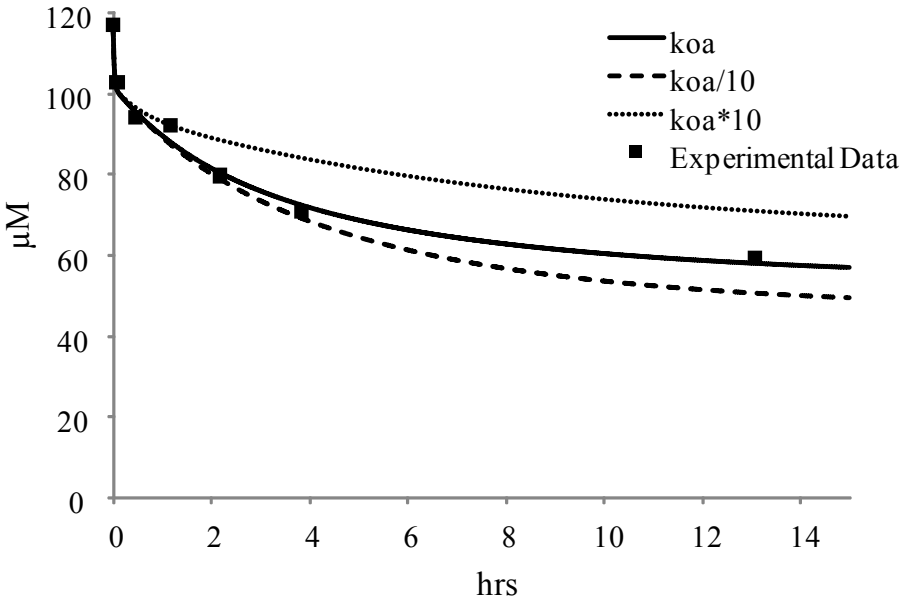

Figure 4.12 Simulated BSANO concentration profiles using the base-case kinetic parameters along with variations in the k_{oa} parameter. The transnitrosation experimental data for the base-case scenario is also shown (solid squares).

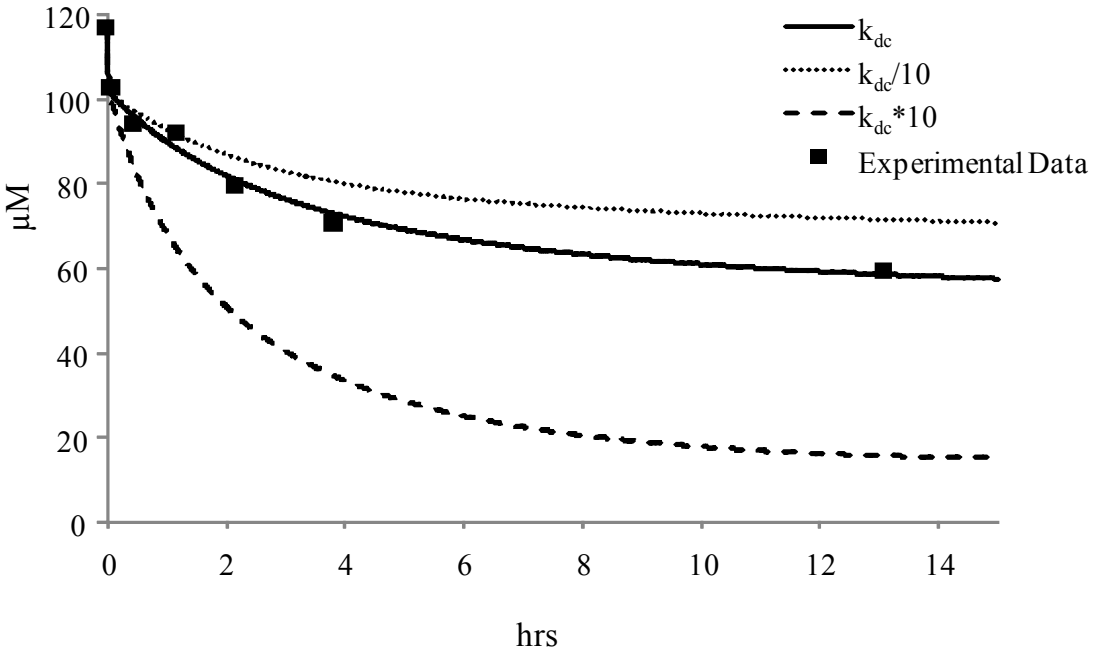

Figure 4.13 Simulated BSANO concentration profiles using the base-case kinetic parameters along with variations in the k_{dc} parameter. The transnitrosation experimental data for the base-case scenario is also shown (solid squares).

$$[AA^-]=2290[AA] \quad (4.36)$$

$$[AA^{2-}]=0.2630[AA] \quad (4.37)$$

Plugging Equations 4.36 and 4.37 into 4.33 gives:

$$-\frac{d[AA]}{dt} = k[Cu^{2+}]^2[AA] \quad (4.38)$$

where k=0.0253 $\mu M^{-2}hr^{-1}$. Comparison with Equation 4.32 in the absence of the CySNO decomposition term shows that k_{oa} is equivalent to $k[Cu^{2+}]^2$.

For a low-purity phosphate buffer which was used in the study, the total heavy metal ion contamination in the salts is around 0.001%wt (based on a Pb analysis) according to the product label. Although Fisher Scientific does not provide detailed compositions regarding the heavy metal content, a common list of heavy metals includes Ag, As, Bi, Cd, Cu, Hg, Mo, Pb, Sb, and Sn [Schmidt *et al.* 2005]. However, according to the Sigma-Aldrich product label, the total Cu is around 5.5%wt and7.7%wt of the total heavy metal ion contamination for high-purity Na_2HPO_4 and NaH_2PO_4 salts, respectively. Thus, in 50 mM low purity buffer (which contains approximately 11.50 g of Na_2HPO_4 and 2.62 g of NaH_2PO_4 in 1L of 100 mM buffer), the total copper concentration is calculated to be 0.067 μM if the same impurity levels as shown in high-purity phosphates salts is used. If all of this was Cu^{2+}, then the maximum value for k_{oa} would be 1.14×10^{-4} hr^{-1}. It is very likely that the maximum rate would be much lower if AA is present since AA would lead to most of the copper being in the form of Cu^+ instead of Cu^{2+}.

Comparing the maximum value of k_{oa} with k_{da}[CySNO], since both terms are shown in Equation 4.32 interacting with AA, provides valuable guidance as to whether k_{oa} can be neglected in the kinetic analysis. Since the CySNO concentration was often higher than 5 μM during the transnitrosation studies (unless BSANO was almost

consumed and transnitrosation almost halted as observed with high AA concentration studies), k_{da}[CySNO] would have a minimum value of 4.7 x 10^{-3} hr^{-1} based on the reported value of k_{da}=0.000941 $\mu M^{-1}hr^{-1}$ at the corresponding pH [Holmes and Williams 2000]. Thus, the maximum value of k_{oa} appears to be more than one order of magnitude smaller than the minimum value of k_{da}[CySNO]. Therefore, it was concluded that kinetics involving k_{oa} in Equation 4.32 could be considered negligible. This reduced the unknown kinetic parameters to four (k_f, k_r, k_{dc}, k_{oc}).

With the values of the four parameters as unknowns, all transnitrosation experimental data was fit to Equations 4.28-4.32 using Scientist 3.0. The best fit values for k_f and k_r are listed in Table 4.3. Figure 4.14 shows an example of the model fit for 50 μM CySH, 62.27 μMBSANO and 500 μM AA. The value of k_f ranged from 0.142 to 0.995 $\mu M^{-1}hr^{-1}$ with an average of 0.332 ± 0.272 $\mu M^{-1}hr^{-1}$. The value of k_r ranged from 0.164 to 0.822 $\mu M^{-1}hr^{-1}$ with an average of 0.504 ± 0.226 $\mu M^{-1}hr^{-1}$. As shown in Figure 4.15, k_f and k_r show no correlation with the AA concentration as expected.

Since k_f and k_r are supposed to be independent of the experiments, the average k_f and k_r were then used to again fit the experimental data to obtain values for k_{dc} and k_{oc}. These two parameters, with fitted values for all experiments shown in Table 4.4, should be functions of AA since they both are pseudo rate constants which include the Cu^{2+} or Cu^{+} concentrations affected by the amount of AA. As noted in the table, both the R^2 and correlation values are above 0.97 for the combined fitting of BSANO and CySNO data, indicating that the model fits the data quite well. The model predictions of BSANO and CySNO are shown for all sets of data in Figure 4.16 through 4.23. In summary, the values used for the model predictions are 0.332 $\mu M^{-1}hr^{-1}$ (average) for k_f, 0.504 $\mu M^{-1}hr^{-1}$

Table 4.3 Values of k_f and k_r for transnitrosation experiments in low purity phosphate buffer at pH=7.4 with different ascorbic acid concentrations.

Ascorbic Acid concentration (μM)	**0**		**20**	**50**		**148**	**198**	**200**	**500**	**Avg.**	**Stdv.**
	Run #1	**Run #2**		**Run #1**	**Run #2**						
k_f ($\mu M^{-1}hr^{-1}$)	0.235	0.229	0.142	0.995	0.362	0.484	0.200	0.160	0.179	0.332	0.272
k_r ($\mu M^{-1}hr^{-1}$)	0.548	0.308	0.164	0.706	0.822	0.485	0.234	0.595	0.678	0.504	0.226

Figure 4.14 Scientist 3.0 regression result graphic output for the transnitrosation with 500 μM AA and 50 μM CySH with initial BSANO concentration at 62.27 μM. The lines are the fitted model and the solid and open square markers are the experiment data for BSANO and CySNO concentration respectively.

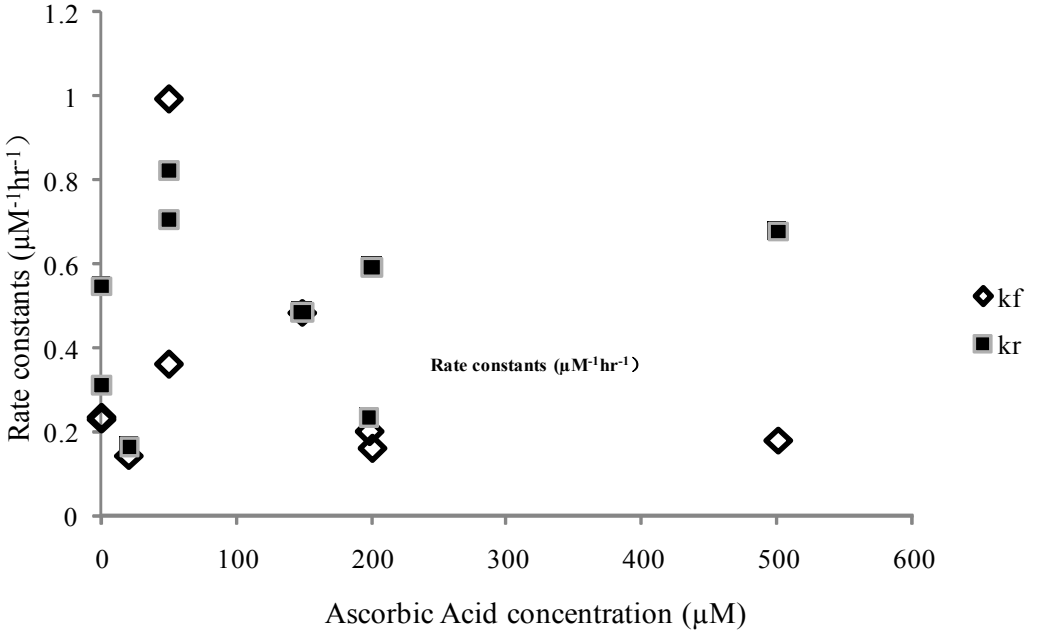

Figure 4.15 Result of data fitting for variable k_f (open diamond) and k_r (solid square) showed that there is no sign of correlation between the two constant and ascorbic acid concentration. Also, the range of the kinetic constant are within 0.1 to 0.7 $\mu M^{-1} hr^{-1}$, except a few outliers, which indicating a good consistency of the data fitting.

Table 4.4 Values of k_{dc} and k_{oc}, with fixed average k_f and k_r values (as shown in Table 4.3), for transnitrosation experiments in low purity phosphate buffer at pH=7.4 with different ascorbic acid concentrations.

Ascorbic Acid concentration (μM)	**0**		**20**	**50**		**148**	**198**	**200**	**500**
	Run #1	**Run #2**		**Run #1**	**Run #2**				
k_{dc} (hr^{-1})	0.225	0.207	0.423	3.07	1.729	2.775	3.031	0.957	6.596
k_{oc} (hr^{-1})	0.6192	0.4932	0.4868	0.3144	0.9042	0.319	0.1064	0.1522	0.0348
R^2	0.999	0.999	0.999	0.986	0.990	0.987	0.993	0.998	0.977
Correlation	0.999	0.998	0.998	0.990	0.990	0.990	0.995	0.999	0.985

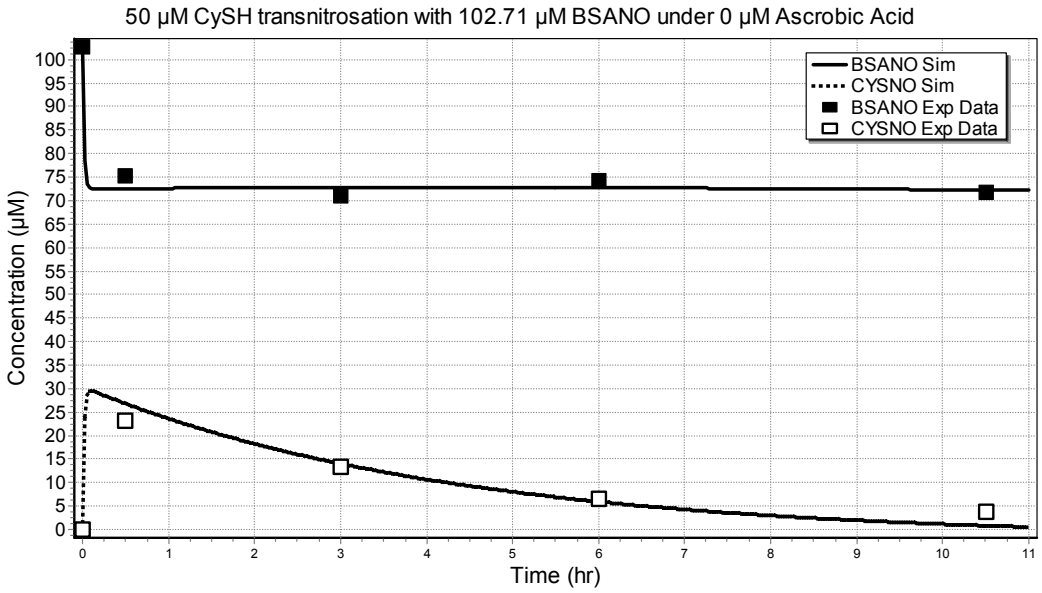

Figure 4.16 Scientist 3.0 regression result graphic output for the transnitrosation with 0 µM AA and 50 µM CySH (Run #1). The lines are the fitted model and the solid and open square markers are the experiment data for BSANO and CySNO concentration respectively.

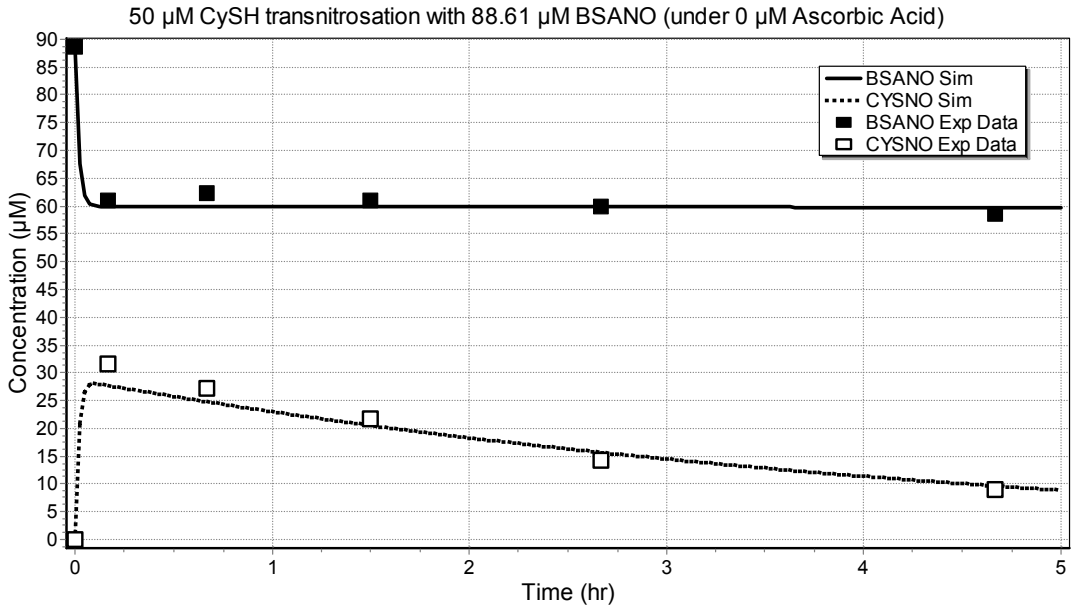

Figure 4.17 Scientist 3.0 regression result graphic output for the transnitrosation with 0 µM AA and 50 µM CySH (Run #2). The lines are the fitted model and the solid and open square markers are the experiment data for BSANO and CySNO concentration respectively.

Figure 4.18 Scientist 3.0 regression result graphic output for the transnitrosation with 50 μM AA and 50 μM CySH (Run #1). The lines are the fitted model and the solid and open square markers are the experiment data for BSANO and CySNO concentration respectively.

Figure 4.19 Scientist 3.0 regression result graphic output for the transnitrosation with 50 μM AA and 50 μM CySH (Run #2). The lines are the fitted model and the solid and open square markers are the experiment data for BSANO and CySNO concentration respectively.

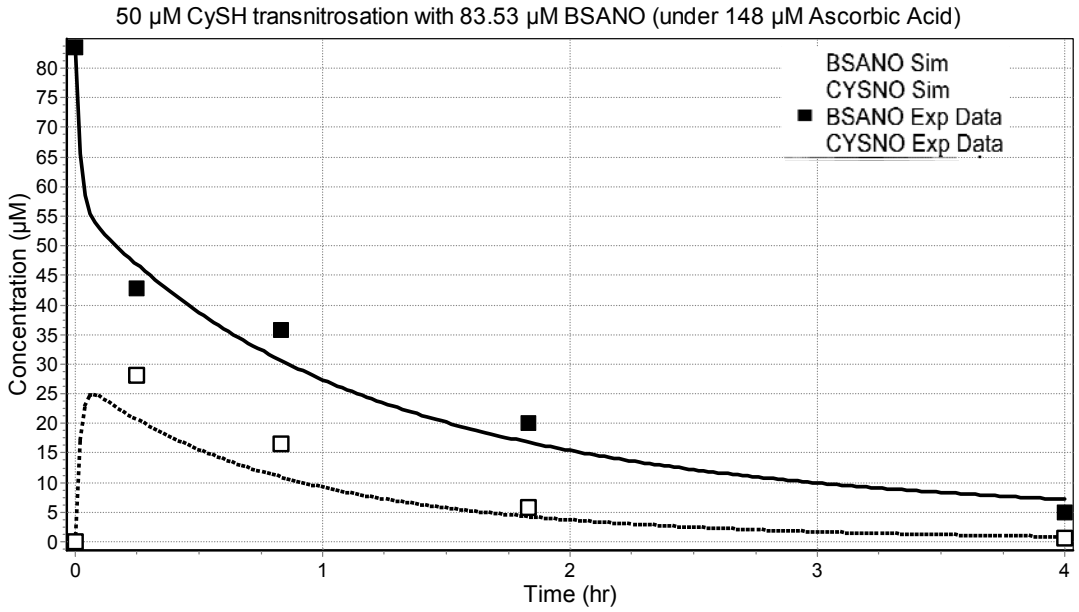

Figure 4.20 Scientist 3.0 regression result graphic output for the transnitrosation with 148 µM AA and 50 µM CySH. The lines are the fitted model and the solid and open square markers are the experiment data for BSANO and CySNO concentration respectively.

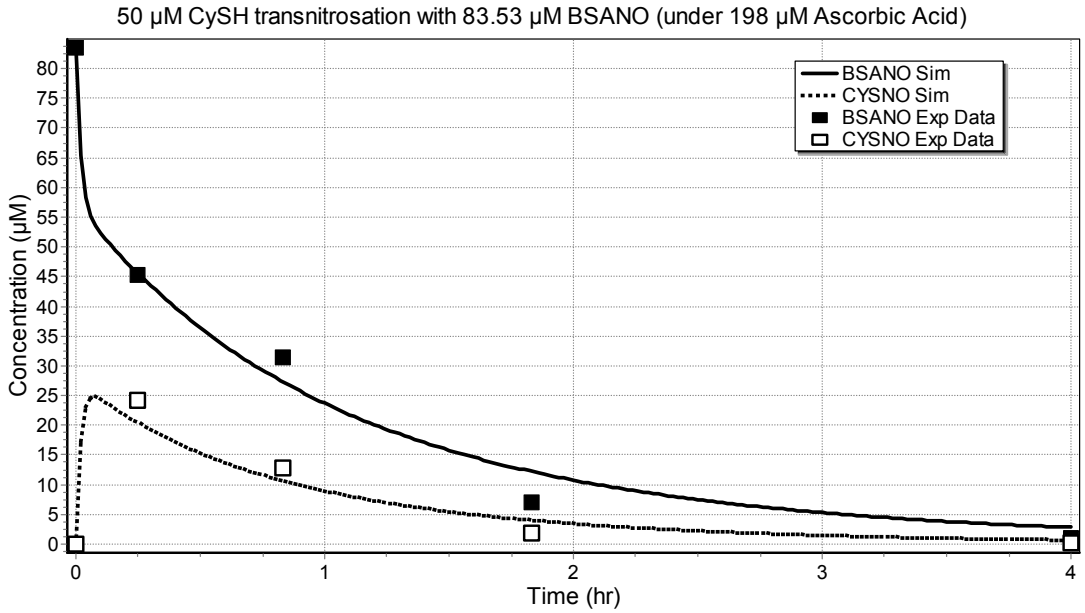

Figure 4.21 Scientist 3.0 regression result graphic output for the transnitrosation with 198 µM AA and 50 µM CySH. The lines are the fitted model and the solid and open square markers are the experiment data for BSANO and CySNO concentration respectively.

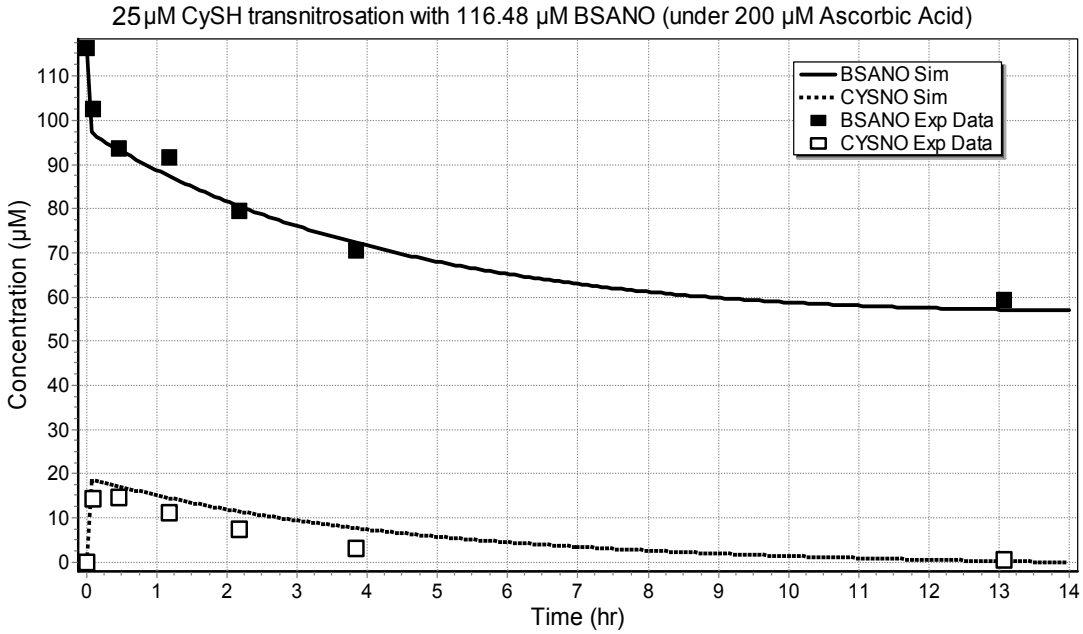

Figure 4.22 Scientist 3.0 regression result graphic output for the transnitrosation with 200 µM AA and 25 µM CySH. The lines are the fitted model and the solid and open square markers are the experiment data for BSANO and CySNO concentration respectively.

Figure 4.23 Scientist 3.0 regression result graphic output for the transnitrosation with 500 μM AA and 50 μM CySH. The lines are the fitted model and the solid and open square markers are the experiment data for BSANO and CySNO concentration respectively.

(average) for k_r, 0.00094 hr^{-1} for k_{da}, 0.002 to 0.011 hr^{-1} (the value determined for each experiment) for k_{db}, 0.7103 $\mu M \cdot hr^{-1}$ for k_{oo}, and the fitted parameters for k_{dc} and k_{oc}. As previously noted, the reaction involving k_{oa} was assumed negligible.

Further analysis of k_{dc} and k_{oc} with regards to the AA concentration is shown in Figures 4.24 and 4.25, respectively. Figure 4.24 shows a general trend (with the exception of a few outliers) in which k_{dc} increases as the AA concentration increases. Since k_{dc} is a pseudo parameter that includes the Cu^+ concentration, this trend is consistent since AA contributes to the conversion of Cu^{2+} to Cu^+. Figure 4.25 shows a general trend (with the exception of a few outliers) in which k_{oc} decreases as the AA concentration increases. Since k_{oc} is a pseudo parameter that includes the Cu^{2+} concentration, this trend is consistent since AA contributes to the conversion of Cu^{2+} to Cu^+.

4.4 Discussion

Two methods for detecting NO_2^- or S-nitrosothiols were evaluated in this chapter, namely the Saville method and the Chemiluminescence method. Both techniques are robust as they usually give very small standard error. However, the Saville test is not as sensitive as the chemiluminescence method as described earlier and it also has the potential for interference problems with low molecular weight S-nitrosothiol detection [Tashimo *et al.* 2003]. Thus, it should only be used when a quick and semi-quantitive analysis is needed.

The transnitrosation results showed that transnitrosation is not as simple as previously thought, especially when there is ascorbic acid present. The key reactant of

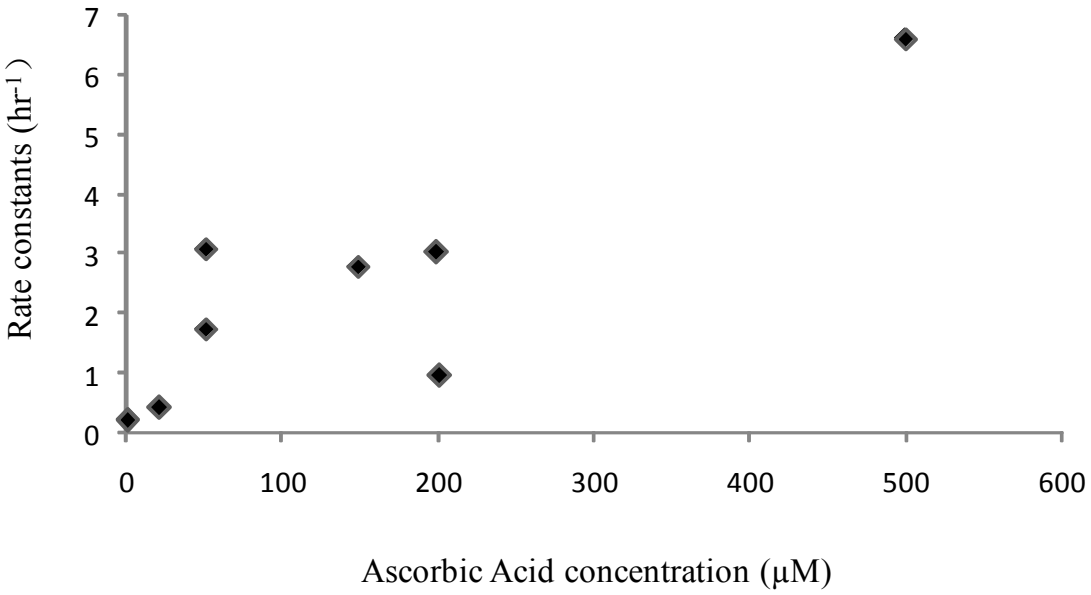

Figure 4.24 Result of data fitting for CySNO decomposition kinetic parameter k_{dc} versus ascorbic concentration (with fixed transnitrosation kinetic parameter k_f and k_r).

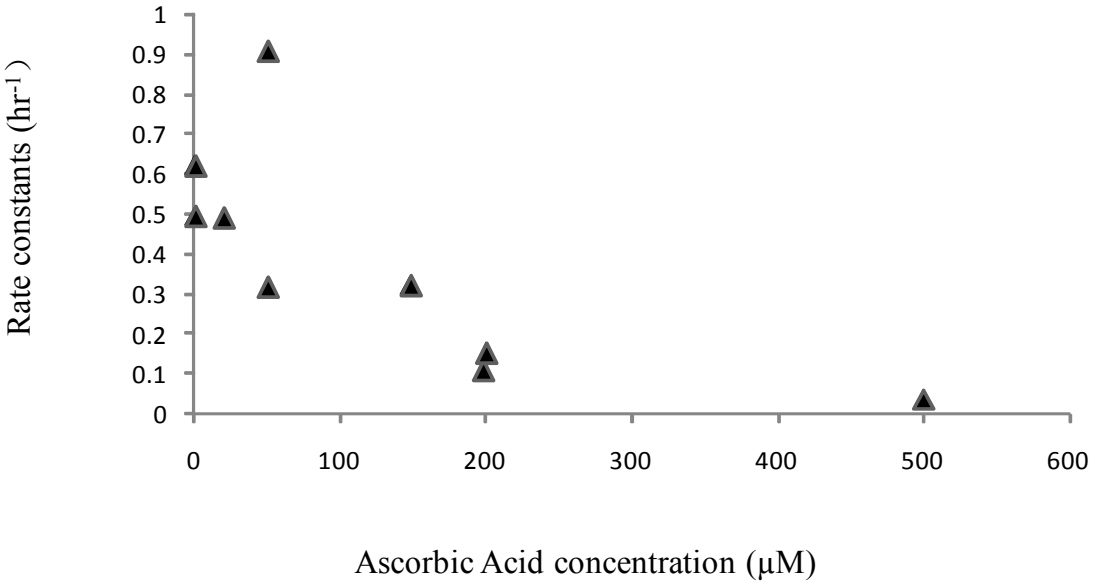

Figure 4.25 Result of data fitting for CySH oxidation (by copper ion) kinetic parameter k_{oc} versus ascorbic concentration (with fixed transnitrosation kinetic parameter k_f and k_r).

transnitrosation, CySH, can be affected by various reductants or oxidants, thus changing the kinetics drastically. Oxygen is one of the key oxidants that oxidizes CySH and makes it less effective for transnitrosation. Since in this work all reactions were performed in aerobic conditions, the experimental results showed that transnitrosation was affected by CySH oxidation. In physiological conditions, it is possible that this autoxidation might be counter played by various reducing agents in the blood such as glutathione [Flagg *et al.* 1993; Guan *et al.* 2003]. On the other hand, although the kinetic study showed zero order for the CySH autoxidation, it is feasible that a lower oxygen concentration can result in different kinetics. Ehrenberg *et al.* found that the oxygen pressure did affect the pseudo zero order rate constant [Ehrenberg *et al.* 1989]. In blood vessels, the oxygen partial pressure (95 mmHg) [Martin 1999] is much lower than the atmosphere oxygen partial pressure (159.6 mmHg), thus the autoxidation rate can also be reduced and more cysteine can be kept in the reduced form. Copper is another oxidant that plays an important role during the CySNO decomposition. As Cu^{+} needs to be regenerated to cause decomposition of CySNO, two reactions (reaction 4.20 and 4.21) compete with each other to scavenge Cu^{2+} and convert it back to Cu^{+}. When the ascorbic acid concentration is high, more CySH can be saved from oxidization by Cu^{2+}, thus more BSANO will be transnitrosated with CySH. This effect was shown by the decrease of the k_{oc} value with increasing concentration of ascorbic acid as shown in Figure 4.25. On the other hand, as Cu^{2+} decreases, Cu^{+} increases which causes an increase in k_{dc} as shown in Figure 4.24. However, the k_{dc} value at 0 μM ascorbic acid concentration during transnitrosation (~0.2 hr^{-1}) is much lower than the result from Chapter 3 (~7.2 hr^{-1}) which measured k_{dc} in the absence of transnitrosation (no BSANO present). As noted

previously, k_{dc} is a pseudo rate constant which includes the Cu^{+} concentration. In the presence of BSA, it has been shown that BSA can chelate the copper ion [Dicks and Williams 1996]. Therefore, in the presence of BSA, the k_{dc} value should be smaller than in the absence of BSA.

From a modeling standpoint, the high correlation value calculated from least square fitting at all ascorbic concentrations indicated that the model described the transnitrosation mechanism quite well. However, compared to the k_f and k_r values reported in literature for transnitrosation involving CySH (see Table 4.1), the values reported in this work are at least an order of magnitude higher due to unknown reasons. However, the calculated equilibrium transnitrosation constant $K=k_f/k_r$ obtained in this work (0.657) is similar to the literature value of HSANO and CySH transnitrosation (0.75) as shown in Table 4.1.

It should be noted that the model was based on the assumption that the Cu^{+}/Cu^{2+} ratio remained constant during the reaction. This requires that the ascorbic acid concentration remains virtually stable during the reaction because AA can react with Cu^{2+} to form Cu^{+} as showed in Equation 4.21. In order assess this aspect, a simulation for the AA concentration for 25 μM CySH, 200 μM AA and 116.48 μM BSANO was performed. The result showed that the AA concentration decreased less than 5% within 15 hours (graph not shown), thus demonstrating that the AA was essentially constant for the timeframe of modeling. However, it would be better to experimentally measure the oxidized ascorbic acid (DHA) concentration to further prove this assumption.

4.5 Conclusions

In this chapter, transnitrosation between BSANO and free CySH (not immobilized CySH) was studied and a mathematic model was successfully developed to model the experimental data. The major achievements are:

1) An improved nitrite/S-nitrosothiol detection method based on ammonium sulfamate treatment and KI/I_2 based chemiluminescence method was established, which gives less standard error and more data consistency.
2) Transnitrosation between BSANO and free CySH was found to be sensitive to various reductants and oxidants. Oxygen and Cu^{2+} both can oxidize CySH, while ascorbic acid can react with Cu^{2+} so that less CySH will be oxidized. The NO transferred from BSANO increases significantly when the ascorbic acid concentration increases.
3) A mathematic model which includes transnitrosation between BSANO and CySH, CySNO decomposition and CySH oxidation was developed to model the experimental data. The results showed that the model described the transnitrosation reactions very well.
4) Experimental results showed that ascorbic acid increases the CySNO decomposition rate constant k_{dc} value and reduces the CySH oxidation rate constant k_{oc}, which is consistent with the reaction mechanisms.
5) Model sensitivity analysis showed that the transnitrosation rate constants k_f and k_r; and the CySNO decomposition rate constant k_{dc} have the most impact on the BSANO concentration time profile, while the ascorbic acid oxidation rate constant k_{oa} has less influence.

CHAPTER 5

IMMOBILIZATION OF L-CYSTEINE ON PET SURFACE

5.1 Introduction

In order to utilize endogenous NO to improve the haemocompatibility of polymer surfaces as proposed in Chapter 2, L-cysteine (CySH) needs to be attached to the polymer surface. Currently, polyethylene terephthalate (PET) has been widely used in the biomedical field, especially blood contacting applications such as vascular grafts, heart valves and surgical mesh [Vinard *et al.* 1988; Tweden *et al.* 1997] because of its relatively good haemocompatibility, good mechanical properties and good biochemical stability *in vivo* [Bùi *et al.* 1993; Greenwald *et al.* 1994]. Thus, it is ideal to use PET as the model polymer for surface modifications as an example. Previously, researchers in this group have established a protocol for covalently attaching CySH or related thiol molecules onto the PET surface [Duan and Lewis 2002; Gappa-Fahlenkamp and Lewis 2005].

Surface modifications have been widely used to immobilize diverse molecules such as antibodies, peptide and proteins, and even cells onto different material surface in order to change the surface properties, such as improving blood compatibility, altering cell adhesion and growth, changing the hydrophilicity or lubricity and enhancing

corrosion resistance all while retaining the key bulk properties of the material [Ratner and Castner 1997].

Immobilization can be mainly divided into two categories based on the interaction between the immobilized molecules/cells and the supporting material: non-covalent and covalent. Non-covalent immobilization is basically physical absorption of a chemical on the material surface which is usually for short term applications. It, however, does have the advantage of a high degree of order and uniformity [Whitesides *et al.* 1991; Knobler 2007]. Covalent immobilization usually involves chemical bond formation. This can be achieved by either physical methods (such as plasma or UV radiation treatment) or chemical treatments [Jiao and Cui 2007]. For polymer surface modifications, chemical treatments are usually considered first as the process is relatively easy to control (less side reactions) and less expensive (no special equipments needed).

As an inert polymer, PET needs to be activated first to form reactive groups, so that CySH can form covalent bonds with the surface. As introduced earlier in Chapter 2, PET films were treated with ethylenediamine to introduce primary amine groups on the surface. The formation of a primary amine occurs via a polymer chain breakage as illustrated in Figure 5.1 [Avny and Ludwig Rebenfeld 1986]. The amine group was then used to react with glutaraldehyde (GA) to introduce the aldehyde group via imine bond (-C=N-) formation. Finally, another unreacted aldehyde group of the GA was used to react with the amine group of CySH [Duan and Lewis 2002; Fahlenkamp 2003]. However, the imine formation reaction is reversible in aqueous solution and can be catalyzed by acid [Carey and Sundberg 2007]. The imine involved in the modified polymer has already been shown to be susceptible to acid as CySH gets detached from the polymer completely

Figure 5.1 Reaction scheme for PET aminolysis by ethylenediamine. The reaction leads to chain breakage in the ester bond and the formation of a primary amine group.

within one hour in acidic nitrite solution [Duan 2001]. Therefore, the stability of the imine bond in neutral solution can be questionable, as water itself can serve as a weak acid. Although glutaraldehyde cross-linking has been widely used for immobilizing functional groups on different biomaterials for a long time [Bùi *et al.* 1993; Marconi *et al.* 1996; Seifert *et al.* 1997; Liu *et al.* 2008], the stability of the imine bond has rarely been addressed in these applications. However, a study done by Vazquez *et al.* reveals that the structure of the imine compound can significantly improve the stability of the imine bond due to the lack of ionic groups or the existence of bulky hydrophobic substituent groups near the imine bond [Vazquez *et al.* 1990]. Thus, for the imine bonds between CySH and GA or the imine bond between GA and ethylenediamine on the polymer, the bonds either lack one or both of the above two stabilizing factors which makes it highly possible that CySH can be detached from the polymer easily even at neutral pH. Another drawback of this modified polymer is the polymer bulk property changes after ethylendiamine treatment. As mentioned earlier, ethylenediamine causes polymer chain scission when inserting itself into the polymer, thus this treatment weakens the mechanical properties of the polymer [Avny and Ludwig Rebenfeld 1986].

In order to overcome the above problems, a new surface modification carboxylation treatment is introduced in this chapter and amide bond (-C-NH-) formation is used to attaching CySH to the polymer surface. For attaching via the amide bond, there are two functional groups on CySH that can be used: the carboxyl group and the amine group. Thus, PET needs to be activated to acquire amine or carboxyl groups on the surface, respectively, in order for attachment to occur. The amine group can be introduced by the aminolysis method as discussed above using ethylenediamine although

the polymer can be weakened. In contrast, the carboxylation treatment can add a carboxyl group on the benzene ring of PET without breaking the polymer chain (Figure 5.2) [Löfås and Johnsson 1990; Massia and Hubbell 1990]. Peptide bond formation is also a widely used method for immobilization [Hermanson 1996]. Although peptide bonds can also be hydrolyzed in neutral pH and the reaction is thermodynamically favored (equilibrium constant is around 10^3-10^4), the hydrolysis is kinetically unfavored under physiological conditions with a reaction half life of years. Thus, peptide bonds are still considered to be stable in physiological time scale [Aslam and Dent 1998]. In this chapter, two different surface modification methods (imine bond and amide bond) were evaluated and their potential stability problems were also studied in detail. In addition, polymer surface changes were briefly characterized after different modifications.

In addition to the bond stability of modified PET, the stability of CySH itself, particularly the thiol (-SH) group, is critical for the long term performance of a CySH-modified polymer in biomedical applications. Thiol groups have been reported to be sensitive to light, oxygen and ozone in either dry conditions or aqueous conditions [Gerdes *et al.* 1999; Ferris and Rowlen 2000]. Although the applications of modified PET are mostly in aqueous conditions and without light (*in vivo*), studying the behavior of CySH on PET without exposure to aqueous solution is beneficial for determining an optimized storage condition for CySH-modified PET. Therefore, this work also evaluated the stability of CySH following attachment to PET.

5.2 Materials and Methods

5.2.1 Materials

Polyethylene terephthalate (PET) was generously provided by DuPont (Hopewell, VA). Glacial acetic acid, potassium iodide, tetrahydrofuran (THF) acetone, formaldehyde and sodium nitrite were purchased from Fisher Scientific (Fairlawn, NJ). 10× Gibco Phosphate-Buffered Saline (PBS), pH 7.4 was purchased from Invitrogen. 1M NaOH and 1 M HCl were purchased from Cole-Parmer (Vernon Hills, IL). ethylenediamine (ED), ammonia sulfamate, sulfanilamide, iodine, L-cysteine (CySH), 1-ethyl-3-(3-dimethylaminopropyl)-carbodiimide hydrochloride (EDC), glutaraldehyde, bromoacetic acid, N,N'-dicyclohexylcarbodiimide (DCCI), N-(tert-butoxycarbonyl)-S-trityl-L-cysteine [Boc-Cys(Trt)-OH], 1-hydroxybenzotriazole (HOBt), 4-Ethylmorpholine, 2-(N-morpholino)ethanesulfonic acid (MES), 5,5-dithiobis (2-nitrobenzoic acid) (DTNB) and all the other reagents were purchased from Sigma Chemical Co. (St. Louis, MO). Kimble 4 mL and 1.8 mL amber vials were purchased from VWR (West Chester, PA).

5.2.2 PET Modification

PET film was cut into 1×5 cm size and soaked in acetone for 24 hours followed by drying in petri dishes for 12 hours before any surface modification. The acetone treatment is for removing possible surface contaminants.

Two surface modifications: aminolysis and carboxylation were used to add either amine or carboxyl groups on the PET surface, respectively.

Aminolysis: Acetone treated PET was placed in an 8 mL glass culture tube and then 5 mL 40% or 60% ED solution was added into the tube to cover the entire polymer. Then, the tube was placed in a 40 ˚C water bath and shaken at 130 times/min for 24 hours [Gappa-Fahlenkamp and Lewis 2005]. The polymer was then washed by DI water in culture tubes for 3 cycles, each cycle consisting of three quick rinses (using 5 mL DI water each time) followed by one soaking for 5 min (in 5 mL DI water). Finally, the aminolyzed PET (PET-NH_2) was placed in a nitrogen glove box for 12 hours to let it dry.

Carboxylation: PET was carboxylated using the protocol described by Yang et al. [Yang *et al.* 2000]. Briefly acetone treated PET was placed in the culture dish and 5 mL 18.5% formaldehyde solution in 1 M acetic acid was added to cover the entire polymer. The tubes were then set on the hand motion shaker, shaking for 4 hours followed by DI water wash as previously described. This process hydroxylates the PET surface by adding a methanol residue on the benzene ring [Massia and Hubbell 1990] (Figure 5.2). After drying the hydroxylated PET (PET-OH) for 12 hours in the nitrogen glove box, PET-OH was then treated with 5 mL 1 M bromoacetic acid solution in 2 M sodium hydroxide in a glass culture tube for 16 hours followed by DI water rinsing and drying in a nitrogen glove box for 12 hours. This finally introduced the carboxyl group to the PET surface (PET-COOH) [Löfås and Johnsson 1990].

5.2.3 CySH Immobilization

After PET surface activation, cysteine can then be attaching using different methods. Three different approaches were attempted as follows.

Glutaraldehyde cross-linking (imine bond): This method was based on the previous works done by Fahlenkamp [Fahlenkamp 2003]. PET-NH_2 was put into a

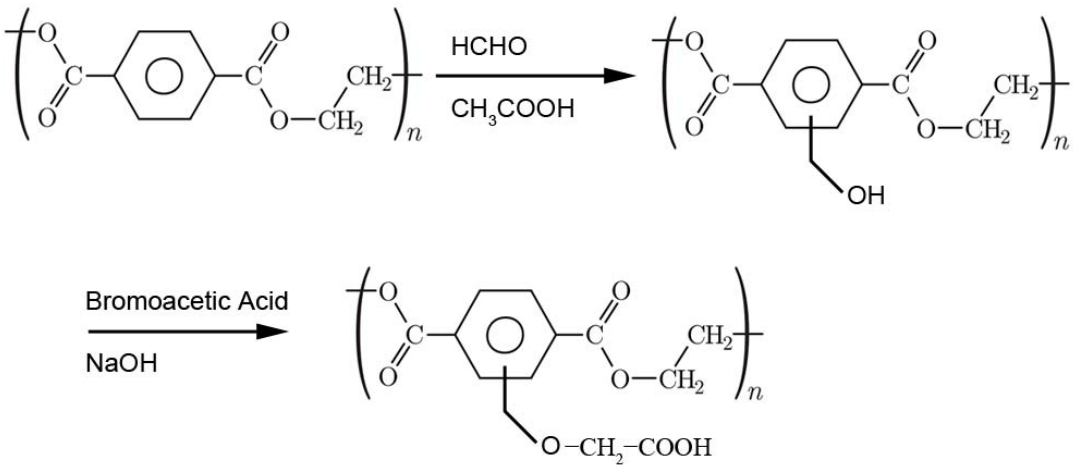

Figure 5.2 Reaction scheme for PET carboxylation. The reaction adds a carboxyl group on the benzene ring without causing chain breakage.

glass tube filled with 5 mL 0.02% GA in Gibco 1×PBS (pH 7.4) buffer. Then, the tube was set on the hand motion shaker, shaking at 1 time/sec while blowing nitrogen into the tubes slowly for 15 min followed by DI water rinsing. This formed the glutaraldehyde modified polymer (PET-GA). Then PET-GA was placed in a new glass tube filled with 5 mL 0.2% CySH in Gibco 1×PBS (pH 7.4) buffer. Finally, the tube was set on the hand motion shaker, shaking at 1 time/sec for 12 hours, followed by DI water rinsing. This modified polymer with CySH on the aminolyzed PET via the imine bond is denoted as PET-N(i)-CySH.

DCCI coupling (amide bond): This method was modified from M. Bodanszky and A. Bodanszky [Bodanszky and Bodanszky 1994]. Briefly, PET-NH_2 was put into a glass culture tube and then 5 mL 4˚C THF mixture (including 20 mM of HOBt, EMP, Boc-Cys(Trt)-OH and 22 mM DCCI) was added into the tube, followed by shaking on a hand motion shaker for 1 hour at 4 ˚C and 1 hour at room temperature. The DCCI was slightly in excess because it is the coupling reagent. The CySH had a protecting group on both its amine and thiol groups, thus preventing CySH self-polymerization and also keeping the thiol from reacting with DCCI [Hermanson 1996]. Another experiment using higher concentration reactant (200 mM) was also made accordingly. During the reaction, white precipitate was observed which was due to the formation of dicyclohexylurea [Barany and Merrifield 1979]. After coupling, the modified polymer was rinsed by THF for 3 cycles similarly to DI water rinsing. Then, the thiol of the cysteine was de-protected by incubating the modified polymer in 80 mM I_2 dissolved in methanol for 1 hour at room temperature. Finally, the modified polymer was incubated in 1M $Na_2S_2O_3$ solution to remove the excess iodine on the polymer surface (The color of the polymer turn from

brown to white), followed by 3 cycles of DI water rinsing. A brief summary of these steps is illustrated in Figure 5.3. This modified polymer with CySH on the aminolyzed PET via the amide bond is denoted as PET-N(a)-CySH. A Boc-glycine modified PET was also made similarly as the blank sample and it is denoted as PET-N(a)-Gly.

EDC coupling (amide bond): This method was modified from Wissink *et al*. Briefly, PET-COOH was incubated with 0.25 M EDC and 0.25 M CySH in 0.1 M phosphate buffer (pH 6.8) in a culture tube which was shaken on a hand motion shaker for 16 h at 4 ˚C, followed by 1 cycle of 1 M NaCl solution rinsing and 3 cycles of DI water rinsing at 4˚C [Wissink *et al.* 2001]. The CySH used here was unprotected since the thiol protected CySH used in the DCCI method was not water soluble and EDC is preferred to be used in aqueous solution [Hermanson 1996]. The only water soluble thiol protected cysteine commercially available is extremely expensive and currently there is no known method to deprotect it. However, a carboxyl group protected CySH — cysteine ethyl ester (CySH(E)) was also immobilized using the similar method in order to study the self-polymerization effect on immobilization. These two modified PET had an amide bond between the carboxyl group on the PET-COOH and the amine group on cysteine and they are denoted as PET-C(a)-CySH and PET-C(a)-CySH(E), respectively. In addition, a set of experiments with lower reactant concentrations (0.1 M EDC and 0.1M CySH) were performed in order to study the concentration effect on immobilization. A modified polymer in which glycine, rather than cysteine, was attached served as a control. This polymer is denoted as PET-C(a)-Gly.

EDC coupling was also used for ethylenediamine treated PET for attaching CySH. The immobilization is similar to the above protocol, except that 100 mM MES buffer (pH

Figure 5.3 CySH immobilization on the aminolyzed PET using DCCI coupling. The amide bond forms between the carboxyl group of CySH and the amine group on PET-NH_2. The thiol group was de-protected after coupling.

5.5) was used instead of 100 mM Na_2HPO_4-NaH_2PO_4 buffer (pH 6.8). This polymer is denoted as PET-N(a,e)-CySH.

5.2.4 Cysteine Surface Concentration Analysis

Immobilization of cysteine on PET-N(i)-CySH was verified using a protocol modified from Duan and Lewis [Duan and Lewis 2002]. Briefly, the polymer was cut into a 1×1 cm piece and put in a 1.8mL amber vial. Then, 250 µL 1 N HCl and 750 µL 100 µM $NaNO_2$ was added into the vial followed by hand motion shaking for 1 hour at room temperature. After that, 500 µL 200 µM ammonium sulfamate was added into the vial with continued shaking for 5 min to quench the excess nitrite. In this process, cysteine detaches and is nitrosated to form S-nitrosocysteine. S-nitrosocysteine was then measured by a Sievers NO chemiluminescence analyzer NOA 270B (Sievers Medical Instruments, Inc., Boulder, CO) using a potassium iodide/iodine (KI/I_2) reducing solution as mentioned in Chapter 4, Section 4.2.5. Since the excess nitrite is removed, only CySNO was measured. The surface cysteine concentration was calculated as follows:

$$[CySH]_{surface} = [CySNO]_{solution} \bullet V / A \qquad (5.1)$$

where $[CySNO]_{solution}$ is the CySNO concentration in the solution measured via chemiluminescence, V is the volume of the solution, and A is the surface area of the polymer film.

For the cysteine modified polymer via the amide bond (PET-N(a)-CySH and PET-C(a)-CySH) the amide bond is stable in the acidic condition and the above method cannot detect any S-nitrosocysteine in the solution. Therefore, an indirect method was used. Briefly, the modified polymer was incubated with 500 µL 100 µM $NaNO_2$ and 500 µL 1 N HCl for 30 min followed by 500 µL 1N NaOH neutralization. This reaction

reduces the nitrite concentration in the solution since the thiols on the surface are nitrosated. Meanwhile, a similar acidic nitrite solution was prepared, without exposure to a polymer, to be used as a blank since during the nitrosation some of the nitric acid can decompose to form NO and be released into the head space of the vial which can also cause a decrease of total nitrite in the solution. Then, 20 μL samples were taken from both the polymer-exposed solution and the blank solution and the nitrite concentration was measured by the KI/I_2-based chemiluminescence method as previously described. The surface cysteine concentration was estimated by the following equation:

$$[CySH]_{surface} = ([NO_2^-]_{blank} - [NO_2^-]_{sample}) \bullet V / A \quad (5.2)$$

where $[NO_2^-]_{blank}$ is the nitrite concentration of the blank solution, $[NO_2^-]_{sample}$ is the nitrite concentration of the solution containing the modified PET, V is the volume of the solution and A is the area of the polymer film.

In addition to measuring the surface cysteine concentration, cysteine concentration in solution was measured during some studies using Ellman's method [Ellman 1959; Rootwelt 1967] as mentioned in the Chapter 4, Section 4.2.7. Briefly, a 100 μL sample solution was mixed with an equal volume of Ellman's reagent (5 mM DTNB in 100 mM pH 7.2 phosphate buffer and 0.1 mM EDTA) in a 96-well microplate (Falcon 353228, BD, Franklin Lakes, NJ). After 10 min, the absorbance of the solution was measured at 410 nm using a Packard® SpectraCount™ Microplate Photometer BS10000 (Packard Instrument Co., Meriden, IL).

5.2.5 Imine Bond and Amide Bond Stability Test

All three polymers, PET-N(i)-CySH, PET-N(a)-CySH and PET-C(a)-CySH, were cut into a smaller size (usually 1×1 cm) and placed in an 4 mL amber vial which was

filled with 1.5 mL 50 mM low purity NaH_2PO_4-Na_2HPO_4 buffer (pH=7.4). All the vials were set on the hand motion shaker, shaking at 30 times/min at either room temperature or in a 37 ˚C incubator. At specific times, sample polymers were taken out of the vials, wiped by tissue paper and then measured by the chemiluminescence method mentioned earlier. The liquid samples were measured by Ellman's method as previously mentioned.

5.2.6 Cysteine Modified Polymer Surface Property Analysis

The modified polymer surface was briefly characterized by scanning electron microscope (SEM) using a Jeol JSM 6360 scanning electron microscope (Jeol USA, Inc., Peabody, MA). Images of the surface were taken for unmodified polymer, aminolyzed PET (treated by different concentration of ethylenediamine) and carboxylated PET. Also, the polymer thickness change after aminolysis was analyzed by micrometer calipers.

5.2.7 Light and Air Effect on CySH Modified Polymer and Long Term Storage Test

CySH-modified PET was made by ethylenediamine treated PET followed by glutaraldehyde cross-linking immobilization as previously described. The reason for using this unstable polymer for this oxidation test was because 1) the oxidation test was under dry conditions which does not have the potential problem arising from the imine bond breakage; 2) This method was the easiest and fastest one to make the CySH modified PET; 3) This method can introduce more cysteine on the PET surface than the other methods, which will make it easier to detect the change in the surface concentration.

The PET-N(i)-CySH was cut into 1×1 cm pieces and divided into three petri dishes. One of the petri dishes was placed in the nitrogen glove box with a 60 W

incandescent light bulb turning on constantly at the distance of 20 cm. This experiment will show only the light effect on the modified PET. The other two petri dishes were exposed to air but with one of them covered with aluminum foil and one placed under a constant 60 W incandescent light bulb at a distance of 20 cm. Therefore, these two petri dishes were used for studying CySH modified PET oxidation in air only and in light + air, respectively. At specific times, one piece of the modified polymer was removed from each petri dish and treated with acidic nitrite, followed by KI/I_2 based chemiluminescence analysis as previously mentioned.

In order to study the possibility of long term storage of the modified polymer under dry conditions, one piece of a 1×5 cm polymer was placed in a 4 mL amber vial and the vial was placed in the -20 ˚C freezer for 62 days. Then, the polymer was cut into 1×1 cm pieces and measured by the same method which was used to analyze the PET-N(i)-CySH polymer as above.

The CySH surface concentration for oxidation in air only, light only and air + light were plotted versus time. Since the kinetic mechanism of the oxidation is unknown for the modified polymer, TableCurve2D v5.01 (Systat Software, Inc, Chicago, IL) was used to fit the graph with various embedded kinetic models in the software and then a best fit model was determined.

5.3 Results

5.3.1 Cysteine Surface Concentration Measurement

The chemiluminescence analysis for all three modified polymer showed that cysteine was attached. The surface concentrations are shown in Figure 5.4. However, the

surface concentrations are not consistent among different modification methods. The surface concentrations ranged from around 2 nmol/cm^2 to 20 nmol/cm^2, with PET-N(i)-CySH having the highest concentration and the PET-C(a)-CySH showing the lowest value. This is probably due to surface area changes or cross-linking effect, which will be addressed later. On the other hand, it is evident that increasing the reactant concentration during the carbodiimide coupling (DCCI method and EDC method) leads to a higher surface concentration of CySH (PET-N(a)-CySH (20 mM) versus PET-N(a)-CySH (200 mM) and PET-C(a)-CySH (0.1 M) versus PET-C(a)-CySH (0.25 M)). However, for DCCI coupling, since the protected CySH is relative expensive, only a 200 mM reactant concentration was tried.

For EDC coupling, two different treated PET were assessed: aminolyzed PET and carboxylated PET. The resulting surface concentrations are much lower (below 5 nmol/cm^2) compared to PET-N(i)-CySH and PET-N(a)-CySH, with the modified PET coupled with cysteine ethyl ester (CySH(E)) having a relatively higher surface concentration. Also, it was also observed that a higher (around 0.5 M) concentration of CySH during the coupling is not recommended because when large amount of CySH is oxidized during the reaction, it forms a substantial amount of white precipitation (disulfide CySH) which can stick on the polymer surface and significantly interfere with coupling reaction (data not shown).

As expected, two blank polymer using glycine as the reactant: PET-N(a)-Gly and PET-C(a)-Gly showed virtually zero CySH surface concentration (data not shown).

5.3.2 Stability of Imine Bond and Amide Bond

Although the polymer using the ethylenediamine treatment and glutaraldehyde

Figure 5.4 CySH surface concentrations on PET modified by different methods. PET-N(i)-CySH: PET treated by ethylenediamine, followed by glutaraldehyde cross-linking with CySH. PET-N(a)-CySH: PET treated by ethylenediamine, followed by DCCI coupling. PET-C(a)-CySH: PET treated by carboxylation, followed by EDC coupling. PET-C(a)-CySH(E) same as PET-C(a)-CySH, but cysteine ethyl ester was used instead of cysteine. Concentrations in the parenthesis are the reactant concentrations during the coupling reaction.

cross-linking yielded the highest CySH surface concentration, the imine bond was not stable even at neutral pH. Figure 5.5 shows that cysteine detached from the polymer surface and went into the solution (The total cysteine loss is more than 70% at 37 ˚C and less than 50% at 25 ˚C). Notice that the y axis of Figure 5.5 is the total moles of cysteine on the polymer (or in the solution) instead of the CySH surface concentration (nmol/cm^2) as shown in Figure 5.4. Thus, it is easy to find show that CySH loss from the polymer and the CySH increase in the solution are virtually comparable if considering the factor that some of the CySH (either on polymer or in solution) is oxidized due to the reasons which were discussed in the previous chapter. Figure 5.5 also showed that the hydrolysis is initially fast (within 5 hours) and then slows down. Increasing the temperature only increased the initial imine bond hydrolysis and the free CySH oxidation in the solution but exerted no noticeable effect on CySH detachment after 5 hours. This is evident since two curves showed the same trend of CySH surface concentration loss which is probably due to oxidation and not imine bond hydrolysis.

For the CySH modified polymer made by aminolysis followed by DCCI coupling through an amide bond (PET-N(a)-CySH), the polymer showed good stability in acidic condition as mentioned earlier. However, at neutral pH, there was still significant CySH detachment from the polymer as shown in Figure 5.6. The detaching trend was similar to the modified polymer using an imine bond (PET-N(i)-CySH). Ellman's method again detected that there was CySH existing in the solution and the amount was comparable to the CySH amount lost from the polymer surface.

For the polymer made by carboxyl modification followed by EDC coupling (amide bond), PET-C(a)-CySH also showed significant CySH surface concentration loss

Figure 5.5 CySH surface amount and amount in the solution when the modified polymer (PET-N(i)-CySH) was incubated in low purity phosphate buffer at 25 ˚C and 37 ˚C. (n=2) The cysteine is slowly detached from the polymer (compared to acidic condition). An increase in temperature can accelerate this imine bond hydrolysis within the initial 5 hours.

as shown in Figure 5.7 (more than 80% of the CySH detached from the polymer surface). Again, CySH was detected in the solution. However, the total CySH amount in the solution was more than the amount on the polymer (almost 3 times). This inconsistency of the data will be discussed in detail later. As shown in Figure 5.8, the carboxyl group protected CySH showed instability similar to the unprotected polymer.

For the polymer made by ethylenediamine modification followed by EDC coupling (amide bond), PET-N(a,e)-CySH showed that the bond between CySH and the polymer had much better stability as shown in Figure 5.9. The CySH surface concentration decrease was probably due to oxidation, which is consistent with previous results (virtually zero order oxidation as shown in Figure 5.5 after 5 hours). Ellman's method could not detect any CySH in the solution, thus confirming that there was no CySH detached from the polymer.

5.3.3 Polymer Surface Change after Modification

SEM images (Figure 5.10) showed that the original PET surface is quite smooth with only minor defects (some dots and lines). The carboxylated polymer also showed no polymer surface deterioration. However, for the ethylenediamine (ED) treated PET, there were many cracks formed and the size of the cracks increased with increasing ED concentration (The entire dark part of Figure 5.10(d) is one crack with a width around 5 μm while in Figure 5.10(c), the width of the cracks are less than 1 μm). The polymer thickness for the ED treated polymer also changed significantly after modification, reducing from 0.0855±0.0053 mm to 0.0525±0.0039 mm with about 60% loss after 60% ethylenediamine treatment.

Figure 5.6 CySH surface amount and amount in the solution when the modified polymer (PET-N(a)-CySH) was incubated in low purity phosphate buffer at 25 ˚C. (n=2) The cysteine was detached from the polymer similar to PET-N(i)-CySH, indicating that the bond was unstable.

Figure 5.7 CySH surface amount and amount in the solution when the modified polymer (PET-C(a)-CySH) was incubated in low purity phosphate buffer at 25 ˚C. (n=2) The cysteine was detached from the polymer similarly to PET-N(i)-CySH, indicating that the bond was still unstable. However, the CySH lost from the polymer was not consistent with the CySH observed in solution.

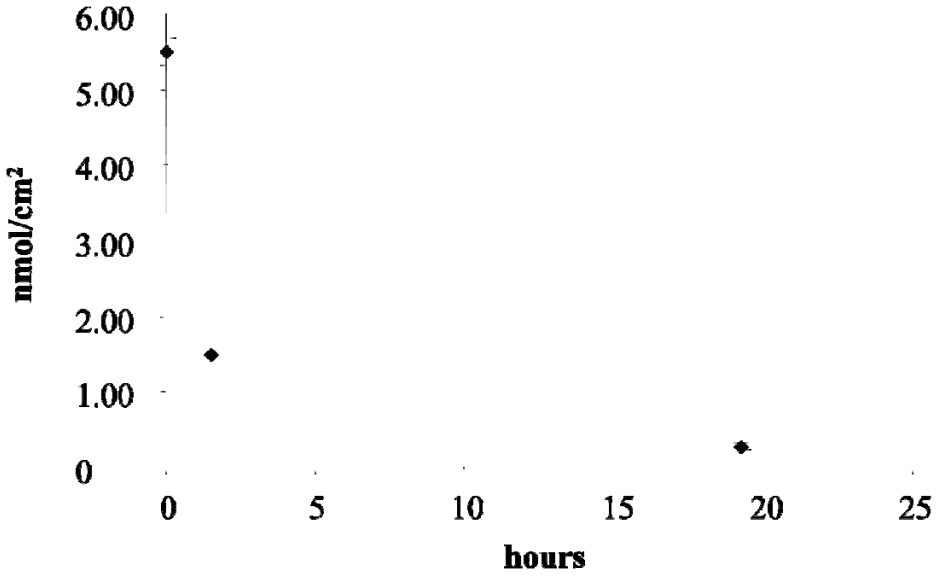

Figure 5.8 CySH surface concentration when the modified polymer (PET-C(a)-CySH(E) was incubated in low purity phosphate buffer at 25 ˚C. (n=2) The cysteine was detached from the polymer similarly to PET-N(i)-CySH, indicating that the bond was still unstable. The solution CySH was not measured in this case.

Figure 5.9 CySH surface concentration when the modified polymer (PET-N(a,e)-CySH was incubated in low purity phosphate buffer at 25 ˚C. (n=2) CySH surface concentration was reduced mostly by oxidation because there was no detectable CySH in the solution (data not shown).

Figure 5.10 SEM image of PET surface change after different treatment. (a) untreated PET, (b) carboxylated PET, (c) 40% ethylenediamine treatment, (d) 60% ethylendiamine treatment. The carboxylated PET showed similar surface as the original one while the ethylenediamine treated PET showed many cracks and the size of the cracks increased with higher ethylenediamine concentrations.

5.3.4 Light and Air Effect on CySH Modified Polymer and Long Term Storage Test.

The results shown in Figure 5.11 with only light + air treatment showed significant CySH oxidation (40% loss within 110 hours) while light or air alone virtually did not show any CySH oxidation (<10% within 110 hours). A 3rd-order simple decay model (Equation 5.3) fit the data the best with R^2 of 0.999:

$$C = \frac{C_0}{\sqrt{1 + 2 \cdot C_0^2 \cdot k \cdot t}} \tag{5.3}$$

where C_0 is the initial CySH surface concentration, k is the 3rd-order decay rate constant. The fitting gives the value of C_0=26.07 nmol/cm^2 and k=(3.32±0.1)×10^{-5} nmol^{-2}·cm^4·hr^{-1}. Long term freezer storage (Figure 5.12) showed that the CySH surface concentration remained stable at -20 ˚C freezer for 62 days.

5.4 Discussion

The theoretical maximum cysteine surface concentration can be estimated by assuming a tightly packed monolayer of spherical cysteine molecules on the polymer surface. The following equation can be used to estimate the radius of cysteine molecule [Fournier 1999]:

$$R = \left(\frac{3M}{4\pi\rho N_A} \right)^{1/3} \tag{5.4}$$

where, M is the molecular weight of the molecule (121.16 g/mol for cysteine) and ρ is the density of the molecule (1.523 g/cm^3). Thus, the calculated cysteine molecule radius is 0.32 nm and the maximum surface concentration is 0.52 nmol/cm^2. The ethylenediamine treated PET followed by glutaraldehyde cross-linking or DCCI coupling showed a much

Figure 5.11 PET-N(i)-CySH oxidation under different storage condition. (n=2) The light or air treatment virtually did not cause oxidation, only light combined with air caused CySH oxidation. The solid line is a 3rd-order decay model (Equation 5.3) for fitting the light + air scenario.

Figure 5.12 PET-N(i)-CySH long term storage test. (n=3) CySH surface concentration remained virtually the same after 62 days in a -20 ˚C freezer.

higher value than the theoretical limit. There are two possible reasons for this phenomenon. First, the cracks formed can significantly increase the active surface area for immobilization; second, glutaraldehyde can self polymerize in aqueous solution to form long chains with multiple aldehyde groups [Migneault *et al.* 2004]. On the other hand, aminolyzed PET using the EDC method for coupling did not show a high cysteine surface concentration which was probably due to the fact that EDC was mostly consumed by CySH self-polymerization (because the unprotect CySH can react with each other to form a complex compound, therefore less CySH can be attached to aminolyzed PET).

The instability of the imine bond was verified and the possible reason was discussed above. However, there is a method to improve the imine stability by reducing the imine bond (-C=N-) to an amine bond (-C-NH-) by a strong reducing agent (e.g. $NaCNBH_3$) [Hermanson 1996]. However, this work was not pursued.

The amide bond was supposed to be stable according to many published applications [Hermanson 1996; Aslam and Dent 1998]. However, among the various modified PET that were made in this study using the amide bond, most of them (e.g. PET-N(a)-CySH, PET-C(a)-CySH and PET-C(a)-CySH(E)) appeared to be stable only in acidic conditions, only one (PET-N(a,e)-CySH) was stable at both neutral and acidic pH. One possible reason is the thiol group on the CySH. In EDC coupling, the –SH group can react with the COOH group during the EDC coupling to form a thiol ester bond [Hermanson 1996]. This bond is stable in acidic solution according to Saburo [Saburo 1999], but it is not as stable as the amide bond and can be hydrolyzed in neutral pH. Also, the activated –COOH will preferably react with a NH_2 group, even there is a SH group at the same concentration level [Hermanson 1996]. Therefore, during coupling, since the CySH

concentration is quite high, CySH will first react with each other to form a chain of CySH instead of reacting with the activated –COOH on the PET as shown in Figure 5.13(a). Thus, for this molecule (Figure 5.13(a)), it is easier to react with the activated –COOH on the PET via the –SH rather than the $–NH_2$ group because the –SH is now dominant (see Figure 5.13(b)). Therefore, when this thiol ester polymer is put into the solution, the thiol ester bond will be broken and all the cysteine will be quickly lost. However, in the acidic nitrite condition, the –SH can be nitrosated and the bond is stable. Therefore, –SH can be detected.

On another note, it has been documented that phosphate can also be activated to react with amine to form a phosphoramidate bond [Hermanson 1996], although the stability of this bond is not clear and there is no literature regarding whether activated phosphate can react with the thiol group or not. Similar reactions can still occur even if the carboxyl group of CySH is protected which is in the case of EDC coupling with CySH ethyl ester, because CySH ethyl ester might be hydrolyzed to form unprotected CySH during the long coupling process (16 hours). For EDC coupling using aminolyzed PET and CySH, since there is no thiol ester bond formation between PET and CySH (no carboxyl group on PET), all the CySH are coupled to PET via an amide bond to form a stable CySH-modified PET. This can also be used to explain the reason why in the case of PET-C(a)-CySH, a higher CySH was detected in the solution than the loss of CySH on the polymer, because the CySH chain might form a complex 3-D formation on the PET surface to prevent the thiols from reacting with acidic nitrite. Therefore, when the thiol ester bond is hydrolyzed, the chain is detached from the polymer and all of the thiol groups are exposed to Ellman's reagent. This leads to more CySH detected by Ellman's method as

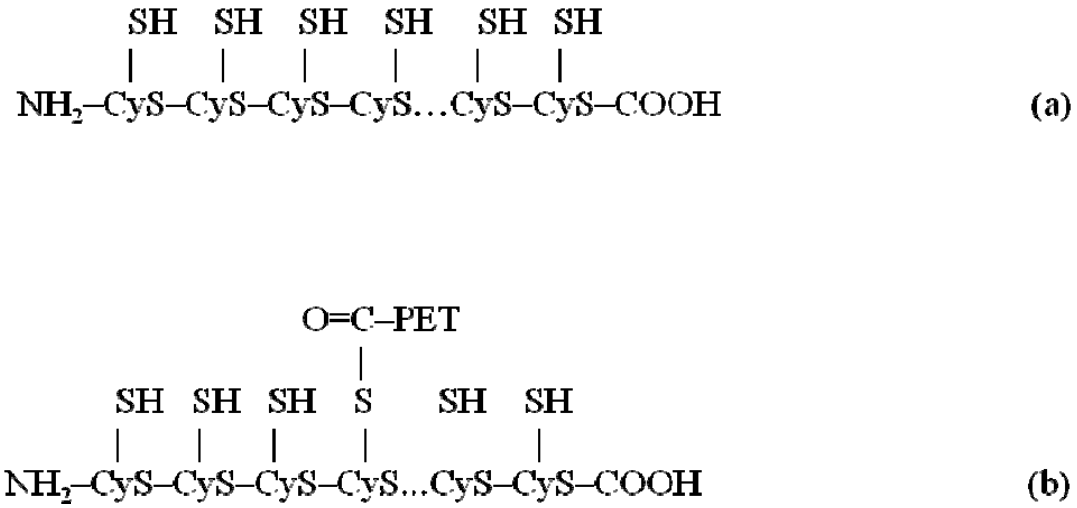

Figure 5.13 Possible CySH chain formation (a) and thiol ester bond formation between the thiol group on the CySH chain and carboxyl group on the PET (b).

compared to the chemiluminescence method.

However, the above mechanism cannot explain why in the DCCI coupling, even when the CySH had both its thiol group and amine group protected, the resulting modified polymer was still unstable. The only explanation could be that the ethylenediamine treated polymer became more unstable after the DCCI coupling which involved a lot of different organic solvent treatments.

Although one CySH modified polymer with a stable bond (PET-N(a,e)-CySH) was finally synthesized, there were still potential problems with this polymer. The aminolyzed PET showed significant surface deterioration as shown by SEM analysis due to the reason that ethylenediamine can diffuse into the polymer fiber to cause further damage of the polymer microstructure [Avny and Ludwig Rebenfeld 1986]. Meanwhile the mechanical properties were significantly weakened as the polymer thickness reduced significantly after 60% ethylenediamine treatment. Thus, it is ideal to find a method to introduce an amine group on the PET surface without breaking the polymer chain or find a water soluble thiol protected CySH which can be deprotected easily.

The CySH surface concentration time profiles (Figure 5.5-5.8) for the unstable polymers (PET-N(i)-CySH, PET-N(a)-CySH, PET-C(a)-CySH and PET-C(a)-CySH(E)) were almost similar, with a fast initial decreasing step within a few hours and then slowing down. The first stage was likely due to bond breakage while the second stage was likely due to cysteine oxidation. By fitting the second stage of Figure 5.5 with zero order kinetics, the decay constant is 0.280 nmol/(cm^2·hr). However, by fitting the data in Figure 5.9, the decay constant is 0.0433 nmol/(cm^2·hr). The inconsistencies between these two constants indicate that different binding can affect the CySH oxidation decay

constant. However, the decay constant might not be affected by the temperature as shown in Figure 5.5, which is different from the free cysteine oxidation in solution mentioned in the Chapter 4.

The light and air influence study showed that except for the bond stability issue, CySH on the surface can also be oxidized in the dry condition when light and oxygen are both present, but under light or air alone, no significant oxidation occurs. A possible explanation for this phenomenon is that light serves as the energy to activate the electron in the thiol group and oxygen serves as the electron acceptor. Thiol photooxidation in dry conditions or in non-aqueous solutions has previously been studied. There is a postulated intermediate for this oxidation in both gas or liquid phase, which involves the thiylperoxyl radical [Robert-Banchereau *et al.* 1997]:

$$\text{R-S}\cdot + \text{O}_2 \rightarrow \text{R-S-O-O}\cdot \rightarrow \text{Oxidation products} \qquad (5.5)$$

where the thiol radical might be generated under light activation. However, this work showed a 3rd-order decay reaction, which is different from photooxidation occurring in aqueous conditions (first or zero order reaction) [Robert-Banchereau *et al.* 1997; Ferris and Rowlen 2000; Bagiyan *et al.* 2003]. Therefore, further studies need to be performed to test whether this is a unique reaction mechanism for CySH photooxidation of a modified polymer.

Cysteine-modified PET long term storage tests showed that when kept at low temperature (-20 ˚C), no CySH oxidation was observed for about two month. This finding is beneficial for future experiments since large amounts of CySH-modified polymer can be made in one batch and kept in the freezer for a long time. This could

potentially reduce possible inter-experimental errors for CySH surface concentration studies.

5.5 Conclusions

Cysteine immobilization using different methods was evaluated and the stability of the bond in buffer as well as cysteine oxidation in both aqueous and dry conditions were studied. The important findings are:

1) The previous protocol for making PET-N(i)-CySH lead to an unstable polymer due to imine bond breakage between either CySH and glutaraldehyde or glutaraldehyde and the amine on PET.
2) Amide bond formation using DCCI or EDC coupling increased the stability of the modified polymer in acidic condition. However at neutral pH, some of the modified polymer still showed bond breakage and only one of the newly developed polymers (ethylenediamine treatment followed by EDC coupling) showed good bond stability in both acidic and neutral pH.
3) Cysteine on all the polymers can also be oxidized slowly just as the free cysteine oxidation which followed the zero order kinetics in solution. Different immobilization methods appear to have a significant effect on the oxidation rate constant.
4) Ethylenediamine treatment can cause substantial amounts of cracks on PET surfaces and the higher concentration of ethylenediamine used, the bigger the cracks. Also, the PET thickness is reduced significantly after ethylenediamine

treatment which potentially affects the mechanical properties or the stability of the modified polymer.

5) Immobilized CySH on PET-N(i)-CySH polymer is susceptible to light and air under dry conditions. However light or air alone does not cause CySH oxidation. This oxidation was found to be represented by a 3rd-order decay reaction with regard to the CySH surface concentration, but a detailed mechanism remains unsolved. CySH modified PET can be stored in an amber vial at -20 ˚C for about 2 months without noticeable oxidation.

As noted in this chapter, a modified polymer that had both structural integrity and stable bonds was not achieved. In order to make a polymer with both good mechanical integrity and bond stability, two approaches can be attempted in the future: a) introduce amine group on the PET without destroying the polymer and then do the EDC coupling; b) find a water soluble thiol protected CySH (which can later be deprotected) and attach it to carboxylated PET using the EDC method.

CHAPTER 6

BSANO TRANSNITROSATION WITH CYSH MODIFIED PET AND MODELING IN FLOW SYSTEM

6.1 Introduction

As described in Chapter 1, the ultimate goal of this work is to develop a kinetic model to predict the NO flux from a CySH-modified polymer surface exposed to BSANO. A model will aid in evaluating the performance of a CySH-modified polymer under various physiological conditions. In addition, by comparing the predicted NO flux to the minimum NO flux for platelet inhibition reported by Ramamurthi and Lewis [Ramamurthi and Lewis 2000], the reason for previously incomplete platelet inhibition might be explained.

Although transnitrosation reaction kinetics in free solution were studied in Chapter 4, it is unknown whether the rate constants will change after immobilization as many enzyme activities have been found to be significantly altered after immobilization [Ollis *et al.* 1976; Jerzy *et al.* 1981; Bickerstaff 1997; Mateo *et al.* 2007]. Thus, in this work, the kinetics of transnitrosation between the immobilized CySH and BSANO in the solution was studied and the key parameters of the transnitrosation reaction, namely k_f and k_r, and k_{dc}, were calculated based on the experimental data.

One potential difficulty of evaluating the kinetics for most CySH-modified polymers addressed in Chapter 5 (e.g. PET-N(i)-CySH) is that the bond stability was not very good. Thus, kinetic parameters could be masked by continual loss of CySH from the polymer. As noted in Chapter 5, only the modified polymer made via aminolysis followed by EDC coupling method (PET-N(a,e)-CySH) had good bond stability (although not good mechanical strength). However, this modified polymer had a very low CySH (~1 nmol/cm^2) surface concentration compared to the modified PET made by aminolysis followed by glutaraldehyde cross-linking (PET-N(i)-CySH) or DCCI coupling (PET-N(a)-CySH) (~20 nmol/cm^2). The low cysteine surface concentration would be difficult for kinetic studies as the BSANO concentration change due to transnitrosation might be too small to be measured accurately. The modified PET made via aminolysis followed by glutaraldehyde cross-linking (PET-N(i)-CySH) showed only a 10% loss of CySH due to imine bond hydrolysis within the first hour at 25 ˚C (Figure 5.5). Therefore, this CySH-modified polymer developed via aminolysis could still provide valuable information regarding the values of k_f and k_r for an immobilized system since these parameters could be estimated from initial transnitrosation data within the first hour. Although these parameters could vary between different types of immobilized CySH polymers, having an estimate of the parameters for one CySH-modified polymer could still provide insights regarding transnitrosation with a modified polymer. Therefore, in this chapter, transnitrosation kinetic studies between immobilized CySH (prepared via aminolysis followed by glutaraldehyde cross-linking) and BSANO were performed.

k_f and k_r can be estimated from experimental data according to [Duan 2001]:

$$\left[\frac{d[BSANO]}{dt}\right]_0 = -k_f[BSANO]_0[CySH]_0 \cdot \frac{S}{V} - k_{db}[BSANO]_0 \quad (6.1)$$

where the left side of Equation 6.1 is the initial slop of the BSANO concentration time profile, $[BSANO]_0$ and $[CySH]_0$ are the initial concentration of BSANO and CySH, respectively, S is the total area of the modified polymer and V is the total volume of the solution. Knowledge of the initial conditions and the value of k_{db} (obtained from BSANO decomposition studies in the absence of polymer—see Chapter 4, Section 4.3.2) enables the calculation of k_f from Equation 6.1. If the equilibrium constant does not change with immobilization, k_r can be calculated by using the free solution transnitrosation equilibrium constant calculated in Chapter 4.

Once the transnitrosation studies were performed to evaluate the k_f and k_r constants following immobilization, a dimensionless mathematical model for predicting transnitrosation and the resulting NO flux was developed to mimic a CySH-modified biomaterial that could be used in a tubular system (e.g. catheters and vascular graft). A laminar flow pattern was used for the model since most of the blood flow in the human body is laminar, except in the aorta which is turbulent flow [Brant 2001]. The model was simplified according to a few assumptions as noted below. Using the model, an assessment of the BSANO concentration, CySH surface concentration and other factors was performed to determine the resulting influence on the NO flux. The predicted NO flux was compared to the minimum NO flux required to minimize platelet adhesion.

6.2 Materials and Methods

6.2.1 Materials

Polyethylene terephthalate (PET) was provided by DuPont (Hopewell, VA). Glacial acetic acid, potassium iodide, acetone and sodium nitrite were purchased from Fisher Scientific (Fairlawn, NJ). 1M NaOH and 1 M HCl were purchased from Cole-Parmer (Vernon Hills, IL). Ethylenediamine (ED), ammonia sulfamate, iodine, L-cysteine (CySH), glutaraldehyde and all the other reagents were purchased from Sigma Chemical Co. (St. Louis, MO). Kimble 4mL and 1.8mL amber vials were purchased from VWR (West Chester, PA).

6.2.2 Transnitrosation Reaction Between PET-N(i)-CySH and BSANO Solution

PET-N(i)-CySH was prepared using the protocol described in Chapter 5. The BSANO solution was prepared using the protocol described in Chapter 4. CySH-modified PET was cut into 1×1 cm pieces and each piece was placed in a 4 mL amber vial filled with 2 mL BSANO to cover the entire polymer. Several vials were prepared. The vials were then set on a hand-motion shaker, shaking at 30 times/min at 25 ˚C. At specific time interval, two vials (duplicate samples) were removed from the hand motion shaker and the polymer samples were taken out of the vials to stop transnitrosation.

The polymer was wiped by tissue paper and treated with acidic nitrite to nitrosate the CySH on the polymer to form CySNO). During acidic treatment, CySNO is also detached from the polymer. The resulting CySNO was then measured using KI/I_2-based chemiluminescence analysis, as previously described in Chapter 5, Section 5.2.4, to obtain the CySH concentration on the surface. In addition to un-nitrosated CySH on the polymer, there would also be CySNO on the polymer as a result of the BSANO transnitrosation. However, preliminary experiments showed that after pulling a polymer out of solution, CySNO was not detectable via chemiluminescence when the polymer

was exposed to an acidic solution (although not acidic nitrite such that any CySH was not nitrosated). Therefore, it appears that once the polymer is pulled out of solution, CySNO on the polymer perhaps undergoes decomposition and is no longer detectable but CySH can still be detected once placed back in solution and nitrosated. Therefore, the method used in this study appears to measure the CySH, but not the CySNO, on the polymer surface.

Meanwhile, 20 μL of the sample BSANO solution was withdrawn from the vials and treated by ammonium sulfamate to scavenge any NO_2^-. The sample was analyzed for BSANO using the KI/I_2-based chemiluminescence method described in Chapter 4, Section 4.2.5 It should be noted that in the solution sample, an unknown concentration of CySNO could be present due to a small amount of CySNO release as a result of bond instability (although less than 10% in first hour). However, this CySNO concentration likely would have a negligible contribution to the BSANO analysis since CySNO decomposes very fast with half life of only 6 min at pH 7.4 (as shown in Chapter 3, Figure 3.1) and not all of the detached thiol will be CySNO (some will likely be CySH). This assumption was implied for the experimental results in Section 6.3.1.

6.2.3 Data Analysis and Modeling

The total RSNO concentration in solution (BSANO and CySNO—although most should be BSANO) and the total CySH surface concentration were plotted against time. The k_f value was estimated using the first two data points of RSNO versus time according to Equation 6.1. Since the transnitrosation reaction equilibrium constant is related to the Gibbs free energy which is independent of immobilization, the free solution transnitrosation equilibrium constant calculated in Chapter 4 was used to predict k_r from

the k_f value. Additionally, k_{dc}, which represents NO release from CySNO, was also evaluated.

The modeling of transnitrosation and NO release in a tubular system through which a fluid continually flows is derived as follows. First, if CySH is maintained in a fully reduced state (i.e. never oxidized due to either CySNO decomposition or autoxidation), the CySNO surface concentration will reach a steady state value since the rate at which CySNO is generated would be a constant as a result of continuously replenished S-nitroso human serum albumin (HSANO) in a flowing system. This assumption was validated after one hour (see Figure 6.1) for CySNO in a solution using the solution transnitrosation model described in Chapter 4. It is very possible for CySH to remain in the reduced state since blood contains abundant ascorbic acid [Khaw *et al.* 2001; Jamaati *et al.* 2006] and glutathione [Svardal *et al.* 1990; Lim *et al.* 1995; Abukhalaf *et al.* 2002; Elena Sbrana 2004]. Ascorbic acid can keep CySH in the reduced form after CySNO decomposition according to Chapter 4 and glutathione can reduce the cystine back to cysteine [Conrad 2009]. Based on these assumptions, the following model was developed.

Similar to section 4.3.3, the transnitrosation reaction between HSANO and immobilized CySH, followed by CySNO decomposition can be illustrated as follows:

$$\mathrm{HSANO} + \mathrm{CyS}^- \underset{k_r}{\overset{k_f}{\rightleftharpoons}} \mathrm{HSA}^- + \mathrm{CySNO} \tag{6.2}$$

$$\mathrm{CySNO} \xrightarrow{k_{dc}} \mathrm{CyS}^- + \mathrm{NO}\uparrow \tag{6.3}$$

$$\mathrm{CySNO} + \mathrm{AA} \xrightarrow{k_{da}} \mathrm{CyS}^- + \mathrm{DHA} + \mathrm{NO}\uparrow \tag{6.4}$$

The major difference between these reactions and the reactions in Chapter 4 is that both CyS^- and CySNO are immobilized on the polymer rather than in solution. Additionally,

the oxidation reactions (Equations 4.20 and 4.23) of CyS^- were ignored since, as mentioned above, CyS^- oxidation is not as likely in a blood system due to reducing agents.

Figure 6.1 Simulation of CySNO surface concentration time profile when PET-CySH contacts a constant concentration of HSANO. A continuously reduced CySH was assumed.

According to the above reactions, the rate of [CySNO] change is:

$$\frac{d[CySNO]}{dt} = k_f[HSANO][CySH]_T - k_r[CySNO][HSA]_T - k_{dc}[CySNO] - k_{da}[CySNO][AA] \tag{6.5}$$

where $[CySH]_T$ and $[HSA]_T$ are the total thiol concentrations composed of both the thiol and thiol anions that are in equilibrium (see Chapter 4, section 4.3.3). It should be noted that [HSANO] and [HSA] are volumetric concentrations while [CySH] and [CySNO] are surface concentrations. Based on a k_{da} value of 0.00094 $\mu M^{-1}hr^{-1}$ [Holmes and Williams 2000] and a maximum AA physiological concentration of 60 μM [Khaw *et al.* 2001; Jamaati *et al.* 2006], $k_{da}[AA]_{max}$ is 0.0564 hr^{-1}. For k_{dc} of 2.4 hr^{-1} in the presence of 50 μM AA (which is the blood concentration), $k_{dc} >> k_{da}[AA]_{max}$. Thus, the k_{da} term is negligible and Equation 6.5 can be simplified to:

$$\frac{d[CySNO]}{dt} = k_f[HSANO][CySH]_T - k_r[CySNO][HSA]_T - k_{dc}[CySNO] \tag{6.6}$$

When CySNO is at steady state as discussed above, Equation 6.6 becomes:

$$k_f[HSANO][CySH]_T - k_r[CySNO][HSA]_T - k_{dc}[CySNO] = 0 \tag{6.7}$$

Because the mass balance for cysteine is:

$$[CySH]_T = [CySH]_0 - [CySNO] \tag{6.8}$$

where $[CySH]_0$ is the initial CySH concentration, Equation 6.8 can be substituted into Equation 6.7 to give:

$$k_f[HSANO]_T([CYSH]_0 - [CySNO]) - k_r[CySNO][HSA]_T - k_{dc}[CySNO] = 0 \quad (6.9)$$

Rearrangement provides an estimate for the steady state CySNO concentration as a function of the original CySH loading on the polymer ($[CySH]_0$) and the amount of S-nitroso albumin (HSANO) or albumin (HSA) in blood according to:

$$[CySNO] = \frac{[CySH]_0}{1 + \frac{k_r}{k_f}\frac{[HSA]_T}{[HSANO]} + \frac{k_{dc}}{k_f[HSANO]}} \quad (6.10)$$

To further simplify Equation 6.10, the total albumin concentration (HSANO + HAS) in blood is approximately 44g/L [Rodriguez-Segade *et al.* 2005] and [HSANO] is below 0.2 μM [MacArthur *et al.* 2007]. Accordingly, [HSA] is approximately 667 μM. (based on HSA MW of 66 kDa [Zunszain *et al.* 2003]). As shown in Chapter 4, k_f is of the same order as k_r, thus $\frac{k_r}{k_f}\frac{[HSA]}{[HSANO]} >> 1$. Therefore, Equation 6.10 can be simplified to:

$$[CySNO] = \frac{[CySH]_0}{\frac{[HSA]}{K} + \frac{k_{dc}}{k_f}}[HSANO] \quad (6.11)$$

where K is the equilibrium constant, equal to k_f/k_r, for the reversible transnitrosation.

Once CySNO can be approximated, the approximation can be using in the HSANO balance which is:

$$\frac{d[HSANO]}{dt} = -k_f[HSANO][CySH]_T \cdot \frac{S}{V} + k_r[CySNO][HSA]_T \cdot \frac{S}{V} - k_{db}[HSANO] \quad (6.12)$$

where S denotes the surface area and V denotes the volume of the liquid. Substituting Equation 6.7 into Equation 6.12 followed by substituting Equation 6.11 into the resulting equation gives:

$$\frac{d[HSANO]}{dt} = -\frac{[CySH]_0}{\frac{[HSA]}{K \cdot k_{dc}} + \frac{1}{k_f}} \cdot \frac{S}{V} \cdot [\text{HSANO}] - k_{db}[HSANO] \tag{6.13}$$

Since [HSA]>>[HSANO], HSA will likely remain at the concentration in blood due to rapid equilibrium between HSANO and HSA during transnitrosation. Thus, Equation 6.13 can be simplified to

$$-\frac{d[HSANO]}{dt} \cdot \frac{V}{S} = k_{A,S}[HSANO] = R_{A,S} \tag{6.14}$$

where $k_{A,S} = \frac{[CySH]_0}{\frac{[HSA]}{K \cdot k_{dc}} + \frac{1}{k_f}} + k_{db}\frac{V}{S}$.

The first term of $k_{A,S}$ is the polymer surface consumption rate of HSANO and the second term is the self-decomposition consumption rate of HSANO in the bulk solution. The total consumption rate is $R_{A,S}$ (in mol/(area·time)). As noted, $R_{A,S}$ can be approximated as a first-order irreversible reaction for HSANO under physiological conditions. As shown below for the model conditions, the second term of $k_{A,S}$ is negligible such that $k_{A,S}$ represents only the consumption at the surface.

For modeling transnitrosation and NO release in a tube through which a solution continuously flows, the model is described by a tube which has CySH coated on the inner wall. A mixture of HSANO and HSA passes through the tube (Figure 6.2). The reactions (Equations 6.2 through 6.4) only occur on the surface. Thus, the consumption of HSANO

(Equation 6.14) appears only in the boundary condition, not in the mass balance equation of the bulk liquid.

Thus, for HSANO in the bulk solution, the continuity equation is [Bird *et al.* 2006]:

$$\rho\left(\underline{\frac{\partial C_A}{\partial t}}+v_r\underline{\frac{\partial C_A}{\partial r}}+\frac{v_\theta}{r}\underline{\frac{\partial C_A}{\partial \theta}}+v_z\frac{\partial C_A}{\partial z}\right)=\rho D_A\left[\frac{1}{r}\frac{\partial}{\partial r}\left(r\frac{\partial C_A}{\partial r}\right)+\frac{1}{r^2}\underline{\frac{\partial^2 C_A}{\partial \theta^2}}+\underline{\frac{\partial^2 C_A}{\partial z^2}}\right]+\underline{r_A}$$

(1) (2) (3) (3) (4) (5)

(6.15)

where C_A denotes the HSANO concentration, ρ is the density of the fluid and D_A is molecular diffusivity of HSANO. The following assumptions were made to simplify Equation 6.15:

1) Steady State for C_A: $\frac{\partial C_A}{\partial t}=0$.
2) No convective transport of reactant toward the wall: $v_r = 0$.
3) Reactant concentration profile is angularly symmetric: $\frac{\partial C_A}{\partial \theta}=0$.
4) Axial diffusion can be neglected compared to axial convection: $\frac{\partial^2 C_A}{\partial \theta^2}=0$.
5) No reaction in the bulk liquid: $r_A = 0$. Convective transport vanishes on the stationary surface. Thus, the mass transfer of A towards the inner wall of the tube equals the consumption rate of A on the surface.
6) Constant ρ and D_A.

Based on the above assumptions, the fives terms which are underscored can be neglected, resulting in the following partial differential equation (PDE):

$$v_z \frac{\partial C_A}{\partial z} = D_A \frac{1}{r} \frac{\partial}{\partial r}\left(r \frac{\partial C_A}{\partial r} \right) \tag{6.16}$$

For laminar flow, the velocity profile is a function of the radius location in the tubes [Polyanin *et al.* 2001]:

$$v_z(r) = 2\bar{v}\left[1 - \left(\frac{r}{R} \right)^2 \right] \tag{6.17}$$

where v_z is the axial velocity, R is the inner radius of the tube, and $\bar{v}$ is the average velocity within the tube. Substituting Equation 6.17 into Equation 6.16 gives:

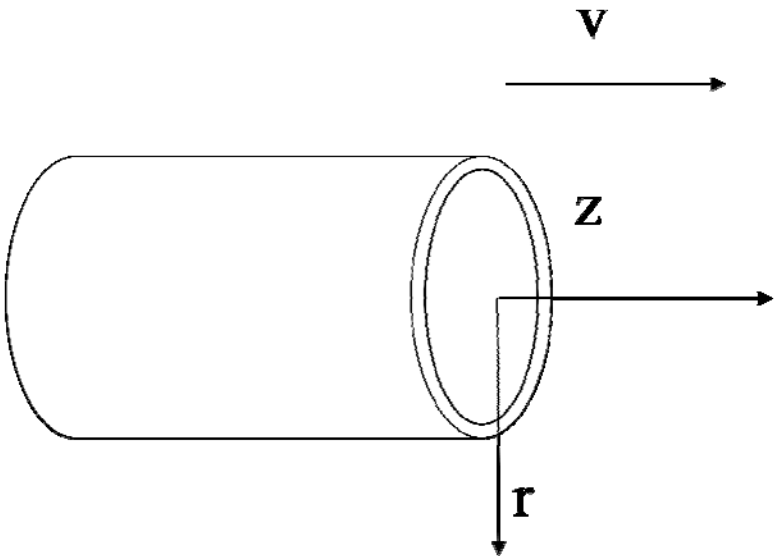

Figure 6.2 Modeling geometry. A round tube with CySH coated on the inner war of the tube was assumed with blood flowing inside the tube with a laminar flow pattern of velocity v. A cylindrical coordinate system with z for the axial axis and r for the radius axis is used.

$$2\overline{v}\left[1-\left(\frac{r}{R}\right)^2\right]\frac{\partial C_A}{\partial z}=D_A\left(\frac{1}{r}\frac{\partial C_A}{\partial r}+\frac{\partial^2 C_A}{\partial r^2}\right) \tag{6.18}$$

Rearrangement gives:

$$D_A\frac{\partial^2 C_A}{\partial r^2}=\frac{2\overline{v}}{R^2}\left[R^2-r^2\right]\frac{\partial C_A}{\partial z}-\frac{D_A}{r}\frac{\partial C_A}{\partial r} \tag{6.19}$$

The boundary equations to solve Equation 6.19 are:

At z=0 and r>0, $C_A(r) = C_{A0} = 2\times10^{-4}$ mol/m^3 (the concentration of HSANO in blood)

At r=R and z>0, $k_{A,s}C_A=-D_A\frac{\partial C_A}{\partial r}$

At r=0 and z>0, $C_A(z) = C_{A0} = 0.2$ μmol/m^3. This latter boundary condition was initially assumed and then validated with the modeling results. Generally, this assumption implies that very little HSANO is consumed in the bulk solution.

When solving a model, it is best to use a non-dimensional form of the model. With r=γR, $C_A=\varphi C_{A0}$ and z=ζL, Equation 6.19 becomes:

$$\frac{\partial^2\varphi}{\partial\gamma^2}=\kappa\left(1-\gamma^2\right)\frac{\partial\varphi}{\partial\zeta}-\frac{1}{\gamma}\frac{\partial\varphi}{\partial\gamma} \tag{6.20}$$

where, $\kappa=\frac{2\overline{v}R^2}{D_AL}$

The associated boundary conditions become:

at ζ=0 and γ>0, $\varphi(\gamma)=\varphi_0=1$

at γ=1 and ζ>0, $k_{A,s}\varphi=\frac{-D_A}{R}\frac{\partial\varphi}{\partial\gamma}$

Since γ cannot be 0 in the second term on the right hand side of Equation 6.20, a very small value of γ was chosen as the boundary condition for γ=0:

at γ=0.000001 and ζ>0, $\varphi(\zeta)=1$.

By solving the above PDE numerically in MathCAD (PTC, Needham, MA), the C_A concentration profile within the tube can be predicted as a function of γ and ζ. The surface concentration of C_A can then be used to calculate the CySNO surface concentration by Equation 6.11. Finally, the estimated NO flux can be calculated according to:

$$[NO]_{flux} = k_{dc}[CySNO] \tag{6.21}$$

The following parameters were used for the model. Since BSA has a diffusivity of 5×10^{-7} cm^2/s [Cha and Beissinger 1996] and BSA has a similar molecular structure as HSANO, the diffusivity of HSANO was assumed to be the same. The radius was chosen to be similar to an artery with a radius of 0.2 cm. For this size of an artery, the average velocity is around 10 cm/s [Stoner *et al.* 2004]. The length of the polymer tube was chosen as 1 m. Although this length is extremely long for polymer applications, this length would give a good idea as to how the HSANO concentration and NO flux change through the polymer tube. Based on the above information, κ in Equation 6.20 is 16,000.

To estimate $k_{A,S}$ (Equation 6.14) used in the boundary condition, the constant cysteine surface concentration, $[CySNO]_0$, was chosen as 4 $nmol/cm^2$, which was a typical value shown in Chapter 5 and was also a typical surface concentration used in previous platelet inhibition studies in which incomplete inhibition was observed [Duan and Lewis 2002; Gappa-Fahlenkamp and Lewis 2005]. [HSA] was assumed to be the typical value in blood which is 667 μM. K was assumed to be 0.66 as measured from the free solution transnitrosation studies in Chapter 4. The value of k_{dc} was assumed to be 2.4 hr^{-1}, which was the average value for the free transnitrosation studies in Chapter 4 involving 50 μM AA (which is the typical concentration in blood). The validity of this

assumption is shown in Section 6.3.1. The k_{db} value is 0.001 hr^{-1} from experimental conditions as shown in section 6.3.1. Finally, $k_f = 0.33\ \mu M^{-1}hr^{-1}$ from the free transnitrosation studies of Chapter 4 was used (see discussion section to validate this reasoning). Based on these values, $k_{A,S}$ is approximately 0.0096 cm/hr of which the k_{db} term of Equation 6.14 only contributed to 1% of the value. Thus, the $k_{A,S}$ term is representative of just the consumption of HSANO at the polymer surface, which was assumed for the boundary condition. As an additional point, the k_f contribution was negligible such that $k_{A,S}$ is only strongly dependent upon K, [HSA], and k_{dc}.

6.3 Results

6.3.1 Transnitrosation between BSANO and Immobilized CySH

Figure 6.3 shows the BSANO concentration profile when BSANO was incubated with CySH-modified PET. Also, the BSANO concentration time profile (without CySH modified PET) is also shown in the graph for comparison. The BSANO profile without the polymer showed a first order decay constant, k_{db}, of 0.001 hr^{-1}, which is consistent with previous results in Chapter 4 (0.002 hr^{-1}). However, the BSANO concentration decreased significantly when CySH-modified PET existed in the system, indicating that transnitrosation followed by CySNO decomposition (on surface or in solution) played an important role.

As shown in Figure 6.4, the CySH surface concentration during transnitrosation dropped very fast within the first 6 hours (about 60% loss) and then began to stabilize. According to Figure 5.5 where no transnitrosation occurred, the CySH loss from bond instability appeared to be only 30%. Therefore, the “apparent” increase in CySH loss

during transnitrosation may be a result of some of the CySH on the polymer being converted to CySNO and this CySNO is likely not detected by the chemiluminescence method as mentioned in section 6.2.2.

When the CySH surface concentration remained approximately constant (between 7 and 60 hours), the BSANO concentration showed a decrease with a constant slope of 0.446 μM/hr. This constant slope indicates a pseudo-steady state CySNO (and CySH) concentration which is similar to the simulation in Figure 6.1. It should be noted that although bond instability was observed at early times in Chapter 5, bond instability was not as appreciable between 6 and 30 hours, leading to the possibility of CySNO reaching pseudo-steady state value. At this point, all of the change in BSANO would be equivalent to the NO release rate, such that

$$\frac{d[BSANO]}{dt} = -k_{dc}[CySNO]\frac{S}{V} \tag{6.22}$$

The NO release rate was obtained from Equation 6.22. The left side of Equation 6.22 is the constant slope of -0.446 μM/hr noted above. S is 2 cm^2 and V is 2 mL. To approximate [CySNO], the [CySH] value of 7 nmol/cm^2 (see Figure 6.4) was used. Since the polymer initially had 24 nmol/cm^2, and approximately 60% is lost after 30 hours due to hydrolysis (see Figure 5.5), then that should leave 9.6 nmol/cm^2 on the surface. Therefore, [CySNO] should be approximately 2.6 nmol/cm^2. Based on this, k_{dc} is calculated to be 0.17 hr^{-1}. This is very close to the value of 0.22 hr^{-1} observed in Chapter 4 for free transnitrosation in the absence of AA (see Table 4.4). Thus, it appears that immobilization doesn't significantly change the constant. Therefore, the value of k_{dc} used in the model, based on 50 μM AA, was assumed to be the same as observed in Chapter 4 for free transnitrosation.

Figure 6.3 BSANO concentration change during transnitrosation with immobilized cysteine (using PET-N(i)-CySH). (n=2) Solid diamond: BSANO without PET-N(i)-CySH, Solid square: BSANO with PET-N(i)-CySH, dashed line is the first order decay model for the data based on Equation 4.16.

Figure 6.4 CySH surface concentration (PET-N(i)-CySH) change during transnitrosation with BSANO. (n=2) The CySH surface concentration dropped very fast within the first 6 hours and then slowed down. CySH loss within 6 hours (~60%) is more than that of Figure 5.5 (~30%).

From this study, the initial surface concentration of CySH was measured as 24 nmol/cm^2. Based on Equation 6.1 and the initial slop of the BSANO concentration profile, together with the initial BSANO concentration, k_f was calculated to be 0.0037 $\mu M^{-1}hr^{-1}$. This value is much lower than the value for free solution transnitrosation as calculated in Chapter 4 (0.33 $\mu M^{-1}hr^{-1}$) but is within the wide range reported in Table 4.1. The significantly lower value suggests that immobilization reduced the effectiveness of transnitrosation. As noted in the discussion section, the reduced effectiveness may have been due to mass transfer limitations.

6.3.2 Transnitrosation Modeling in Flow System

The results for the model simulation are shown in Figure 6.5. The dimensionless HSANO concentration is also indicated by the darkness of the grey color (the deeper color for higher concentration). It shows that concentration drops slightly near the wall and the outlet of the tube has a greater concentration gradient than the inlet of the tube. In order to get a more detailed concentration profile near the wall, a contour graph of the dimensionless concentration focusing on the dimensionless radius range from 0.9 to 1 (Figure 6.6) shows the concentration drop between the bulk solution and the surface. The maximum concentration drop is around 5%, which occurs at the outlet of the tube. As noted, the concentration in the bulk solution remains the same as the inlet, thus validating the boundary condition at r=0.

Based on the dimensionless HSANO concentration profile near the wall, the NO flux was calculated by Equation 6.11 and 6.21. Figure 6.7 shows the NO flux based on the simulated HSANO concentration profile near the inner wall of the tube. The NO flux is virtually constant throughout the entire tube, a little higher than 5.2×10^{-12} mol/(m^2·s),

Figure 6.5 Dimensionless simulation of Human Serum albumin (HSANO) concentration profile within a tube with inner surface covered with Cysteine (CySH). The graph shows only the concentration near the wall ($0.8 \leq \gamma \leq 1$), since the concentration is essentially constant throughout the tube except near the wall. The depth of grayscale indicates the dimensionless concentration (the darker for the lower concentration).

while the minimum NO flux to inhibit platelet adhesion is around $3\text{-}6\times10^{-12}$ mol/(m^2·s) [Ramamurthi and Lewis 2000]. Therefore, the polymer used in previous experiments may have been sufficient to minimize platelet adhesion. However, uncertainties in physiological conditions, such as the HSANO concentration (as shown in Table 6.1), exert significant impact on the NO flux, leading to possible insufficient NO flux as discussed in detail later.

6.4 Discussion

6.4.1 Transnitrosation Reaction between BSANO and Immobilized CySH

Although the CySH modified polymer used for this analysis is an unstable polymer with CySH detaching from the polymer surface with time, it still showed that the modified polymer is capable of continuously transferring NO. For instance, according to Figure 6.3, 90 nmol of BSANO was transferred in the 2 ml solution compared to the 48 nmol of initial CySH on the polymer. Thus, even without ascorbic acid, CySH on the polymer performs better than free CySH in solution since CySH in solution only could transfer less NO than the amount of CySH. This finding is probably due to the reason that immobilized CySH, even if it forms a thiol radical (which is the oxidation product of thiol anion by either Cu^{2+} [Dicks *et al.* 1996] or O_2 [Ehrenberg *et al.* 1989]), may not be easy to react with each other as a result of steric hindrance to form a disulfide bond (CyS-CyS). Instead, the unreacted thiol may be reduced from other molecules (e.g. free thiol group on BSA) to form reduced cysteine.

As noted above, the transnitrosation kinetics data was different between the free solution study and the immobilized study. The value of k_f for the immobilized study was

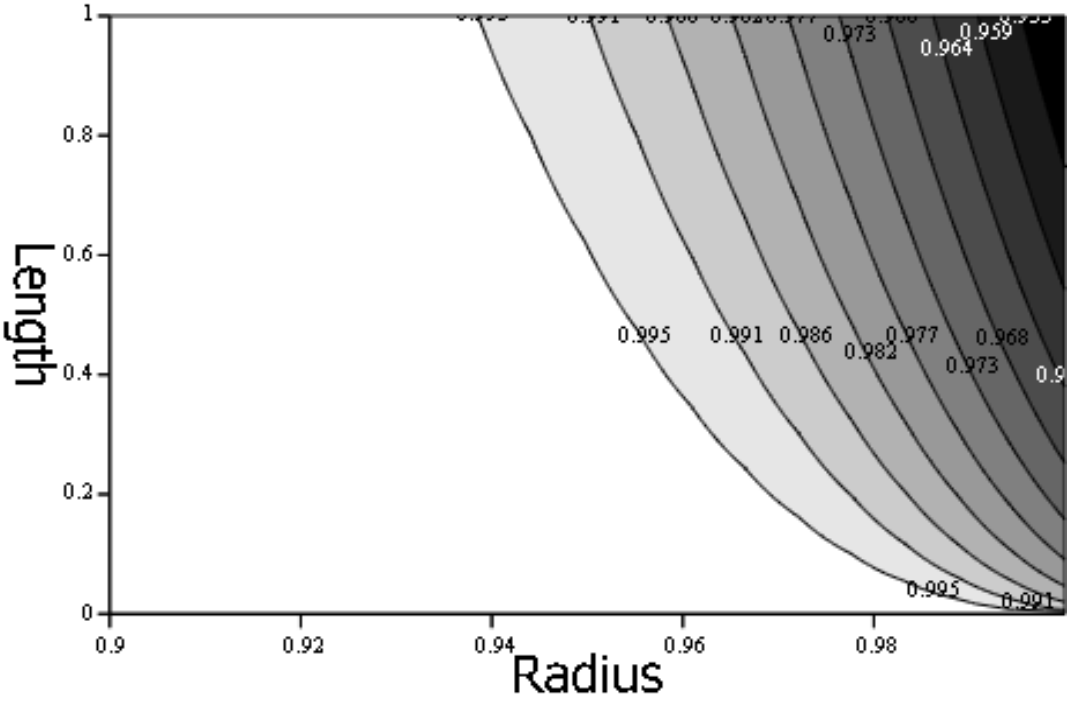

Figure 6.6 2-D contour (with concentration gradient) graph for dimensionless simulation of HSANO concentration profile within a tube with inner surface covered with CySH. The depth of the darkness indicates the concentration (lighter for higher concentration and darker for lower concentration). The graph shows part of the tube which is near the wall (dimensionless radius from 0.9 to 1). The number on the contour line is the dimensionless concentration.

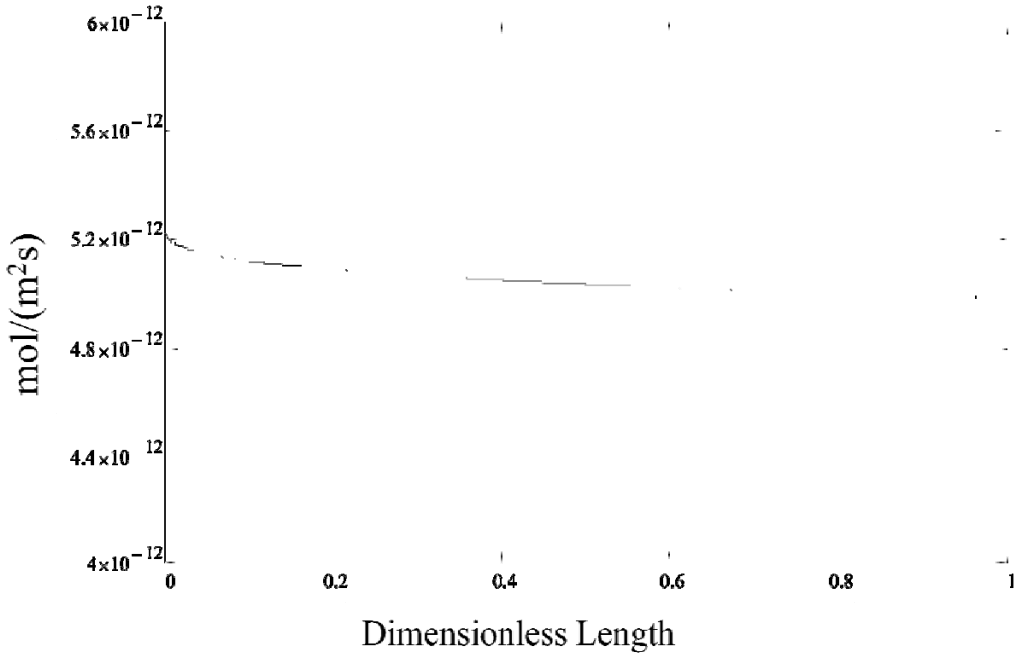

Figure 6.7 NO flux profile along the length of the tube at the inner wall surface (γ=1) of the tube calculated from the dimensionless simulation of Human Serum albumin (HSANO) concentration profile within a tube with the inner surface covered with Cysteine (CySH).

Table 6.1 S-nitroso human serum albumin (HSANO) concentration in plasma.

Concentration	Method	Reference	Note
181±150 nM	GC-MS + $HgCl_2$	[Tsikas *et al.* 1999]	
4.2±1 μM	Fluorometric Assay	[Tyurin *et al.* 2001]	non-pregnancy women
156±64 nM	GC-MS + $HgCl_2$	[Tsikas *et al.* 2002]	
205±96 nM	GC-MS + cysteine/$CuSO_4$	[Tsikas *et al.* 2002]	
62±24 nM	HPLC + Saville	[Jourd'heuil *et al.* 2000]	
7.2±1.1 nM	Chemiluminescence	[Rassaf *et al.* 2003]	
0.59±0.31 nM	Chemiluminescence	[Wang *et al.* 2004]	

approximately two orders of magnitude smaller than the free solution value. One possibility of the lower value, compared to free transnitrosation, is that mass transfer is controlling the rate rather than kinetics. Since BSANO is a large molecule and the nitrosated cysteine residue (Cys-34) is located in the center of the BSA molecule [Gryboś *et al.* 2005], the immobilized CySH within the cracks of the polymer (ethylenediamine forms crack on PET) might not be able to easily come in contact with BSANO.

According to Equation 6.1 and the measured initial values and slope, the far right side of the equation (self decomposition) is negligible. Thus, Equation 6.1 can be rewritten as:

$$\left[\frac{d[BSANO]}{dt}\right]_0 = -k_f\left[BSANO\right]_0\left[CySH\right]_0 = -k\left[BSANO\right]_0 \qquad (6.23)$$

where $k=k_f[\mathrm{CySH}]_0$. It is interesting to note that Equation 6.23 is also consistent with a model for mass transfer limitations where k is the volumetric mass transfer coefficient for BSANO. In other words, mass transfer limitations could result in an "apparent" k_f that is lower than a "true" k_f and the apparent k_f would be related to the slower mass transfer rate. This appears to be a likely explanation for the lower k_f and further work would need to be performed to test this hypothesis. From a modeling standpoint, the model parameters noted at the end of Section 6.2 assumed a k_f of 0.33 $\mu M^{-1}hr^{-1}$ (from free transnitrosation) rather than the apparent value shown above. The reason is that the model must include the "true" value of k_f to accurately represent the reaction at the surface as the diffusivity of the HSANO has already been included in the model.

Unlike the transnitrosation kinetics, the NO release (i.e., CySNO decomposition) rate constant was similar to the free CySNO decomposition rate constant. This seems

feasible since the rate is primarily a function of the copper ion which should easily be able to come into contact with the polymer due to its small size.

6.4.2 Factors that influence NO flux from the CySH modified polymer

There are numerous environmental factors that can affect the NO flux from the polymer. The HSANO concentration might be the most important one according to Equations 6.11 and 6.21 which shows that the predicted HSANO concentration will significantly affect the NO flux. So far there are still significant inconsistencies regarding the HSANO concentration in blood [Rassaf *et al.* 2003; Giustarini *et al.* 2007]. Table 6.1 shows recent results with the range from sub-nM to μM. Thus, if the HSANO concentration is lower than the simulation value (200 nM), the NO flux will decrease significantly. For example, if assuming the HSANO concentration is one-tenth of 200 nM (20 nM), the NO flux would be reduced to around 0.52×10^{-12} mol/(m^2·s), although the NO flux will still remain almost constant throughout the tube (figure not shown here). This NO flux is one order of magnitude less than the minimum required NO flux to inhibit platelet inhibition. According to Table 6.1, most of the reported HSANO concentrations are below 200 nM, with an average concentration of 102 nM (not including the 4.2 μM value, because of the potential artifact reported for this flurorimetric analysis [Giustarini *et al.* 2007]). Therefore, with this average value, the predicted NO flux is estimated to be 2.6×10^{-12} mol/(m^2·s), which will likely still cause incomplete platelet inhibition. Thus, for the previous incomplete inhibition, the possible reason could be the low HSANO concentration in the blood. However, this assumption needs to be verified in the future.

Another important parameter in the model is the initial surface CySH concentration. The 4 nmol/cm^2 used in the simulation is the ethylenediamine treated polymer used by Duan and Fahlenkamp [Duan and Lewis 2002; Fahlenkamp 2003], which had a lot of cracks to increase the cysteine surface concentration. The theoretical CySH concentration on the polymer should be around 1 nmol/cm^2, unless a branch structure can be formed on the polymer by attaching a molecule with multiple thiol groups. Under the condition of 1 nmol/cm^2 CySH initial concentration, the NO flux would be around 1.3×10^{-12} mol/(m^2·s), which is much less than the minimum required flux. Therefore, in order to make a polymer with complete platelet inhibition and good mechanical and chemical stability, attaching a compound with multiple thiol groups or forming branches with multiple activation sites on the polymer surface might be the direction for future research.

To test the sensitivity of the decomposition rate constant k_{dc} effect on NO flux, the value of k_{dc} was set to 6.6 hr^{-1} which was the highest value measured previously in Chapter 4, Table 4.4., the NO flux will be around 13×10^{-12} mol/(m^2·s) throughout the tube. Compared to the NO flux prediction (k_{dc}= 5.2×10^{-12} mol/(m^2·s)) at the base value (2.4 hr^{-1}), the model is also sensitive to k_{dc} which is also a strong function of the copper ion concentration. Under physiological conditions, metal ions are usually in bound form. For example, the majority of the copper is bound to ceruloplasmin while the rest is bound to serum albumin or amino acid [Twomey *et al.* 2005]. Although the bound copper can still catalyze NO release from CySNO, the catalyzing rate is significantly reduced [Dicks and Williams 1996]. Therefore, the k_{dc} could be much lower *in vivo* compared to the

value measured in chapter 4 which could be a potential problem for the modified polymer.

For the flow rate and tube diameter, these parameters only affected the HSANO concentration profile (figure not shown here) within the tube but not on the surface of the wall (which is reasonable because reaction takes place on the wall).

6.5 Conclusions

In this chapter, BSANO transnitrosation with immobilized CySH was studied in a batch system using the polymer (PET-N(i)-CySH). A mathematical model for predicting the NO flux from the modified polymer surface in a tubular flow system was established and various factors which can influence the NO flux were evaluated. The key findings are:

1) Cysteine on the polymer performs better (transferring more NO from BSANO) than cysteine in the solution even without the help of ascorbic acid.
2) The immobilized transnitrosation reaction appeared to be mass transfer limiting, likely due to the cracks on the polymer, as the k_f value was two orders of magnitude smaller than the free solution transnitrosation value. This may be a result of BSANO being a large molecule and cannot easily diffuse into the cracks. However, these cracks do no effect the surface CySNO decomposition since k_{dc} remained almost the same compared to the free transnitrosation studies.
3) Modeling showed that HSANO and CySH have the most significant effect on the NO flux. Increasing either of them will cause a significant NO flux increase. Also the kinetic constant of k_{dc} could also affect the NO flux rate. However, the

flow rate and tube diameter does no effect the NO flux, they only change the bulk HSANO concentration profile.

4) The modeling results indicate that previous incomplete platelet inhibition by a CySH modified polymer (PET-N(i)-CySH) may likely be due to the low HSANO concentration in blood since the reported HSANO level in the plasma has a wide range (about two orders of magnitude). As the HSANO concentration decreases, the NO flux becomes insufficient if the actual HSANO concentration is about half of the 200 nM value. However, it is still possible to make a successful platelet-inhibiting polymer with good chemical and mechanic stability by attaching a compound with multiple thiol groups or introducing branch structures with multiple activation sites on the polymer for attaching thiol molecules. Such action could increase the NO flux significantly.

CHAPTER 7

CONCLUSIONS AND FUTURE WORK

The haemocompatibility of biomaterials has always been a major issue which interferes with the performance of a medical device and causes severe health threat for patients, especially for the long term applications, as a result of platelet adhesion and aggregation on the material surface. Current treatment of this problem includes systematic administration of heparin and material surface modification with functional groups. Both of these two methods have their own limitations or side effects. For example, heparin treatment can cause side effects, such as platelet depletion, which can lead to thrombocytopenia and hemorrhage [Annich *et al.* 2000]. On the other hand, surface modifications with functional groups always suffer from incomplete platelet inhibition or short term performance [Bamford and Al-Lamee 1992]. Nitric oxide (NO), a small signal messenger, has been found to be a key player for platelet inhibition. NO is naturally secreted by endothelia cells to prevent platelet adhesion to the blood vessel [Feldman 1993; Vaughn *et al.* 1998]. Thus, in order to mimic this unique property of blood vessels, a L-cysteine (CySH)-modified polymer was previously developed which can utilize endogenous NO to inhibit platelet adhesion through transnitrosation followed by fast S-nitrosocysteine (CySNO) decomposition. However, the experimental results

showed only 60% inhibition, rather than complete inhibition [Duan and Lewis 2002; Gappa-Fahlenkamp and Lewis 2005].

In this work, in order to reveal the reason for the incomplete platelet inhibition, the mechanism of transnitrosation followed by decomposition, as well as the stability of the polymer, was studied in detail. Several alternative immobilization methods were also evaluated and compared to the previous method. Finally, a kinetic model for predicting the NO flux from the polymer surface was established and various environmental effects on the NO flux were evaluated and compared to the previously identified minimum NO flux required for platelet inhibition [Ramamurthi and Lewis 2000].

7.1 Major Accomplishments of the Study

The ultimate goal of this work was to study the transnitrosation kinetics between BSANO in solution and immobilized CySH, as well as the NO release from immobilized CySNO. Following the experimental studies, a mathematical model was developed to predict the NO flux from the CySH-modified polymer under various conditions. By comparing the predicted NO flux with the minimum required NO flux established earlier, the direction for future improvement of the polymer could be established. The significant findings from this work are listed as follows.

- CySNO decomposition (which includes NO release) maximizes near physiological pH regardless of the buffer due to trace metal ions existing in all buffer salts. The buffer purity and chelating agent greatly affects the decomposition rate, especially at near physiological pH. A model involving metal ions and the associated equilibrium between different forms of the metal

ions agreed well with experimental observations. The model provided a plausible explanation for the pH dependence on CySNO decomposition.

- An improved nitrite/S-nitrosothiol detection method based on ammonium sulfamate pre-treatment and KI/I_2-based chemiluminescence method was established, which gave less standard error and more data consistency.
- Transnitrosation between BSANO and free CySH was found to be sensitive to various reductants and oxidants. Oxygen and Cu^{2+} both can oxidize CySH, while ascorbic acid can react with Cu^{2+} so that less CySH will be oxidized. The NO transferred from BSANO increases significantly when the ascorbic acid concentration increases. A mathematic model which included transnitrosation between BSANO and CySH, CySNO decomposition and CySH oxidation was developed to model the experimental data. The results showed that the model described the transnitrosation reactions very well. Experimental results showed that ascorbic acid increases the CySNO decomposition rate constant and reduces the CySH oxidation rate constant, which is consistent with the reaction mechanisms. Model sensitivity analysis showed that the transnitrosation rate constants k_f and k_r, and the CySNO decomposition rate constant k_{dc}, have the most impact on the BSANO concentration time profile. However, the ascorbic acid oxidation rate constant k_{oa} has less influence.
- The previous protocol for making immobilized CySH on PET (PET-N(i)-CySH) lead to an unstable polymer due to imine bond breakage between either CySH and glutaraldehyde or glutaraldehyde and the amine on PET.

Amide bond formation using DCCI or EDC coupling increased the stability of the modified polymer in acidic condition. However at neutral pH, some of the modified polymer still showed bond breakage and only one of the newly developed polymers (ethylenediamine treatment followed by EDC coupling) showed good bond stability in both acidic and neutral pH. In addition to bond stability issues, cysteine on all the polymers can also be oxidized slowly just as the free cysteine oxidation which followed zero order kinetics in solution. Different immobilization methods appear to have a significant effect on the oxidation rate constant.

- Ethylenediamine treatment can cause substantial amounts of cracks on PET surfaces and the higher concentration of ethylenediamine used, the bigger the cracks. Also, the PET thickness is reduced significantly after ethylenediamine treatment which potentially affects the mechanical properties or the stability of the modified polymer. Immobilized CySH on PET-N(i)-CySH polymer is susceptible to light and air under dry conditions. However light or air alone does not cause CySH oxidation. This oxidation was found to be represented by a 3^{rd}-order decay reaction with regard to the CySH surface concentration, but a detailed mechanism remains unsolved. It was also discovered that CySH-modified PET can be stored in an amber vial at -20 ˚C for about 2 months without noticeable oxidation.
- The transnitrosation reaction between the CySH modified polymer (PET-N(i)-CySH) and BSANO showed that cysteine on the polymer performs better

(transferring more NO from BSANO) than cysteine in the solution even without the help of ascorbic acid.

- The transnitrosation reaction could be affected by mass transfer limitations as the k_f value was two orders of magnitude smaller than the free solution transnitrosation value. This may be a result of BSANO being a large molecule and cannot easily diffuse into the cracks. However, these cracks do not affect the surface CySNO decomposition since k_{dc} remained almost the same compared to the free transnitrosation studies.
- Modeling of CySH modified polymer contacting blood in a tubular flow system showed that the S-nitroso-human albumin (HSANO) concentration and CySH surface concentration have the most significant effect on the NO flux prediction. Also the kinetic constant of k_{dc} could also affect the NO flux rate. However, the flow rate and tube diameter primarily only change the bulk HSANO concentration profile. The model also predicts that using the CySH modified polymer made by previous researchers in this group (PET-N(i)-CySH with about 4 nmol/cm2 CySH surface concentration) may not achieve complete platelet inhibition mainly because of the low HSANO concentration in the blood. The HSANO level has been reported to range from 0.6 nM to 200 nM, based on different analysis methods. The NO flux will be insufficient if the actual concentration is about one-half of the 200 nM value. However, this assumption needs to be verified by accurately measuring the HSANO concentration in blood, which is very challenging so far.

7.3 Future Work

In order to improve the performance of the CySH-modified polymer in physiological conditions for long terms, there are still many issues that need to be addressed.

- A modified polymer is needed that has both structural integrity and stable bonds. In order to make a polymer with both good mechanical integrity and bond stability, two approaches can be attempted in the future: a) introduce amine groups on the PET without destroying the polymer and then do the EDC coupling or b) find a water soluble thiol protected CySH (which can later be deprotected) and attach it to carboxylated PET using the EDC method.
- Transnitrosation kinetics between the modified polymer and CySNO decomposition at 37 ˚C need to be studied to predict the NO flux. The current studies were only at 25 ˚C and the kinetics of transnitrosation and CySNO decomposition reaction rate constants are likely to be different due to a change in the temperature.
- Glutathione effects on cysteine oxidation need to be studied since glutathione is a much stronger reducing agent compared to ascorbic acid. Glutathione is present in the blood [Svardal *et al.* 1990; Flagg *et al.* 1993; Lim *et al.* 1995] and has been used to reduce various thiol compounds. The transnitrosation under both ascorbic acid and glutathione also needs to be studied so that a more detailed and realistic kinetic model can be established.
- An unsteady state model for the flow system needs to be developed to predict the temporal profile of the NO flux. The model can further be improved by including

a laminar pulse flow pattern that is more consistent with blood flow as compared to the constant flow pattern considered in this work. This change would give a more realistic prediction of the NO flux under physiological conditions.

- Despite the possible low HSANO *in vivo*, which could bring a real challenge for a successful platelet-inhibiting CySH modified polymer, the performance of the CySH-modified polymer can be improved by either modifying the polymer surface with multiple carboxyl groups such as polymethymethacrylate followed by CySH attachment or by immobilizing compounds with multiple thiol groups on the polymer surface. Increasing CySH can significantly increase the NO flux, therefore compensating for the negative effect from the low HSANO concentration.

REFERENCES

Abukhalaf IK, NA Silvestrov, JM Menter, DA von Deutsch, MA Bayorh, RR Socci and AA Ganafa (2002). High performance liquid chromatographic assay for the quantitation of total glutathione in plasma. *Journal of Pharmaceutical and Biomedical Analysis* **28**(3-4): 637-643.

Adam C, L Garcia-Rio, JR Leis and L Ribeiro (2005). Nitroso Group Transfer in S-Nitrosocysteine: Evidence of a New Decomposition Pathway for Nitrosothiols. *J. Org. Chem.* **70**(16): 6353-6361.

Aldred SE, DLH Williams and M Garley (1982). Kinetics and mechanism of the nitrosation of alcohols, carbohydrates, and a thiol. *Journal of the Chemical Society, Perkin Transactions 2*: 777-82.

Aleryani S, E Milo, Y Rose and P Kostka (1998). Superoxide-mediated Decomposition of Biological S-Nitrosothiols. *J. Biol. Chem.* **273**(11): 6041-6045.

Amiji M and K Park (1993). Surface modification of polymeric biomaterials with poly(ethylene oxide), albumin, and heparin for reduced thrombogenicity. *Journal of Biomaterials Science, Polymer Edition* **4**(3): 217-234.

Änggård E (1994). Nitric oxide: mediator, murderer, and medicine. *The Lancet* **343**(8907): 1199-1206.

Annich GM, JP Meinhardt, KA Mowery, BA Ashton, I Merz S, RB Hirschl, ME Meyerhoff and RH Bartlett (2000). Reduced platelet activation and thrombosis in extracorporeal circuits coated with nitric oxide release polymers. *Critical care medicine* **28**(4): 915-20.

Aquart DV and TP Dasgupta (2004). Dynamics of interaction of vitamin C with some potent nitrovasodilators, S-nitroso-N-acetyl-,-penicillamine (SNAP) and S-nitrosocaptopril (SNOCap), in aqueous solution. *Biophysical Chemistry* **107**(2): 117-131.

Archer S (1993). Measurement of nitric oxide in biological models. *FASEB J.* **7**(2): 349-360.

Arnelle DR and JS Stamler (1995). NO^+, $NO^\cdot$, and NO^- Donation by S-Nitrosothiols: Implications for Regulation of Physiological Functions by S-Nitrosylation and Acceleration of Disulfide Formation. *Archives of Biochemistry and Biophysics* **318**(2): 279-285.

Ashby B, J Daniel and J Smith (1990). Mechanisms of platelet activation and inhibition. *Hematology/oncology clinics of North America* **4**(1): 1-26.

Askew SC, DJ Barnett, J McAninly and DLH Williams (1995). Catalysis by Cu^{2+} of nitric oxide release from S-nitrosothiols (RSNO). *Journal of the Chemical Society, Perkin Transactions 2*: 741-745.

Aslam M and A Dent (1998). *Bioconjugation: Protein Coupling Techniques for the Biomedical Sciences* New York Grove's Dictionnaries.

Authi KS, SP Watson and VV Kakkar, Eds. (1993). *Mechanisms of Platelet Activation and Control*. Advances in Experimental Medicine and Biology. New York, Plenum Press.

Avny Y and Ludwig Rebenfeld (1986). Chemical modification of polyester fiber surfaces by amination reactions with multifunctional amines. *Journal of Applied Polymer Science* **32**(3): 4009-4025.

Azuma H, M Ishikawa and S Sekizaki (1986). Endothelium-dependent inhibition of platelet aggregation. *Br J Pharmacol* **88**(2): 411-415.

Bagiyan GA, IK Koroleva, NV Soroka and AV Ufimtsev (2003). Oxidation of thiol compounds by molecular oxygen in aqueous solutions. *Russian Chemical Bulletin* **52**(5): 1135-1141.

Bagiyan GA, IK Koroleva, NV Soroka and AV Ufimtsev (2004). Kinetics of the Catalytic Oxidation Reactions of Thiol Compounds in Aqueous Solutions in the Presence of Copper Ions. *Kinetics and Catalysis* **45**(3): 372-380.

Bamford CH and KG Al-Lamee (1992). Chemical methods for improving the haemocompatibility of synthetic polymers. *Clinical Materials* **10**(4): 243-261.

Barany G and RB Merrifield (1979). *The Peptides* E. Gross and J. Meienhofer. New York, Academic Press. **2:** 1-284.

Bennett B, S Kobus, J Brien, K Nakatsu and G Marks (1986). Requirement for reduced, unliganded hemoprotein for the hemoglobin- and myoglobin-mediated biotransformation of glyceryl trinitrate. *J Pharmacol Exp Ther* **237**(2): 629-635.

Beynon RJ (1996). Buffer Solutions: The Basics.

Bhat SV (2002). *Biomaterials*, Kluwer Academic Publishers.

Bickerstaff GF (1997). Characterization of Enzyme Activity, Protein Content and Thiol Groups in Immobilized Enzymes. *Immobilization of Enzymes and Cells*. G. F. Bickerstaff. Totowa, Humana Press Inc.**:** 253-259.

Bird RB, WE Stewart and EN Lightfoot (2006). *Transport Phenomena*, Wiley, John & Sons, Incorporated.

Blockmans D, H Deckmyn and J Vermylen (1995). Platelet activation. *Blood Reviews* **9**(3): 143-156.

Bodanszky M and A Bodanszky (1994). *The Practice of Peptide Synthesis*. Berlin, Springer-Verlag.

Bohl KS and JL West (2000). Nitric oxide-generating polymers reduce platelet adhesion and smooth muscle cell proliferation. *Biomaterials* **21**(22): 2273-2278.

Brant WE (2001). *The Core Curriculum, Ultrasound: Ultrasound*, Lippincott Williams & Wilkins.

Brass LF (1991). The biochemistry of platelet activation. *Hematology: Basic Principles and Practice*. R. Hoffman. New York, Churchill Livingstone Inc.**:** 1177-1193.

Brass LF, JA Hoxie, T Kieber-Emmons, DR Manning, M Poncz and M Woolkalis (1993). Agonist Receptors and G Proteins as Mediators of Platelet Activation. *Mechanisms of Platelet Activation and Control*. K. S. Authi, S. P. Watson and V. V. Kakkar. New York, Plenum Press**:** 17-36.

Brune B, A Knethen and K Sandau (1998). Nitric Oxide and its Role in Apoptosis. *European Journal of Pharmacology* **35**: 261-272.

Bùi LN, M Thompson, NB McKeown, AD Romaschin and PG Kalman (1993). Surface modification of the biomedical polymer poly(ethylene terephthalate). *Analyst* **118**:

463 - 474.
Burg A, H Cohen and D Meyerstein (2000). The reaction mechanism of nitrosothiols with copper(I). *Journal of Biological Inorganic Chemistry* **5**(2): 213-217.
Butler AR, SC Askew, FW Flitney and I Megson (1994). The vasodilator action of S-nitrosoglutathione: Evidence for nitric oxide transfer. *Portland Press Proceedings* **8**(Biology of Nitric Oxide, 4): 259-262.
Butler AR, FW Flitney and DLH Williams (1995). NO, nitrosonium ions, nitroxide ions, nitrosothiols and iron-nitrosyls in biology: a chemist's perspective. *Trends in Pharmacological Sciences* **16**(1): 18-22.
Butler AR and DLH Williams (1993). The physiological role of nitric oxide. *Chemical Society Reviews* **22**(4): 233-41.
Byler DM, DK Gosser and H Susi (1983). Spectroscopic estimation of the extent of S-nitrosothiol formation by nitrite action on sulfhydryl groups. *Journal of Agricultural and Food Chemistry* **31**(3): 523-7.
Carey FA and RJ Sundberg (2007). *Advanced Organic Chemistry: Part B: Reaction and Synthesis*. New York, Springer.
Carter DC and JX Ho (1994). Structure of serum albumin. *Adv Protein Chem.* **45**: 153-203.
Cha W and RL Beissinger (1996). Macromolecular Mass Transport to a Surface: Effects of Shear Rate, pH, and Ionic Strength. *Journal of Colloid and Interface Science* **177**(2): 666-674.
Christopherson KS and DS Bredt (1997). Nitric oxide in excitable tissues: physiological roles and disease. *J Clin Invest* **100**(10): 2424-2429.
Conboy JJH, Joseph H. (1989). Photolytic interface for high-performance liquid chromatography-chemiluminescence detection of nonvolatile N-nitroso compounds. *Analyst (Cambridge, United Kingdom)* **114**(2).
Conrad DR. (2009). "Glutathione in Cell Culture." Retrieved 04/06, 2009, from http://www.sigmaaldrich.com/life-science/cell-culture/learning-center/media-expert/glutathione.html.
Cooney D (1976). *Biomedical Engineering Principles: an Introduction to Fluid, Heat, and Mass Transport Processes*. New York, M. Dekker.
Courtney JM, NMK Lamba, S Sundaram and CD Forbes (1994). Biomaterials for blood-contacting applications. *Biomaterials* **15**(10): 737-744.
De Queiroz AAA, ÉR Barrak, HAC Gil and OZ Higa (1997). Surface studies of albumin immobilized onto PE and PVC films. *Journal of Biomaterials Science, Polymer Edition* **8**(9): 667-681.
Dicks AP, HR Swift, DLH Williams, AR Butler, HH Al-Sa'doni and BG Cox (1996). Identification of Cu^{+} as the effective reagent in nitric oxide formation from S-nitrosothiols (RSNO). *Journal of the Chemical Society, Perkin Transactions 2*: 481-7.
Dicks AP and DLH Williams (1996). Generation of nitric oxide from S-nitrosothiols using protein-bound Cu^{2+} sources. *Chemistry & Biology* **3**(8): 655-659.
Dimmeler S and B Brüne (1992). Characterization of a nitric-oxide-catalysed ADP-ribosylation of glyceraldehyde-3-phosphate dehydrogenase. *European Journal of Biochemistry* **210**(1): 305-310.
Duan X (2001). Exploiting Endogenous Nitric Oxide to Improve the Haemocompatibility

of Biomaterials. *Chemical Engineering*. Stillwater, Oklahoma State University. **Doctor of Philosophy:** 182.

Duan X and RS Lewis (2002). Improved haemocompatibility of cysteine-modified polymers via endogenous nitric oxide. *Biomaterials* **23**(4): 1197-1203.

Ehrenberg L, M Harms-Ringdahl, I Fedorcsák and F Granath (1989). Kinetics of the Copper- and Iron-Catalysed Oxidation of Cysteine by Dioxygen. *Acta Chemica Scandinavica* **43**: 177-187.

Ellman GL (1959). Tissue sulfhydryl groups. *Arch Biochem Biophys* **82**(1): 70-77.

Fahlenkamp H (2003). The Characterization, Optimization and Utilization of Immobilized Thoil Groups on a Polymeric Surface. *Chemical Engineering*. Stillwater, Oklahoma State University. **Doctor of Philosopy**.

Fang K, R Johns, T Macdonald, M Kinter and B Gaston (2000). S-nitrosoglutathione breakdown prevents airway smooth muscle relaxation in the guinea pig. *Am J Physiol Lung Cell Mol Physiol* **279**(4): L716-721.

Fasman GD (1976). Physical Chemical Data. *CRC Handbook of Biochemistry and Molecular Biology*. Cleveland, CRC Press. **1**.

Feldman PLG, Owen W.; Stuehr, Dennis J. (1993). The surprising life of nitric oxide. *Chemical & Engineering News* **71**(51): 26-38.

Ferris MM and KL Rowlen (2000). Direct Evidence of Ozone as the Active Oxidant in "Photooxidation" of Alkanethiols on SERS-Active Silver. *Applied Spectroscopy* **54**: 664-668.

Flagg EW, RJ Coates, DP Jones, JW Eley, EW Gunter, B Jackson and RS Greenberg (1993). Plasma total glutathione in humans and its association with demographic and health-related factors. *British Journal of Nutrition* **70**: 797-808.

Folts JDL, Joseph. (2000). Coating arterial and blood contacting surface with NO-donating compounds. *Nitric Oxide and the Cardiovascular System* **4**: 503-514.

Freedman JE, B Frei, GN Welch and J Loscalzo (1995). Glutathione peroxidase potentiates the inhibition of platelet function by S-nitrosothiols. *The Journal of Clinical Investigation* **96**(1): 394-400.

Freedman JE, J Loscalzo, MR Barnard, C Alpert, JF Keaney and AD Michelson (1997). Nitric oxide released from activated platelets inhibits platelet recruitment. *The Journal of Clinical Investigation* **100**(2): 350–356.

Frost MC, MM Reynolds and ME Meyerhoff (2005). Polymers incorporating nitric oxide releasing/generating substances for improved biocompatibility of blood-contacting medical devices. *Biomaterials* **26**(14): 1685-1693.

Furchgott RF (1988). Studies on relaxation of rabbit aorta by sodium nitrite: the basis for the proposal that the acid-activatable inhibitory factor from retractor penis is inorganic nitrite and the endothelium-derived relaxing factor is nitric oxide. *Vasodilation: Vascular Smooth Muscle, Peptides, and Endothelium* P. M. Vanhoutte. New York, Raven Press**:** 401-414.

Furchgott RF and JV Zawadzki (1980). The obligatory role of endothelial cells in the relaxation of arterial smooth muscle by acetylcholine. *Nature* **288**(5789): 373-376.

Gappa-Fahlenkamp H, X Duan and RS Lewis (2004). Analysis of immobilized L-cysteine on polymers. *Journal of Biomedical Materials Research Part A* **71A**(3): 519-527.

Gappa-Fahlenkamp H and RS Lewis (2005). Improved hemocompatibility of poly(ethylene terephthalate) modified with various thiol-containing groups. *Biomaterials* **26**(17): 3479-3485.
Gaston BM, J Carver, A Doctor and LA Palmer (2003). S-Nitrosylation Signaling in Cell Biology. *Mol. Interv.* **3**(5): 253-263.
Gerdes R, O Bartels, G Schneider, D Wöhrle and G Schulz-Ekloff (1999). Photooxidation of sulfide, thiol, phenols, and cyclopentadiene by artificial light and solar light irradiation. *International Journal of Photoenergy* **1**(1): 41-47.
Giustarini D, A Milzani, R Colombo, I Dalle-Donne and R Rossi (2004). Nitric oxide, S-nitrosothiols and hemoglobin: is methodology the key? *Trends in Pharmacological Sciences* **25**(6): 311-316.
Giustarini D, A Milzani, I Dalle-Donne and R Rossi (2007). Detection of S-nitrosothiols in biological fluids: A comparison among the most widely applied methodologies. *Journal of Chromatography B* **851**(1-2): 124-139.
Gladwin MT, JH Crawford and RP Patel (2003). The Biochemistry of Nitric Oxide, Nitrite and Hemoglobin: Role in Blood Flow Regulation. *Free Radical Biology and Medicine* **36**(6): 707-717.
Glusa E (1991). Hirudin and platelets. *Semin Thromb Hemost* **17**: 122-5.
Gordge MP, JS Hothersall, GH Neild and AA Dutra (1996). Role of a copper (I)-dependent enzyme in the anti-platelet action of S-nitrosoglutathione. *Br J Pharmacol* **119**(3): 533-538.
Gordge MP, DJ Meyer, J Hothersall, GH Neild, NN Payne and A Noronha-Dutra (1995). Copper chelation-induced reduction of the biological activity of S-nitrosothiols. *British Journal of Pharmacology* **114**(5): 1083-9.
Gow AJ, DG Buerk and H Ischiropoulos (1997). A Novel Reaction Mechanism for the Formation of S-Nitrosothiol in Vivo. *J. Biol. Chem.* **272**(5): 2841-2845.
Greenwald D, S Shumway, P Albear and L Gottlieb (1994). Mechanical Comparison of 10 Suture Materials before and after in Vivo Incubation. *Journal of Surgical Research* **56**(4): 372-377.
Gryboś J, M Marszałek, M Lekka, F Heinrich and W Tröger (2005). PAC Studies of BSA Conformational Changes. *HFI/NQI 2004***:** 755-761.
Guan X, B Hoffman, C Dwivedi and DP Matthees (2003). A simultaneous liquid chromatography/mass spectrometric assay of glutathione, cysteine, homocysteine and their disulfides in biological samples. *Journal of Pharmaceutical and Biomedical Analysis* **31**(2): 251-261.
Guthmann F, B Mayer, D Koesling, WR Kukovetz and E Böhme (1992). Characterization of soluble platelet guanylyl cyclase with peptide antibodies. *Naunyn-Schmiedeberg's Archives of Pharmacology* **346**(5): 537-541.
Hausladen A, CT Privalle, T Keng, J DeAngelo and JS Stamler (1996). Nitrosative Stress: Activation of the Transcription Factor OxyR. **86**(5): 719-729.
Hayakawa K, S Minami and S Nakamura (1973). Kinetics of the Oxidation of Ascorbic Acid by the Copper (II) Ion in an Acetate Buffer Solution. *Bulletin of the Chemical Society of Japan* **46**(9): 2788-2791.
Hayashi F, Y Okuda, M Nakata and K Natori (2003). Development of a Small-Diameter Expanded Polytetrafluoroethylene Vascular Graft. *SEI Tech Rev* **55**: 83-88.
Haynes DH (1993). Effects of cyclic nucleotides and protein kinases on platelet calcium

homeostasis and mobilization. *Platelets* **4**: 231-242.
Hayward JA and D Chapman (1984). Biomembrane surfaces as models for polymer design: the potential for haemocompatibility. *Biomaterials* **5**(3): 135-142.
Hermanson GT (1996). *Bioconjugate techniques*.
Hinderling PH and D Hartmann (2005). The pH dependency of the binding of drugs to plasma proteins in man. *Therapeutic Drug Monitoring* **27**(1): 71-85.
Hogg N (1999). The Kinetics of S-Transnitrosation—A Reversible Second-Order Reaction. *Analytical Biochemistry* **272**(2): 257-262.
Hogg N (2002). The Biochemistry and Physiology of S-nitrosothiols. *Annual Review of Pharmacology and Toxicology* **42**(1): 585-600.
Hogg N, RJ Singh, E Konorev, J Joseph and B Kalyanaraman (1997). S-Nitrosoglutathione as a substrate for gamma-glutamyl transpeptidase. *Biochemical Journal* **323**(2): 477–481.
Holmes AJ and DLH Williams (2000). Reaction of ascorbic acid with S-nitrosothiols: clear evidence for two distinct reaction pathways. *Journal of the Chemical Society, Perkin Transactions 2*: 1639-1644.
Hongu T and GO Phillips (1997). *New fibers*. Sound Parkway, CRC Press.
Hou Y, Z Guo, J Li and PG Wang (1996). Seleno Compounds and Glutathione Peroxidase Catalyzed Decomposition ofS-Nitrosothiols. *Biochemical and Biophysical Research Communications* **228**(1): 88-93.
Hu T-M and T-C Chou (2006). The Kinetics of Thiol-mediated Decomposition of S-Nitrosothiols. *AAPS Journal* **8**(3): 8.
Huang K-J, W-Z Xie, H Wang and H-S Zhang (2007). Sensitive determination of S-nitrosothiols in human blood by spectrofluorimetry using a fluorescent probe: 1,3,5,7-tetramethyl-8-(3',4'-diaminophenyl)-difluoroboradiaza-s-indacene. *Talanta* **73**(1): 62-67.
Ignarro LJ, RE Byrns and KS Wood (1988). Biochemical and pharmacological properties of endothelium-derived relaxing factor and its similarity to nitric oxide radical. *Vasodilation: Vascular Smooth Muscle, Peptides, and Endothelium* P. M. Vanhoutte. New York, Raven Press**:** 427-436.
Ivanova K, WA Buechler, G Wolfram, C Drummer, J-M Heim and R Gerzer (1994). Soluble Guanylyl Cyclase and Platelet Function. *Annals of the New York Academy of Sciences* **714**(1): 151-157.
Jamaati HR, P Pajouh, M Nayebi, N Baghaie, N Baghaie and H Khosravani (2006). Ascorbic Acid Concentration in Plasma and White Blood Cells of Patients with Bronchial Asthma. *Tanaffos* **5**(4): 29-35.
Jayakrishnan A and SR Jameela (1996). Glutaraldehyde as a fixative in bioprostheses and drug delivery matrices. *Biomaterials* **17**(5): 471-484.
Jerzy, Lstrok and obarzewski (1981). Comparison of some properties of immobilized and soluble forms of fungal peroxidase. *Biotechnology and Bioengineering* **23**(9): 2161-2165.
Jia L, C Bonaventura, J Bonaventura and JS Stamler (1996). S-nitrosohaemoglobin: a dynamic activity of blood involved in vascular control. *Nature* **380**(6571): 221-226.
Jiao Y-P and F-Z Cui (2007). Surface modification of polyester biomaterials for tissue engineering. *Biomedical Materials* **2** (R24-R37): 1748-6041.

Jobgen WS, SC Jobgen, H Li, CJ Meininger and G Wu (2007). Analysis of nitrite and nitrate in biological samples using high-performance liquid chromatography. *Journal of Chromatography B* **851**(1-2): 71-82.

Jocelyn PC (1987). Spectrophotometric assay of thiols. *Methods Enzymol* **143**: 44-67.

Jourd'heuil D, K Hallen, M Feelisch and MB Grisham (2000). Dynamic state of S-nitrosothiols in human plasma and whole blood. *Free Radical Biology and Medicine* **28**(3): 409-417.

Keaney JF, simon, D.I., Stamler, J.S., Jaraki, O., Scharfstein, J., Vita, J.A., and Loscalzo, J. (1993). NO forms an adduct with serum albumin that has endothelium-derived relaxing factor-like proterties. *The journal of clinical investigation, Inc* **91**: 1582-1589.

Kelm M (1999). Nitric oxide metabolism and breakdown. *Biochimica et Biophysica Acta* **1411**(2-3): 273-289.

Kelm M and J Schrader (1990). Control of coronary vascular tone by nitric oxide. *Circ Res* **66**(6): 1561-1575.

Khaw K-T, S Bingham, A Welch, R Luben, N Wareham, S Oakes and N Day (2001). Relation between plasma ascorbic acid and mortality in men and women in EPIC-Norfolk prospective study: a prospective population study. *The Lancet* **357**(9257): 657-663.

Kluge I, U Gutteck-Amsler, M Zollinger and KQ Do (1997). S-Nitrosoglutathione in Rat Cerebellum: Identification and Quantification by Liquid Chromatography-Mass Spectrometry. *Journal of Neurochemistry* **69**(6): 2599-2607.

Knobler CM (2007). Recent Developments in the Study of Monolayers at the Air-Water Interface. *Advances in Chemical Physics*. I. Prigogine and S. A. Rice**:** 397-449.

Knowles RG (1997). Nitric Oxide, Mitochondria and Metabolism. *Biochemistry Soc. Trans.* **25**(3): 895-901.

Knowles RG and S Moncada (1994). Nitric oxide synthases in mammals. *Biochem J.* **298**(2): 249-258.

Kuo W-NK, Joseph M.; Robinson, Marvin J.; Nibbs, Janna; Nayar, Ram. (2003). Further study on S-nitrosation by nitrite. . *Frontiers in Bioscience* **8**: A143-A147.

Lahann J, D Klee, W Pluester and H Hoecker (2001). Bioactive immobilization of r-hirudin on CVD-coated metallic implant devices. *Biomaterials* **22**(8): 817-826.

Lander H (1997). An essential role for free radicals and derived species in signal transduction. *FASEB J.* **11**(2): 118-124.

Lander HM, AT Jacovina, RJ Davis and JM Tauras (1996). Differential Activation of Mitogen-activated Protein Kinases by Nitric Oxide-related Species. *J. Biol. Chem.* **271**(33): 19705-19709.

Lewis RS and WM Deen (1994). Kinetics of the Reaction of Nitric Oxide with Oxygen in Aqueous Solutions. **7**(4): 568-574.

Lim HL, BM Myers, BA Hamilton, GL Davis and JYN Lau (1995). Plasma glutathione concentration in patients with chronic hepatitis C virus infection. *Journal of Viral Hepatitis* **2**(4): 211–214

Lin J-C and S-M Tseng (2001). Surface characterization and platelet adhesion studies on polyethylene surface with hirudin immobilization. *Journal of Materials Science: Materials in Medicine* **12**(9): 827-832.

Liu Y, J-R Chen, Y Yang and F Wu (2008). Improved blood compatibility of

poly(ethylene terephthalate) films modified with L-arginine. *Journal of Biomaterials Science, Polymer Edition* **19**: 497-507.
Loeppky RN, W Tomasik and BE Kerrick (1987). Nitroso transfer from {alpha}-nitrosamino aldehydes: implications for carcinogenesis. *Carcinogenesis* **8**(7): 941-946.
Löfås S and B Johnsson (1990). A novel hydrogel matrix on gold surfaces in surface plasmon resonance sensors for fast and efficient covalent immobilization of ligands. *J. Chem. Soc., Chem. Commun.*: 1526-1528.
Loscalzo J (2001). Nitric Oxide Insufficiency, Platelet Activation, and Arterial Thrombosis. *Circ Res* **88**(8): 756-762.
Louis JI (1999). Nitric Oxide: A Unique Endogenous Signaling Molecule in Vascular Biology (Nobel Lecture). *Angewandte Chemie International Edition* **38**(13-14): 1882-1892.
Maalej N, R Albrecht, J Loscalzo and JD Folts (1999). The potent platelet inhibitory effects of S-nitrosated albumin coating of artificial surfaces. *Journal of the American College of Cardiology* **33**(5): 1408-1414.
MacArthur PH, S Shiva and MT Gladwin (2007). Measurement of circulating nitrite and S-nitrosothiols by reductive chemiluminescence. *Journal of Chromatography B* **851**(1-2): 93-105.
Marconi W, A Galloppa, A Martinelli and A Piozzi (1996). New polyurethane compositions able to bond high amounts of both albumin and heparin : II: Copolymers and polymer blends. *Biomaterials* **17**(18): 1795-1802.
Marley R, Feelisch M, Holt S and M K (2000). A chemiluminescense-based assay for S-nitrosoalbumin and other plasma S-nitrosothiols. *Free Radic Research* **32**(1): 1-9.
Marozkina N, B Gaston and A Doctor (2008). Transnitrosation Signals Oxyhemoglobin Desaturation. *Circ Res* **103**(5): 441-443.
Martin L (1999). *All You Really Need to Know to Interpret Arterial Blood Gases*, Lippincott Williams & Wilkins.
Massia SP and JA Hubbell (1990). Covalently Attached GRGD on Polymer Surfaces Promotes Biospecific Adhesion of Mammalian Cells. *Annals of the New York Academy of Sciences* **589**(Biochemical Engineering): 261-270.
Mateo C, JM Palomo, G Fernandez-Lorente, JM Guisan and R Fernandez-Lafuente (2007). Improvement of enzyme activity, stability and selectivity via immobilization techniques. *Enzyme and Microbial Technology* **40**(6): 1451-1463.
Mathews WR and SW Kerr (1993). Biological activity of S-nitrosothiols: the role of nitric oxide. *J Pharmacol Exp Ther* **267**(3): 1529-1537.
Mayer B, S Pfeiffer, A Schrammel, D Koesling, K Schmidt and F Brunner (1998). A New Pathway of Nitric Oxide/Cyclic GMP Signaling Involving S-Nitrosoglutathione. *J. Biol. Chem.* **273**(6): 3264-3270.
McAninly J, DLH Williams, SC Askew, AR Butler and C Russell (1993). Metal ion catalysis in nitrosothiol (RSNO) decomposition. *Journal of the Chemical Society, Chemical Communications*: 1758-9.
Meyer DJ, H Kramer, N Ozer, B Coles and B Ketterer (1994). Kinetics and equilibria of S-nitrosothiol--thiol exchange between glutathione, cysteine, penicillamines and serum albumin. *FEBS Letters* **345**(2-3): 177-180.
Michel T and O Feron (1997). Nitric oxide synthases: which, where, how, and why?

Journal of Clinical Investigation **100**(9): 2146-2152
Migneault I, C Dartiguenave, MJ Bertrand and KC Waldron (2004). Glutaraldehyde: behavior in aqueous solution, reaction with proteins, and application to enzyme crosslinking. *Biotechniques* **37**(5): 790-796.
Mochizuki S, Y Chiba, O Hiramatsu, H Tachibana, H Nakamoto, E Toyota, Y Ogasawara and F Kajiya (2005). Direct measurement of nipradilol-derived nitric oxide in the vascular wall of canine femoral arteries. *Heart and Vessels* **20**(4): 175-178.
Moncada S, RM Palmer and EA Higgs (1991). Nitric oxide: physiology, pathophysiology, and pharmacology. **43:** 109-142.
Muntean W (1999). Coagulation and Anticoagulation in Extracorporeal Membrane Oxygenation. *Artificial Organs* **23**(11): 979-983.
Murayama T and Y Nomura (1998). The Actions of NO in the Central Nervous System and in Thymocytes. *The Japanese Journal of Pharmacology* **76**(2): 129-139.
Nathan C (1992). Nitric oxide as a secretory product of mammalian cells. *FASEB J.* **6**(12): 3051-3064.
Nathan C (1997). Inducible Nitric Oxide Synthase: What Difference Does It Make? *Journal of Clinical Investigation* **100**(10): 2417-2423
Noble DR and DLH Williams (2000). Structure-Reactivity Studies of the Cu^{2+}-Catalyzed Decomposition of Four S-Nitrosothiols Based around the S-Nitrosocysteine/S-Nitrosoglutathione Structures. *Nitric Oxide* **4**(4): 392-398.
Ollis DF, R Datta and M Klaus (1976). Activity correlations between similarly modified soluble and immobilized enzymes. *Methods in Enzymology*, Academic Press. **Volume 44:** 444-450.
Palmer DA, P Benezeth and JM Simonson (2004). The solubility of copper oxides around the water/steam cycle. . *PowerPlant Chemistry* **6**(2): 81-88.
Palmerini CAS, Carla; Arienti, Giuseppe; Palombari, Roberto. (2002). Formation of nitrosothiols from gaseous nitric oxide at pH 7.4. *Journal of Biochemical and Molecular Toxicology* **16**(3): 135-139.
Park J-W (1988). Reaction of S-nitrosoglutathione with sulfhydryl groups in protein. *Biochemical and Biophysical Research Communications* **152**(2): 916-920.
Persichini T, M Colasanti, GM Lauro and P Ascenzi (1998). Cysteine Nitrosylation Inactivates the HIV-1 Protease. *Biochemical and Biophysical Research Communications* **250**(3): 575-576.
Pietraforte D, Mallozzi, C., Scorza, G., and Minetti, M. (1995). Role of Thiols in the Targeting of S-NitrosoThiols to Red Blood Cells. *Biochemistry* **34**: 7177-7185.
Polyanin AD, AM Kutepov, DA Kazenin and AV Vyazmin (2001). *Hydrodynamics, Mass and Heat Transfer in Chemical Engineering* New York, Taylor & Francis.
Puri RN and RW Colman (1997). ADP-induced platelet activation. *Crit Rev Biochem Mol Biol* **32**: 437-502.
Radomski MW and S Moncada (1993). The Biological and Pharmocological Role of Nitric Oxide in Platelet Function. *Mechanisms of Platelet Activation and Control*. K. S. Authi, S. P. Watson and V. V. Kakkar. New York, Plenum Press**:** 251-266.
Radomski MW, DD Rees, A Dutra and S Moncada (1992). S-nitroso-glutathione inhibits platelet activation in vitro and in vivo. *British journal of pharmacology* **107**(3): 745-9.

Ramamurthi A and RS Lewis (1997). Measurement and Modeling of Nitric Oxide Release Rates for Nitric Oxide Donors. *Chemical Research in Toxicology* **10**(4): 408-413.

Ramamurthi A and RS Lewis (1998). Design of a Novel Apparatus to Study Nitric Oxide (NO) Inhibition of Platelet Adhesion. *Annals of Biomedical Engineering* **26**(6): 1036-1043.

Ramamurthi A and RS Lewis (2000). Influence of Agonist, Shear Rate, and Perfusion Time on Nitric Oxide Inhibition of Platelet Deposition. *Annals of Biomedical Engineering* **28**(2): 174-181.

Rassaf T, NS Bryan, M Kelm and M Feelisch (2002). Concomitant presence of N-nitroso and S-nitroso proteins in human plasma. *Free Radical Biology and Medicine* **33**(11): 1590-1596.

Rassaf T, NS Bryan, RE Maloney, V Specian, M Kelm, B Kalyanaraman, J Rodriguez and M Feelisch (2003). NO adducts in mammalian red blood cells: too much or too little? *Nature Medicine* **9**: 481 - 482

Ratner BD. (2004). "Biomaterials Tutorial: An Introduction to Biomaterials." Retrieved 07/12, 2008, from http://www.uweb.engr.washington.edu/research/tutorials/introbiomat.html.

Ratner BD and DG Castner (1997). *Surface Modification of Polymeric Biomaterials*. New York, Springer.

Ratner BD, AS Hoffman, FJ Schoen and JE Lemons (2004). *Biomaterials Science, Second Edition: An Introduction to Materials in Medicine* San Diego, Academic Press.

Richardson G and N Benjamin (2002). Potential therapeutic uses for S-nitrosothiols. *Clinical Science* **102**(1): 99-105.

Richie JP, Jr., P Abraham and Y Leutzinger (1996). Long-term stability of blood glutathione and cysteine in humans. *Clin Chem* **42**(7): 1100-1105.

Robak J, E Marcinkiewicz, Z Michalska and RJ Gryglewski (1997). Nitric oxide donation and nitrite assays in the presence of thiols and albumin as determined by Griess' and Werringloer's methods. *Polish Journal of Pharmacology* **49**(4): 255-262.

Robert-Banchereau E, S Lacombe and J Ollivier (1997). Unsensitized photooxidation of sulfur compounds with molecular oxygen in solution. *Tetrahedron* **53**(6): 2087-2102.

Roderique EM and JE Wynands (1967). Blood coagulation and haemostasis: a review. *Canadian Anaesthetists' Society journal* **14**(2): 129-151.

Rodriguez-Segade S, J Rodriguez, D Mayan and F Camina (2005). Plasma Albumin Concentration Is a Predictor of HbA1c Among Type 2 Diabetic Patients, Independently of Fasting Plasma Glucose and Fructosamine. **28:** 437-439.

Rootwelt K (1967). Quantitative determination of thiols and disulphides in urine by means of Ellman's reagent and thiolated Sephadex and its application in cystinuria. *Scand J Clin Lab Invest* **19**(4): 325-330.

Rossi R, L Lusini, F Giannerini, D Giustarini, G Lungarella and PD Simplicio (1997). A Method to Study Kinetics of Transnitrosation with Nitrosoglutathione: Reactions with Hemoglobin and Other Thiols. *Analytical Biochemistry* **254**(2): 215-220.

Saburo A (1999). Polypeptide synthesis by the thioester method. **51**(4): 247-265.

Samouilov A and JL Zweier (1998). Development of Chemiluminescence-Based Methods for Specific Quantitation of Nitrosylated Thiols*1. *Analytical Biochemistry* **258**(2): 322-330.
Savi P and JM Herbert (1996). ADP receptors on platelets and ADP-selective antiaggregating agents. *Med Res Rev* **16**: 159-79.
Sbrana E, A Paladini, E Bramanti, MC Spinetti and G Raspi (2004). Quantitation of reduced glutathione and cysteine in human immunodeficiency virus-infected patients. **25:** 1522-1529.
Scharfstein JSK, John F., Jr.; Slivka, Adam; Welch, George N.; Vita, Joseph A.; Stamler, Jonathan S.; Loscalzo, Joseph. (1994). In vivo transfer of nitric oxide between a plasma protein-bound reservoir and low molecular weight thiols. *Journal of Clinical Investigation* **94**(4): 1432-1439.
Schmidt HHHW and U Walter (1994). NO at work. *Cell* **78**(6): 919-925.
Schmidt WE, K Desai, C Foster, C Lowery, LC McBride, R Mehta, J Moody and T Tyner. (2005). "Minutes of the Committee on Analytical Reagents." Retrieved 1/28, 2009, from http://pubs.acs.org/reagents/comminfo/minutes.html.
Scorza G, D Pietraforte and M Minetti (1996). Role of Ascorbate and Protein Thiols in the Release of Nitric oxide from S-Nitroso-Albumin and S-Nitroso-Glutathione in Human Plasma. *Free Radical Biology and Medicine* **22**(4): 633-642.
Seifert B, P Romaniuk and T Groth (1997). Covalent immobilization of hirudin improves the haemocompatibility of polylactide--polyglycolide in vitro. *Biomaterials* **18**(22): 1495-1502.
Shi D (2005). *Introduction to Biomaterials*. Beijing, Tsinghua University Press.
Sigma-Aldrich (2002) "5,5'-Dithio-Bis(2-Nitrobenzoic Acid) Product Information."
Singh RJ, N Hogg, J Joseph and B Kalyanaraman (1996). Mechanism of Nitric Oxide Release from S-Nitrosothiols. *J. Biol. Chem.* **271**(31): 18596-18603.
Smith JN and TP Dasgupta (2000). Kinetics and Mechanism of the Decomposition of S-Nitrosoglutathione by L-Ascorbic Acid and Copper Ions in Aqueous Solution to Produce Nitric Oxide. *Nitric Oxide* **4**(1): 57-66.
Stamler J, D Simon, J Osborne, M Mullins, O Jaraki, T Michel, D Singel and J Loscalzo (1992a). S-Nitrosylation of Proteins with Nitric Oxide: Synthesis and Characterization of Biologically Active Compounds. *PNAS* **89**(1): 444-448.
Stamler JS and M Feelisch (1996). Preparation and Detection of S-Nitrosothiols. *Methods in Nitric Oxide Research*. M. Feelisch and J. S. Stamler. Chichester, John Wiley & Sons Ltd**:** 521-539.
Stamler JS, O Jaraki, J Osborne, DI Simon, J Keaney, J Vita, D Singel, CR Valeri and J Loscalzo (1992b). Nitric oxide circulates in mammalian plasma primarily as an S-nitroso adduct of serum albumin. . *Proceedings of the National Academy of Sciences of the United States of America* **89**(16): 7674-7.
Stamler JS and J Loscalzo (1992). Capillary zone electrophoretic detection of biological thiols and their S-nitrosated derivatives. *Analytical Chemistry* **64**(7): 779-85.
Stamler JS and EJ Toone (2002). The decomposition of thionitrites. *Current Opinion in Chemical Biology* **6**(6): 779-785.
Stoner L, M Sabatier, K Edge and K McCully (2004). Relationship between blood velocity and conduit artery diameter and the effects of smoking on vascular responsiveness. **96:** 2139-2145.

Stubauer G, A Giuffre and P Sarti (1999). Mechanism of S-Nitrosothiol Formation and Degradation Mediated by Copper Ions. *J. Biol. Chem.* **274**(40): 28128-28133.
Svardal AM, MA Mansoor and PM Ueland (1990). Determination of reduced, oxidized, and protein-bound glutathione in human plasma with precolumn derivatization with monobromobimane and liquid chromatography. *Analytical Biochemistry* **184**(2): 338-346.
Swift HR and DLH Williams (1997). Decomposition of S-nitrosothiols by mercury(II) and silver salts. *Journal of the Chemical Society, Perkin Transactions 2*: 1933-1935.
Tashimo O, T Ishibashi, J Yoshida, H Tsuchida and M Nishio (2003). Interference with Saville's method in determination of low-molecular weight S-nitrosothiols by ultrafiltration. *Nitric Oxide* **9**(3): 148-152.
Thorslund S, J Sanchez, R Larsson, F Nikolajeff and J Bergquist (2005). Functionality and stability of heparin immobilized onto poly(dimethylsiloxane). *Colloids and Surfaces B: Biointerfaces* **45**(2): 76-81.
Tong GC (2003). Characterization of Cysteine-34 in Serum Albumin. *Department of Biochemistry*, Ohio State University. **Doctor of Philosophy:** 249.
Trujillo M, MN Alvarez, G Peluffo, BA Freeman and R Radi (1998). Xanthine Oxidase-mediated Decomposition of S-Nitrosothiols. *J. Biol. Chem.* **273**(14): 7828-7834.
Tsikas D, J Sandmann, F-M Gutzki, DO Stichtenoth and JC Frölich (1999). Measurement of S-nitrosoalbumin by gas chromatography-mass spectrometry: II. Quantitative determination of S-nitrosoalbumin in human plasma using S-[^{15}N]nitrosoalbumin as internal standard. *Journal of Chromatography B: Biomedical Sciences and Applications* **726**(1-2): 13-24.
Tsikas D, J Sandmann, S Rossa, F-M Gutzki and JC Frolich (1999). Investigations of S-Transnitrosylation Reactions between Low- and High-Molecular-WeightS-Nitroso Compounds and Their Thiols by High-Performance Liquid Chromatography and Gas Chromatography-Mass Spectrometry. *Analytical Biochemistry* **270**(2): 231-241.
Turitto VT (1982). Blood viscosity, mass transport, and thrombogenesis. *Prog Hemost Thromb* **6**: 139-77.
Tweden KS, JD Cameron, AJ Razzouk, WR Holmberg and SJ Kelly (1997). Biocompatibility of Silver-Modified Polyester for Antimicrobial Protection of Prosthetic Valves. *The Journal of heart valve disease* **6**(5): 553-61.
Twomey PJ, A Viljoen, IM House, TM Reynolds and AS Wierzbicki (2005). Relationship between Serum Copper, Ceruloplasmin, and Non-Ceruloplasmin-Bound Copper in Routine Clinical Practice. *Clin Chem* **51**(8): 1558-1559.
van der Vliet A, PAC Hoen, PS-Y Wong, A Bast and CE Cross (1998). Formation of S-Nitrosothiols via Direct Nucleophilic Nitrosation of Thiols by Peroxynitrite with Elimination of Hydrogen Peroxide. *J. Biol. Chem.* **273**(46): 30255-30262.
Vane J (1994). Towards a better aspirin. *Nature* **367**(6460): 215-216.
Vanin AF, IV Malenkova and VA Serezhenkov (1997). Iron Catalyzes both Decomposition and Synthesis of S-Nitrosothiols: Optical and Electron Paramagnetic Resonance Studies. *Nitric Oxide* **1**(3): 191-203.
Vanin AF, AA Papina, VA Serezhenkov and WH Koppenol (2004). The mechanisms of S-nitrosothiol decomposition catalyzed by iron. *Nitric Oxide* **10**(2): 60-73.

Vaughn MW, L Kuo and JC Liao (1998). Estimation of nitric oxide production and reaction rates in tissue by use of a mathematical model. *Am J Physiol Heart Circ Physiol* **274**(6): H2163-2176.

Vazquez MA, F Muñoz, J Donoso and FG Blanco (1990). Influence of the side chain on the stability of Schiff-bases formed between pyridoxal 5prime-phosphate and amino acids. *International Journal of Chemical Kinetics* **22**(9): 905-914.

Vinard E, R Eloy, J Descotes, JR Brudon, H Guidicelli, JL Magne, P Patra, R Berruet, A Huc and Jacques Chauchard (1988). Stability of performances of vascular prostheses retrospective study of 22 cases of human implanted prostheses. *Journal of Biomedical Materials Research* **22**(7): 633-648.

Walsh PN, DC Mills and JG White (1977). Metabolism and function of human platelets washed by albumin density gradient separation. *Br J Haematol* **36**: 287-96.

Walters CLG, P. N.; Palmer, R. C.; Smith, P. L. R. (1987). A rapid method for the determination of nitrate and nitrite by chemiluminescence. *Food Additives & Contaminants* **4**(2): 133-140.

Wang K, Z Wen, W Zhang, M Xian, J-P Cheng and PG Wang (2001). Equilibrium and kinetics studies of transnitrosation between S-nitrosothiols and thiols. *Bioorganic & Medicinal Chemistry Letters* **11**(3): 433-436.

Wang PG, M Xian, X Tang, X Wu, Z Wen, T Cai and AJ Janczuk (2002). Nitric Oxide Donors: Chemical Activities and Biological Applications. *Chemical Reviews* **102**(4): 1091-1134.

Whitesides G, J Mathias and C Seto (1991). Molecular self-assembly and nanochemistry: a chemical strategy for the synthesis of nanostructures. *Science* **254**(5036): 1312-1319.

Williams DF (1999). *The Williams Dictionary of Biomaterials*. Liverpool, Liverpool University Press**:** 368.

Williams DF (2008). On the mechanisms of biocompatibility. *Biomaterials* **29**(20): 2941-2953.

Williams DLH (1996). S-Nitrosothiols and Role of Metal Ions in Decomposition to Nitric Oxide. *Methods in Enzymology* **268**: 299-308.

Williams DLH (1999). The Chemistry of S-Nitrosothiols. *Acc. Chem. Res.* **32**(10): 869-876.

Williams DLH (2003). A chemist's view of the nitric oxide story. . *Organic & Biomolecular Chemistry* **1**(3): 441-449.

Wink DA, JF Darbyshire, RW Nims, JE Saavedra and PC Ford (1993). Reactions of the bioregulatory agent nitric oxide in oxygenated aqueous media: Determination of the kinetics for oxidation and nitrosation by intermediates generated in the nitric oxide/oxygen reaction. *Chemical Research in Toxicology* **6**(1): 23-7.

Wissink MJB, R Beernink, JS Pieper, AA Poot, GHM Engbers, T Beugeling, WG van Aken and J Feijen (2001). Immobilization of heparin to EDC/NHS-crosslinked collagen. Characterization and in vitro evaluation. *Biomaterials* **22**(2): 151-163.

Wu M, KA Pritchard, Jr, PM Kaminski, RP Fayngersh, TH Hintze and MS Wolin (1994). Involvement of nitric oxide and nitrosothiols in relaxation of pulmonary arteries to peroxynitrite. *Am J Physiol Heart Circ Physiol* **266**(5): H2108-2113.

Xu A, JA Vita and JF Keaney, Jr. (2000). Ascorbic Acid and Glutathione Modulate the Biological Activity of S-Nitrosoglutathione. **36:** 291-295.

Yanagimoto T, T Toyota, N Matsuki, Y Makino, S Uchiyama and T Ohwada (2007). Transnitrosation of Thiols from Aliphatic N-Nitrosamines: S-Nitrosation and Indirect Generation of Nitric Oxide. *Journal of the American Chemical Society* **129**(4): 736-737.

Yang Z, AM Belu, A Liebmann-Vinson, H Sugg and A Chilkoti (2000). Molecular Imaging of a Micropatterned Biological Ligand on an Activated Polymer Surface. *Langmuir* **16**(19): 7482-7492.

Zhang H and GE Means (1996). S-Nitrosation of Serum Albumin: Spectrophotometric Determination of Its Nitrosation by SimpleS-Nitrosothiols. *Analytical Biochemistry* **237**(1): 141-144.

Zhang J, Z Hu and X Chen (2005). Quantification of glutathione and glutathione disulfide in human plasma and tobacco leaves by capillary electrophoresis with laser-induced fluorescence detection. *Talanta* **65**(4): 986-990.

Zhang Y-Y, A-M Xu, M Nomen, M Walsh, JF Keaney, Jr. and J Loscalzo (1996). Nitrosation of Tryptophan Residue(s) in Serum Albumin and Model Dipeptides. BIOCHEMICAL CHARACTERIZATION AND BIOACTIVITY. *J. Biol. Chem.* **271**(24): 14271-14279.

VITA

Jun Gu

Candidate for the Degree of

Doctor of Philosophy

Dissertation: ANALYSIS OF NITRIC OXIDE TRANSFER AND RELEASE RATE FOR A CYSTEINE MODIFIED POLYMER

Major Field: Chemical Engineering

Biographical:

Personal Data: Born in Shanghai, China on January 27, 1979.

Education: Graduated from Shanghai Datong High School, Shanghai, China in 1997, received Bachelor of Science degree in Biochemical Engineering from East China University of Science and Technology, Shanghai, China in July 2001. Completed the requirements for the Doctor of Philosophy degree with a major in Chemical Engineering at Oklahoma State University in May 2010.

Experience: Undergraduate Research Assistant Intern; Shanghai Institute of Industrial Microbiology (SIIM), Shanghai, China, from November 2000 to June 2001. Research Associate; Cygen Biotech Co. Ltd., Shanghai, China, from June 2001 to June 2002. Graduate Research Assistant; Oklahoma State University, Department of Chemical Engineering, 2002 to 2007. Teaching Assistant, Oklahoma State University, Department of Chemical Engineering, 2007 to present.

Professional Memberships: American Institute of Chemical Engineers (AIChE)

Name: Jun Gu Date of Degree: May, 2010

Institution: Oklahoma State University Location: Stillwater, Oklahoma

Title of Study: ANALYSIS OF NITRIC OXIDE TRANSFER AND RELEASE RATE FOR A CYSTEINE MODIFIED POLYMER

Pages in Study: 200 Candidate for the Degree of Doctor of Philosophy

Major Field: Chemical Engineering

Scope and Method of Study: In order to improve the haemocompatibility of biomaterials so that platelet adhesion on the surface can be minimized, a cysteine (CySH) modified polymer was developed previously and preliminary blood contacting test has shown that the modified polymer can inhibit 60% platelet adhesion. The mechanism of this modified polymer is that the immobilized cysteine on the polymer can seize nitric oxide (NO) from S-nitroso-albumin (AlbSNO) in blood through transnitrosation reaction, and then the unstable S-nitroso-cysteine (CySNO) decomposes and release NO, which is a well known platelet inhibitor. However, the reason for incomplete platelet inhibition is unclear since measuring the NO flux from the modified polymer is difficult. Therefore, a detailed kinetic model is required to predict this NO flux. In this study, the kinetics of the associated reactions is investigated and stability of the modified polymer is evaluated and finally, NO flux is estimated by modeling in a tubular flow system.

Findings and Conclusions: CySNO decomposition is sensitive to various environment conditions such as metal ion contamination level, pH and ascorbic acid concentration. Transnitrosation in free solution revealed that CySH is oxidized by metal ion or oxygen in solution during the reaction while ascorbic acid can prevent the oxidation caused metal ion, however, oxidation due to oxygen still exists. On the other hand, previous technique for immobilizing CySH led to an unstable bond which is prone to hydrolyzation in neutral pH. Increased temperature was found to accelerate this hydrolysis significantly. An improved modification method was developed and a stable bond was formed. Out of the aqueous solution, immobilized CySH can also be oxidized when both light and air exists, while at -20˚C, CySH is very stable on the polymer surface for about 2 months. Immobilized transnitrosation showed that CySH on the polymer performs better than CySH in the free solution as it transferred more than three times of its own amount of BSANO before getting totally oxidized even without ascorbic acid. The calculated kinetic rate constants showed that transnitrosation has mass transfer limiting behavior which is likely due to the cracks on the polymer formed during modification while the CySNO decomposition rate constant is not affected by the cracks. The predicted NO flux by a model is sufficient for the platelet inhibition for previous *in vitro* blood test, however this flux is highly sensitive to AlbSNO concentration which can be much lower than the value used in the model setup.

ADVISER'S APPROVAL: Randy S. Lewis